JAIST Repository
https://dspace.jaist.ac.jp/

Title	分散符号化に基づくワイヤレス協調通信の場所率解析とパワー配分最適化問題
Author(s)	程，猛
Citation	
Issue Date	2014-03
Type	Thesis or Dissertation
Text version	ETD
URL	http://hdl.handle.net/10119/12108
Rights	
Description	Supervisor:松本　正，情報科学研究科，博士

JAIST
JAPAN
ADVANCED INSTITUTE OF
SCIENCE AND TECHNOLOGY

Japan Advanced Institute of Science and Technology

OUTAGE ANALYSIS AND OPTIMAL POWER ALLOCATION FOR DISTRIBUTED CODING BASED WIRELESS COOPERATIVE COMMUNICATIONS

MENG CHENG

in partial fulfillment of the requirements
for the degree of
Doctor of Philosophy

School of Information Science
Japan Advanced Institute of Science and Technology

March, 2014

Supervised by
Professor Tadashi Matsumoto

Reviewed by
Professor Dirk Wubben
Professor Sumei Sun
Professor Hidekazu Murata
Professor Kiyofumi Tanaka
Professor Brian M. Kurkoski

Abstract

The primary objective of this dissertation is to analyze performances of distributed coding based wireless cooperative communication systems from the perspective of Slepian-Wolf theorem. The particular system assumption in this dissertation is a one-way decode-and-forward relay model, where the original bit sequence at the source and the re-constructed bit sequence at the relay are independently encoded and transmitted to a common destination. The research fundamental lies in the utilization of the correlation knowledge between the two bit sequences, of which concept has potential of significantly improving wireless communication system performance. In this dissertation, both practical coding/decoding algorithms and the theoretical framework setup are focused on.

First of all, we propose a one-way Slepian-Wolf relay system adopting bit-interleaved coded modulation with iterative decoding (BICM-ID) for high spectrum efficiency. It is shown that the extrinsic information transfer (EXIT) curve of the BICM-ID demapper combined with the decoder of doped accumulator (DACC) is well matched with that of the decoders, which enables the EXIT tunnel open until (1,1) mutual information point. Although errors may happen in the source-relay channel (it is referred to as intra-link errors in this dissertation), the re-constructed sequences that may contain some errors are to forwarded to the destination. Strong codes are not needed, and even the systematic part of the coded bit sequences can be simply extracted at the relay node, regardless of whether or not some errors are occurring in the sequences. Therefore, the computational complexity of the relay can be significantly reduced, which indicates that our proposed system is highly energy-efficient.

Moreover, the theoretical outage probability of the proposed Slepian-Wolf relay system is derived over block Rayleigh fading channels. Two cases are considered: in Case 1, we simplify the intra-link transmission as a bit-flipping model, where some of the bits, re-constructed after decoding at the relay, are the flipped versions of the original information bits transmitted from the source. In other words, the intra-link error probability is used as a parameter representing the correlation between the sequences in the practical transmission chain design. As one of the main contributions, the theoretical outage probability expression is derived on

the basis of the admissible Slepian-Wolf rate region, with transmission channels being either temporally independent or correlated. In addition, asymptotic properties of the outage curves are mathematically proven. The theoretical results are verified through a series of simulations. In Case 2, block Rayleigh fading is also assumed for the intra-link, and we express the intra-link error probability by the Hamming distortion represented by the inverse rate distortion function. The outage probability of the Case 2 setup is derived for different relay location scenarios which provides us with more practical performance assessment than with Case 1.

Finally, the power allocation schemes are proposed for the both cases based on the outage derivations described above. Specifically, we aim to (1) minimize the outage probability while keeping the total transmit power fixed and (2) minimize the total transmit power given a fixed outage requirement. By assuming that the source-destination and the relay-destination channels are with high signal-to-noise power ratios, the approximated closed-form of the outage probability expression is derived in Case 1. It is shown that the power allocation scheme for the proposed Slepian-Wolf relay system can be formulated as a convex optimization problem. In Case 2, the power allocation scheme is also applied for different relay location scenarios.

Keywords: Turbo codes, iterative decoding, relay system, Slepian-Wolf theorem, outage probability, power allocation

Acknowledgments

This dissertation brings me back memories of the days when I was first motivated to pursue a PhD degree. I was really lucky to get in touch with Prof. Tad Matsumoto 3 years ago, who recognized my ambition and encouraged me to make a challenge in a new environment. During the three years' work under his supervision, I have been witnessing my academic progress, as well as some other personal developments. Undoubtedly, Prof. Tad Matsumoto is the first person whom I really want to show my gratitude to.

Secondly, I would like to thank Dr. Khoirul Anwar, assistant professor in our laboratory, for his selfless help. Also, I would like to say thank you to all my lab colleagues, Dr. Xiaobo Zhou, Ormsub Soulisak (Henry), Yasuhiro Takano, Valtteri Tervo, Pen-Shun Lu, Hui Zhou, Yu Cai, Ade Irawan, Xin He, Shen Qian, Kun Wu, Muhammad Reza Kahar Aziz, Ricardo Antonio Parrao Hernandez, Francisco Javier Cuadros Romero, Satou Kaoru and Ryouta Sekiya for their kind help and friendship. This dissertation is also in memory of my senior Mr. Kisho Fukawa, who passed away last October. His research work on BICM-ID greatly inspired me and all our Lab members.

Moreover, I want to thank all the university staffs who manage my living in JAIST well so that I can concentrate to the research work. Finally, thanks to my parents in 1800 km away. Their spiritual support will be treasured forever in my deep heart.

Contents

List of Figures

List of Tables

Chapter 1

Introduction

1.1 Motivation and Method

Generally, the transmit diversity of wireless communications requires more than one antenna equipped at the wireless terminals, such as in multi-input multi-output (MIMO) systems [1] [2]. However, many of the devices are unfortunately limited in size and hardware complexity to accommodate multiple antennas, which stimulates researchers to seek for alternative solutions. It is quite natural that the broadcasted signal sent from the transmitter to a specified destination can be overheard by its surrounding nodes. By further utilizing the information overheard by the surrounding nodes, a virtual multi-user environment can be established allowing mobile users to share their antennas. This idea has been conceptualized as cooperative communications, where the direct transmission between two nodes is enhanced with the aid of the supporting relays or other cooperative users. Consequently, the system throughput as well as power and spectral efficiencies of the whole wireless network can be significantly improved. After the first discussion of the classic three-nodes relay system in [3], cooperative communications have received intensive attentions both in academia and industry. In this dissertation, our discussions are all based on such a simple three-nodes one-way relay system model. However, it is quite reasonable that we first identify the most suitable strategies for a typical and simple structure and then extend to more complex network topologies.

There are different types of relay strategies for practical applications, one of which is called decoded-and-forward (DF) scheme [4] [5]. With DF, the original information bit sequence sent (after being channel-encoded) from the source node is to be decoded at the relay, and then forwarded

to the destination. Conventionally, the bit sequence received at the relay is discarded, if it is found to contain some errors after decoding, in order to avoid error propagation. Such errors are referred to as intra-link errors through out this dissertation. It should be noted that in a setup where the relay forwards data sequences, regardless of either presence or absence of intra-link errors, the two data sequences, one from the source and the other from the relay, are highly correlated because they were originally transmitted from the same source. The Slepian-Wolf theorem states that for lossless compression of correlated sources, by best exploiting the correlation knowledge of the data streams at the receiver, the distributed source coding scheme can achieve the same compression rate as that with an optimum single encoder which compresses the sources jointly. Therefore, the first objective of this research is to propose a practical transmission coding/decoding scheme that is capable of utilizing the correlation knowledge between the bit sequences sent from the source and the relay, which is referred to as the Slepian-Wolf relay system. Since the sequence that may contain some intra-link errors are allowed to be forwarded, this system does not require heavy computational complexity at the relay node.

The author in [6] proposes a simple one-way relay system exploiting source-relay correlation, assisted by a doped accumulator (DACC) with binary phase shift keying (BPSK) modulation. On the basis of this work, we apply the bit-interleaved coded modulation with iterative decoding (BICM-ID) technique to investigate the system performance for higher order modulations [7] [8]. BICM-ID has been well studied as a bandwidth efficient coded modulation scheme, where the encoder and the modulator of the transmission chain are separated by a random interleaver. The extrinsic log-likelihood ratios (LLRs) obtained from the demapper/decoder are exchanged iteratively with the decoder/demapper at the receiver side, via the de-interleaver/interleaver, respectively. The performance of the BICM-ID technique using non-Gray mapping outperforms that with the Gray mapping in the iterative process, which can be observed by the extrinsic information transfer (EXIT) chart analysis [9] [10]. Our technique shows that, the demapper's EXIT curve combined with a DACC decoder can reach a point very close to the (1,1) mutual information point, which matches well with that of the decoder; the convergence tunnel opens until that point and therefor the error floor is eliminated.

In many wireless communication analysis, channels are assumed to suffer from variations due to fading. One of the most reasonable and hence widely accepted model for block-wise transmission is the block Rayleigh fading channel, where the channel realization changes block-by-block but

stays constant within each block. With the block fading assumption, if the channel state information (CSI) is unknown to the transmitter, achieving always error-free transmission is impossible. This is simply because the transmission chain parameters can not be flexibly changed at the transmitter without the knowledge of CSI, which invokes the necessity of the outage analysis. The result of outage analysis provides the system operators with the estimated probability that the quality of service (QoS) requirement can be/can not be satisfied. This dissertation analyzes the theocratical bound of outage probability of such Slepian-Wolf relay systems, and their asymptotic properties as well, by assuming the transmission channels are suffering from block Rayleigh fading. The obtained theoretical bound can be used when evaluating the real, practical system performance, asymptotically, when it is needed to identify how close the performance of the practical systems to the bound.

Based on the outage probability analysis mentioned above, it is straightforward to move on to an optimal power allocation problem, given the requirement that the total transmit power, totalling over the source and relay transmit powers, are fixed. In this dissertation, the optimal power allocation techniques are presented, and the theoretical results are compared between with and without optimal power allocation.

1.2 Summary of Contribution

This research aims to provide a new coding/decoding framework, theoretical bounds and power allocation strategies, all for the cooperative communication systems, which exploits the correlation knowledge of the distributed sources at the destination. The achievements of this dissertation can be summarized as follows:

- We apply the BICM-ID technique with higher order modulations into a simple Slepian-Wolf relay system, where the correlation of the source and the relay is exploited. It is shown that the EXIT curve of the BICM-ID demapper combined with a DACC decoder matches very well with that of the decoder, and the convergence tunnel opens until a point very close to the (1,1) mutual information point.

- A methodology of theoretical outage probability derivation of the correlated source transmission is presented in this research. Its asymptotic properties are analyzed as well.

- In the case the intra-link errors can be represented by a bit-flipping model, a closed-form expression of the theoretical outage probability expression can be mathematically derived, with approximation of high signal-to-noise ratios (SNRs). It is shown that the optimal power allocation problem is formulated by the convex optimization framework.

- The optimal power allocation scheme is also investigated in the case when intra-link errors are assumed to be represented by the Hamming distortion of the inverse rate distortion function.

1.3 Dissertation Outline

This dissertation is organized as follows.

In Chapter 1, the motivation and brief descriptions of this research are introduced. It follows the contribution summaries and organization of this dissertation.

Then, in Chapter 2, some fundamental concepts and background knowledge about information theory and wireless communication systems are discussed for better understanding of the main part of this dissertation.

In Chapter 3, we investigate the proposed Slepian-Wolf relay system combined with BICM-ID technique in detail. Coding/decoding algorithms and the convergency behavior analysis using EXIT charts are provided for different relay location scenarios. The system performances are evaluated through simulations over both AWGN and block Rayleigh fading channels.

The methodology of the outage probability derivation is first introduced in Chapter 4 for the proposed Slepian-Wolf relay system. We consider two cases: in Case 1, a bit-flipping model is assumed for the intra-link errors; we provide the asymptotic analysis of the theoretical outage curves, as well as the comparison between the theoretical performances and the simulation results. In Case 2, to eliminate the flipping model, a rate distortion function with Hamming distortion measure is introduced representing the intra-link bit error probability, so that the account is taken of the fading variation of the intra-link in the analysis. The theoretical outage behaviors are then analyzed under the assumption of high SNRs for different relay scenarios.

In Chapter 5, we formulate an optimal power allocation scheme for the proposed Slepian-Wolf relay system. A closed-form expression of the theoretical outage probability is derived with the assumption of high SNRs in Case 1, and the optimal power allocation to the source and the relay

can be found by solving a convex optimization problem, related to the formulation based on the approximation. In Case 2, it is made possible to evaluate the impact of the relay location on outage, because it is assumed that the intra-link error probability can be expressed by the rate distortion function. Hence, the power allocation can also take into account the different relay location scenarios.

Finally, the conclusions, as well as the future work, are presented in Chapter 6.

Chapter 2

Preliminaries

In this chapter, some earlier work and techniques involved in this research are reviewed. First of all, the block diagram of the current digital communication system is presented, along with brief discussions of basic wireless channel models, such as AWGN and Rayleigh fading channels. In addition, the concept of outage probability is introduced for better understanding of the following chapters. Moreover, the principles of BICM-ID and Turbo codes are also explained, which act as key transmission techniques adopted in our proposed system. Finally, several important relay strategies and distributed source coding concept are also briefly described.

2.1 Review of Wireless Communication Basis

2.1.1 Digital Wireless Communication System Model

The physical layer level block diagram of the standard point-to-point digital communication system is shown in Fig. 2.1 [11]. At the transmitter side, the discrete information bits are first source-encoded in order to reduce the source redundancy. After that, the data is channel-encoded for the protection against transmission errors. Finally, the baseband signals are modulated into radio frequency and transmitted. The received signals via the wireless channel are processed at the receiver step-by-step for the recovery of the transmitted information. It should be emphasized here that our core research interest is not in the issue of the independent point-to-point case, but for the cooperative scenarios, composed of multiple point-to-point channels.

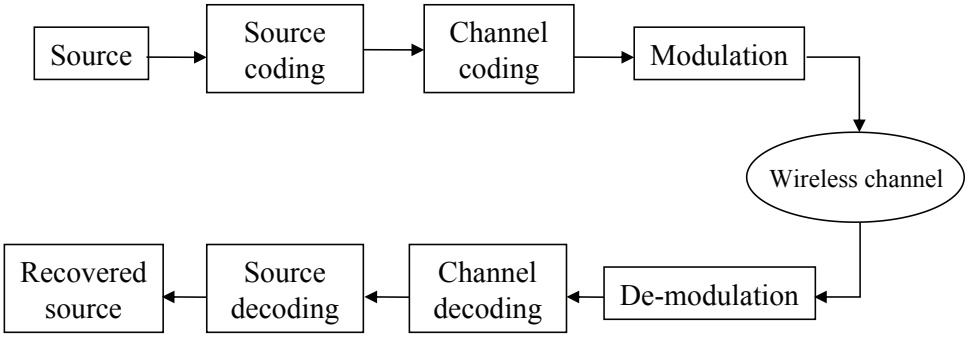

Figure 2.1: Block diagram of general digital communication system.

2.1.2 Wireless Channel Models

Wireless channels can be defined as the physical medium between the output of the transmitter and the input of the receiver. Due to the impact of the practical channel environment, the transmitted signals may suffer from interferences, fading variations, path-loss, shadowing and etc. In this dissertation, only additive white Gaussian noise (AWGN) and block Rayleigh fading channel models are considered when evaluating the system performance. Brief introductions of the both two models [12] are given as follows:

AWGN Channel Model

Without loss of generality, we consider the simplest AWGN channel, where the transceiver only has a single antenna pair. Basically, the received signal $\mathbf{y}$ is a sum of the transmitted signal $\mathbf{s}$ and a white Gaussian noise variables $\mathbf{n}$, as

$$\mathbf{y} = \mathbf{s} + \mathbf{n}. \tag{2.1}$$

Fading, interference, frequency selectivity and other channel properties are not considered in the AWGN channel model, however, it is a useful mathematical model for evaluating the basic system performances before taking into account of other influences. It should also be noted that the AWGN channel model is quite accurate for fixed terrestrial and satellite communications.

Block Rayleigh Fading Channel

Due to the obstacles of large objects such as buildings and vehicles in urban areas, the arrived signals at the receiver may subject to the multi-path propagation, which causes fading. In the Rayleigh fading model, the amplitude of the transmitted signals will vary or fade according to the Rayleigh distribution. It should also be noted that in the Rayleigh fading channel, none of the paths along the transmitter and the receiver has a dominating line-of-sight. Otherwise, it becomes a Rician fading model.

In modern wireless communications, data are usually divided into different frames and transmitted block-by-block. It is quite reasonable to assume that the channel coherence time is almost as long as the duration of the transmitted frame (fading is neither too fast nor too slow), which means that the channel gain changes block-by-block independently. The received signal can be expressed according to the equivalent complex baseband models as:

$$\mathbf{y} = h \cdot \mathbf{s} + \mathbf{n}, \tag{2.2}$$

where h is the complex channel gain, with the real and imaginary parts being modelled by independent and identically distributed (i.i.d.) zero-mean Gaussian processes.

2.1.3 AWGN Channel Capacity

We consider discrete-input continuous-output AWGN channel in the dissertation. According to Shannon's theory, the channel capacity is defined as the maximum number of bits per channel use that could be correctly transmitted through a noisy channel. Let the instantaneous channel SNR and bandwidth be denoted by γ and B, respectively, the channel capacity can be expressed by [13]

$$C = B \log_2(1 + \gamma). \tag{2.3}$$

Without loss of generality, $B = 1$ is assumed. Shannon's coding theorem states that it is possible to design a code at the transmission rate $R \leqslant C$ that can achieve arbitrarily small error probability. Through the exploitation of the equi-partitioning property (AEP) of joint typical sequences, a Gaussian codebook can be designed such that the mutual information between the input and output of the channel is maximized, given γ. For a memoryless time-invariant channel, its mutual information is given by

$$
\begin{aligned}
I(\mathbf{s};\mathbf{y}) &= h(\mathbf{y}) - h(\mathbf{y}|\mathbf{s}) \\
&= h(\mathbf{y}) - h(\mathbf{s}+\mathbf{n}|\mathbf{s}) \\
&= h(\mathbf{y}) - h(\mathbf{n}|\mathbf{s}) \\
&= h(\mathbf{y}) - h(\mathbf{n}),
\end{aligned} \tag{2.4}
$$

where $h(\mathbf{y}) = -\int_{\mathbf{y}} p(y)\log[p(y)]dy$ and $h(\mathbf{y}|\mathbf{s}) = \sum_{s\in\mathbf{s}}\int_{\mathbf{y}} p(s,y)\log[p(y|s)]dy$. It should be noted that the transmitted signal $\mathbf{s}$ and the AWGN noise $\mathbf{n}$ are statistically independent. As stated by Shannon, the channel capacity is equal to the mutual information between the channel input and output, and the maximization is with respect to the input distribution $p(\mathbf{s})$, which can be formulated by

$$
C = \max_{p(\mathbf{s})} I(\mathbf{s};\mathbf{y}). \tag{2.5}
$$

As stated before, the AWGN channel capacity can be achieved by maximizing the transmitted sequences following by a Gaussian codebook.

2.1.4 Outage Probability

It has to be noted that the Shannon theorem provides the capacity only for the deterministic channel. However, the parameters of practical channels usually vary in time, and therefore the instantaneous capacity of the time-varying channel becomes less meaningful. Generally, the ergodic capacity and outage probability are the two practical ways to evaluating the statistical channel capability.

With the ergodic property of the channel, the duration of the communication is assumed to be long enough compared to the speed of the channel variations, so that the receiver experiences all the possible fading channel realizations. Hence, the time average of performance figures in general can be replaced by their expectations. The ergodic capacity can be calculated by averaging the instantaneous Gaussian capacity over the probability density function (PDF) of the instantaneous SNR.

On the contrary, if the communication duration is not sufficiently long, the fading variation will not be ergodic, unless the fading variation is very fast (however unrealistic). It usually happens when channels are suffering from slow fading. In this case, instead of the ergodic capacity, the channel quality can be represented by outage probability.

As stated before, since block fading is assumed in this dissertation, our focus is not on the channel quality over the communication duration. Instead, our focus is on frame-wise quality. Basically, if the channel state information (CSI) is unknown to the transmitter, the adaptive coded modulation (ACM) techniques can not be used, and hence the Shannon capacity supported by the instantaneous channel SNR may become smaller than the required data transmitting rate, when the channel experiences deep fading. Consequently, there is no guarantee that error-free transmission can always be achieved for each frame. The outage probability $P_{out}(R)$ is the probability that the channel can not support the required transmission rate R.

Given the instantaneous SNR γ, it can support a rate $C(\gamma) = \log_2(1+\gamma)$. The outage event happens when $C(\gamma) < R$ or $\gamma < 2^R - 1$, with an outage probability being expressed by [14]

$$\begin{aligned} P_{out}(R) =& \mathrm{P_r}(r < 2^R - 1) \\ =& \int_0^{2^R-1} p_\gamma(\gamma) d\gamma, \end{aligned} \tag{2.6}$$

where $p_\gamma(\gamma)$ represents the PDF of the instantaneous SNR.

2.2 Turbo Codes

The idea of Turbo codes was proposed by Berrou, Glavieux and Thitimajshima in [15] in 1993 for the first time as the practical code that can asymptotically achieve the Shannon-limit performance in terms of bit error rate (BER). The excellent performance provided by the Turbo codes immediately excited researchers both in academia and industry. During the last 20 years, the research community has made a lot of achievements related to the Turbo codes, or more in general, Turbo principle. Basically, a Turbo code is formed by a parallel concatenation of two codes separated by an interleaver. A block diagram of the Turbo code by a the parallel concatenation is shown in Fig. 2.2, where the two input information sequences separated by a random interleaver are independently channel-encoded by each component encoder. The random interleaver aims to make the two encoded bit sequences statistically independent.

At the receiver side, instead of using the entirely optimal decoder requiring high complexity, an iterative decoding precess takes place between two component decoders, where soft information is exchanged in the form of log-likelihood ratio (LLR) defined as:

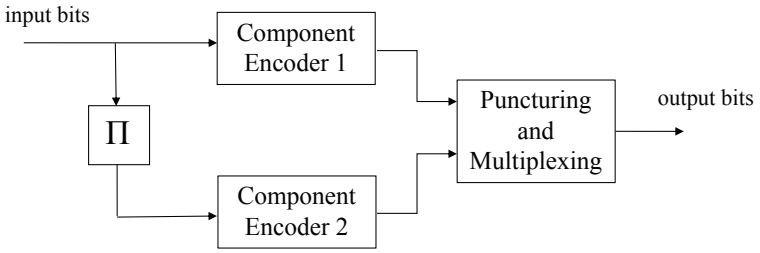

Figure 2.2: The block diagram of a simple Turbo encoder.

$$L(b) = \ln\left[\frac{\mathrm{P_r}(b=1)}{\mathrm{P_r}(b=0)}\right]. \tag{2.7}$$

It can be seen in (2.7) that, the definition of LLR is a logarithm of the ratio of the probabilities of the bit being 1 or 0. During one iteration, soft decoding is performed in each component decoder by using the Bahl-Cocke-Jelinek-Raviv (BCJR) algorithm, to obtain the LLR of each bit, and it is passed to another decoder as the soft input, as illustrated in Fig. 2.3. It should be noted that the iterative decoding process can be evaluated by the EXIT chart analysis. During the last 20 years, Turbo codes are widely used in communication systems under operation, for example, 3G cellular networks, satellite communications and other applications with high reliability requirements.

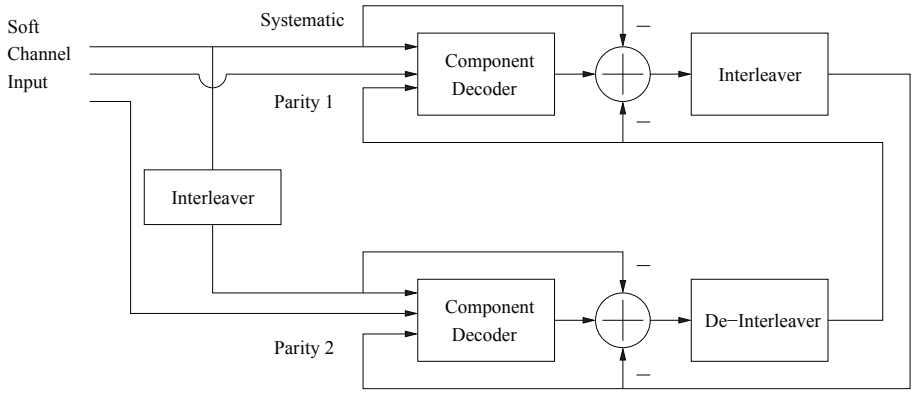

Figure 2.3: The block diagram of a Turbo decoder principle.

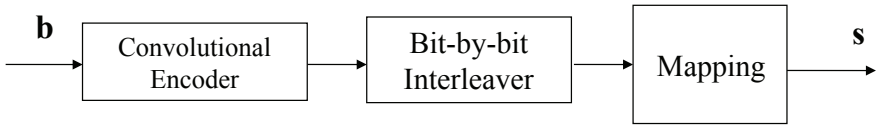

Figure 2.4: The BICM transmitter model.

2.3 BICM-ID Principles

Bit-interleaved coded modulation (BICM) was first proposed by Zehavi in [7], with a purpose of increasing the diversity order of the Trellis-coded-modulation (TCM) scheme [16]. It utilizes independent bit interleaver at the bit level rather than symbol level.

An example of the BICM transmitter model is shown in Fig. 2.4. The original information bits **b** are channel encoded, interleaved bit-by-bit, and mapped on to a symbol **s** with a specified mapping rule.

At the receiver side, in order to improve the system performance, Li and Ritcey applied an iterative decoding process into the original BICM technique in [17], which is called BICM-ID. Importantly, the non-Gray labelling rather than Gray mapping, is more suitable to BICM-ID. The receiver model of BICM-ID is shown in Fig. 2.5. The critical point is that, the *extrinsic* LLR of the coded bits is interleaved and fed back to the demapper as *a priori* LLR, and demapping process is performed with the help of the *a priori* LLR. The demapping output extrinsic LLR is de-interleaved again, and input to the decoder. This process is repeated until no more significant increase of *a posteriori* mutual information can be achieved. Finally, hard decision is made based on *a posteriori* LLR of the systematic bits.

Through iterations, the demapper can obtain more knowledge of the

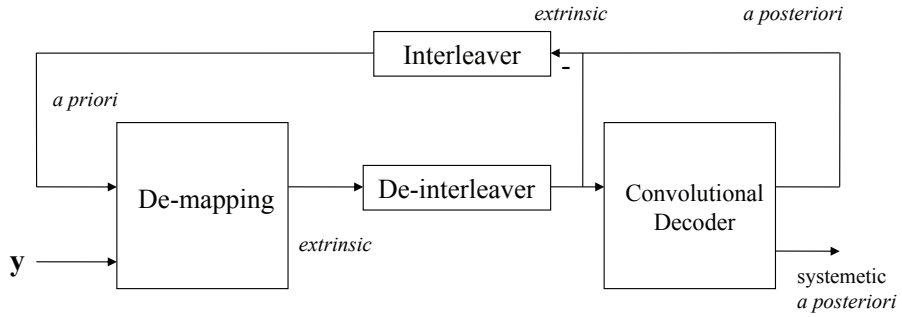

Figure 2.5: The BICM receiver model.

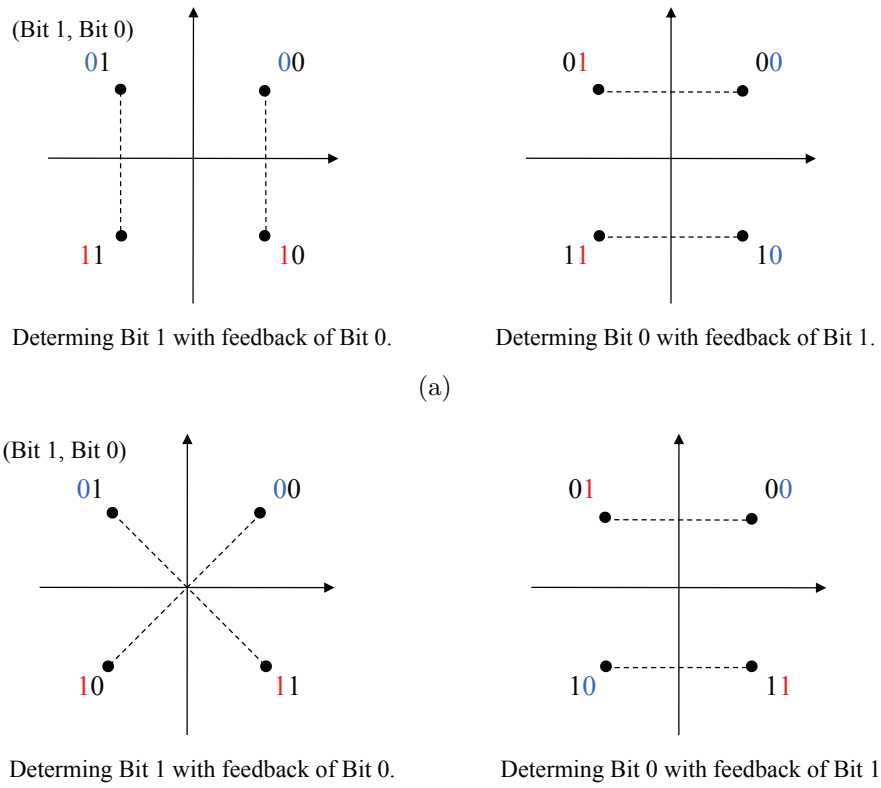

Figure 2.6: QPSK constellations with (a) Gray mapping and (b) non-Gray mapping.

bits, and this process enhances the detection of one bit with the knowledge of its neighbouring bits within one symbol. To explain this mechanism descriptively, we use quaternary phase shift keying (QPSK) modulation as an example of BICM-ID in this sub-section. Obviously, with the full *a priori* information of the bit at the position Bit 0, the bit at the position Bit 1 can be detected by comparing the Euclidean distances between the received signal point and the two candidate constellation points. It is found that with non-Gray mapping, the Euclidean distance to be compared is longer than that with Gray mapping, which is illustrated in the left part of Fig. 2.6(b). The similar properties can be found for 8PSK in Fig. 2.7. Therefore, it is obvious that the non-Gray labeling pattern outperforms the Gray mapping in the iterative decoding-and-demapping process [16].

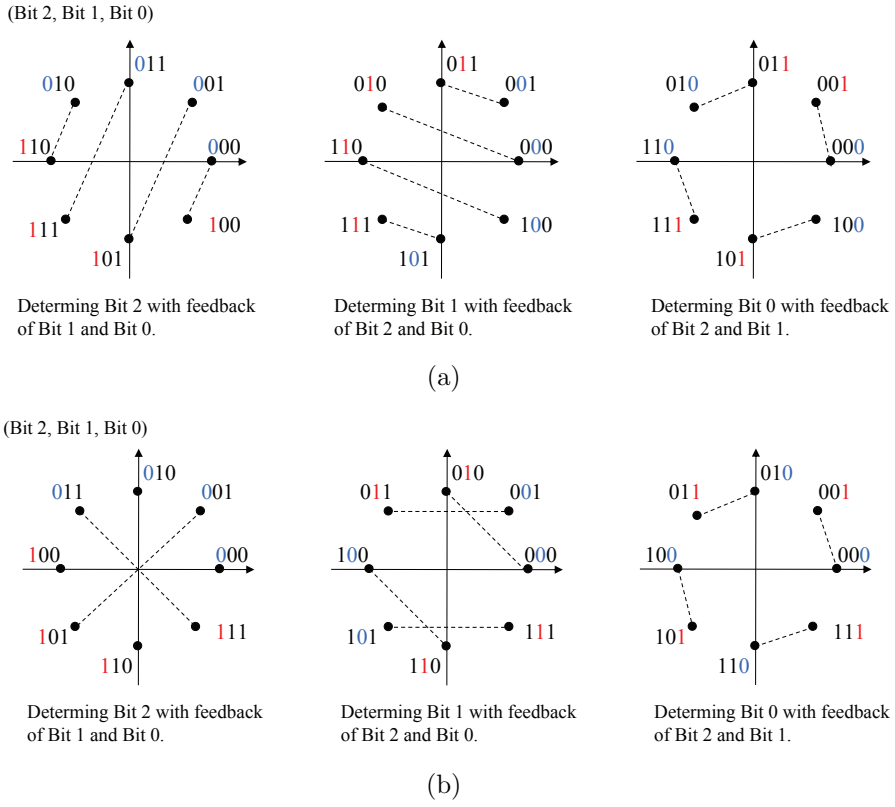

Figure 2.7: 8PSK constellations with (a) Gray mapping and (b) non-Gray mapping.

2.4 Cooperative Communications

With the aims of achieving higher system throughput and transmission reliability in future wireless networks, transmit diversity techniques using multiple antennas, such as space-time block coding (STBC) [18] have been intensively studied in the past decades. The transmit diversity can effectively reduce the detrimental effects of fading. Unfortunately, due to the size and/or cost limitations of mobile devices, multiple antennas can not always be supported in practice. However, with antenna sharing strategies among single-antenna users, it is possible to form a virtual multiple antennas environment. In other words, different mobile users can work cooperatively in order to exploit the spatial diversity without having multiple antennas by each user. The main advantages of the cooperative communication are summarized as follows:

- **High Spatial Diversity** Compared to the point-to-point transmis-

sion, cooperative communications can achieve higher transmission quality. Moreover, the physically separated antennas in a virtual network can better reduce the effect of the shadowing than fixed multiple-input multiple-output (MIMO) systems.

- **High Throughput** Higher throughput can be achieved through cooperation by adopting adaptive resource allocation techniques such as rate adaption and power allocation according to channel conditions.

- **Lower interference and Extended Coverage** Interference can be reduced if the cooperative network is deployed, together with some cognitive frequency management techniques. If the system is not interference-limited, the cooperation can extend the the network coverage without having to introduce cognitive frequency management.

- **Adaptability to Network Condition** According to the channel conditions and interference, the cooperative communication system can adaptively select different relays, change cooperation strategies, and allocate resources available for transmission in the network.

A simple three-nodes relay system model, shown in Fig. 2.8, is described as an example of the cooperative communication. During the time when the source node communicates directly with the destination node via the source-destination (S-D) channel, the broadcasted signals can be naturally overheard by the relay node via the source-relay (S-R) channel. The received signals at the relay are processed according to certain strategies, and then forwarded to the destination through relay-destination (R-D)

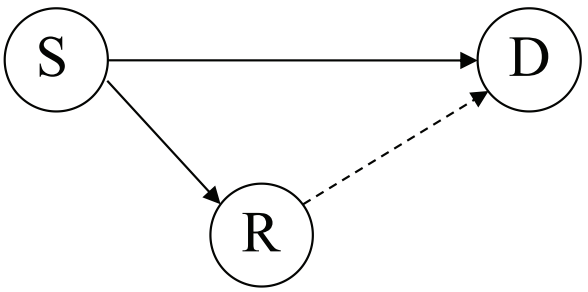

Figure 2.8: A simple three nodes one-way relay model.

channel during the next time slot. Finally, two copies of the original information will arrive at the destination node through the S-D and R-D channels, yielding the diversity gain.

The overheard signals at the relay node can be processed by different relay protocols before being forwarded to the destination. In this subsection, three popular relay strategies are introduced, as follows:

- **Amplify-and-Forward**
  The amplify-and-forward (AF) is one of the simplest relay protocols from the perspective of signal processing complexity. Basically, the relay node only scales the received signals and then directly re-transmit the amplified version to the destination. Finally, two copies of the signals coming from the source and the relay are combined at the destination for achieving spatial diversity. However, in AF, the CSI knowledge of S-R channel is needed in order to select the scaling factor [19] for optimal combining. It has to be noted that noise component will also be amplified in AF, and the final detection would become problematic if the quality of the S-R channel is low. In this dissertation, AF is out of the focus and will not be discussed further in detail.

- **Compressed-and-Forward**
  With the compressed-and-forward (CF) relay strategy, the received signal at the relay is quantized and compressed before being forwarded to the destination (this technique is also known as estimate-and-forward or quantize-and-forward). It is obvious that the received signals at the relay and the destination are correlated, since they are noisy versions of the same signals broadcasted from the source. Hence, the relay node can compress the received signals by utilizing the correlation and re-transmit them to the destination (source coding is applied with the side information from the destination, such as Wyner-Ziv coding) [20] [21].

- **Decode-and-Forward**
  The decode-and-forward (DF) strategy has been applied into most of the practical distributed coding systems because of its excellent performance [22]- [23]. In DF, the relay node performs decoding of the received signals in order to recover the original information sequences. After that, the recovered bits are re-encoded again and forwarded to the destination. Due to the imperfect S-R channel, the decoded bit sequences at the relay may contain some errors, which

may cause significant performance loss if they are forwarded to the destination. Therefore, it is common that the relay only forwards the correctly decoded sequences, which is referred to as the selective DF (S-DF). Nowadays, the DF is widely implemented in practical systems [24] with powerful coding schemes, such as Turbo codes [22] [25] and/or low density parity check (LDPC) codes [26] [23]to avoid such scenario.

2.5 Distributed Source Coding

With traditional centralized source coding strategy, the redundancy of the source information is compressed by a single encoder or multiple-encoders that work jointly. However, due to many limitations such as physical separation of the nodes and network topology, the cooperation between different encoders is not always feasible, which has led to the research direction to the distributed source coding technique (DSC). The DSC deals with correlated source information compression at separated nodes which do not communicate with each other. The theoretical lossless compression bound of two separated sources was first proposed in [27] by David Slepian and Jack Keil Wolf in 1973. It has been proven that, as long as the joint decoder at the receiver side can fully exploit the knowledge of the source correlation, DSC can achieve the same compression rate as an optimal single encoder that jointly encode the source.

The concept of DSC can be well implemented into relay system where the source and relay are regarded as separated transmitting nodes. For instance, with the DF scheme, the re-constructed information sequence to be forwarded to the destination from the relay is highly correlated with the original data sequence sent from the source node, even though some errors may be contained in the re-constructed sequence due to the imperfect S-R channel. At the destination side, both signals transmitted from the source and the relay are processed by one joint decoder, where the correlation knowledge is exploited to improve the system performance. The practical applications of this mechanism, such as distributed Turbo code and distributed LDPC code can be seen in [25], [6] and [26].

2.6 Summary

In this chapter, some conceptional bases are briefly reviewed, such as AWGN and Rayleigh channel models, AWGN channel capacity and out-

age probabilities. Moreover, the Turbo principles, BICM techniques and cooperative communication structures are introduced, as well as the distributed source coding. The preliminary studies will be used in the main part of this dissertation.

Chapter 3

DACC-Assisted Relay System with BICM-ID Allowing Intra-link Errors

Cooperative communication systems, especially the classical relaying techniques, have been well studied in the past decades. In the conventional S-DF assumption, if the relay can not perfectly recover the received bit sequence, it will stop forwarding the sequence to the destination to avoid error propagation. In [6], the author proposed a very simple doped accumulator (DACC) assisted relay model allowing S-R link (intra-link) errors with BPSK modulation. This system enables the relay to always forward the re-constructed bit sequences, regardless of it contains errors or not.

In this chapter, we propose an extended work of [6] for higher order modulations with the BICM-ID technique. First of all, the relay system structure is presented, and the three location scenarios as well. We provide the transmission strategies and coding/decoding algorithms of the proposed system in detail. Convergence behavior analysis using the EXIT charts is also provided. The system performances in terms of BER and frame-error-rate (FER) are then evaluated through simulations over AWGN and block Rayleigh fading channels. In addition, the influences of different relay locations are also studied. Finally, it is shown that by assuming error free transmission for the intra-link, the proposed relay topology is logically equivalent to an automatic repeat request (ARQ) scheme. The throughput performance of the ARQ technique is also evaluated in this chapter.

3.1 System Model

In this section, a very simple wireless one-way relay system is proposed, which consists of three basic components, a source node, a relay node and a destination node. Transmission protocols of the proposed relay system is described as follows. During the first time slot, the original information bit sequence $\mathbf{b}_1$ is broadcasted to both the relay and the destination nodes. At the relay, the original information sequence is first re-constructed by either performing channel decoding or only extracting the systematic part of the coded bits. In the second time slot, the re-constructed bit sequence $\mathbf{b}_2$, which may contain some errors, is interleaved, re-encoded and forwarded to the destination node.

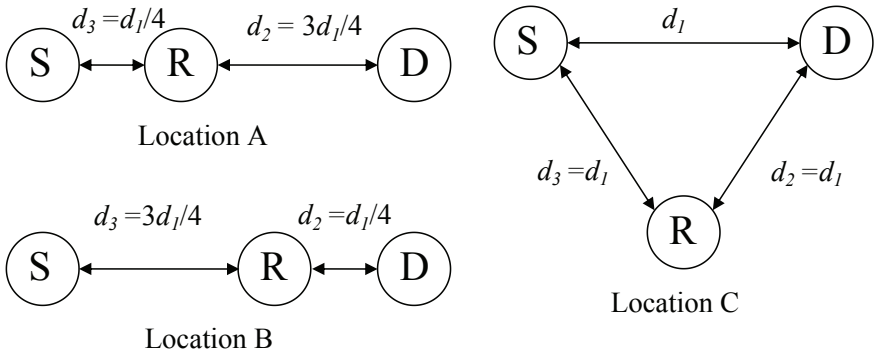

Figure 3.1: System model with different relay location scenarios. d_1 denotes the distance of the direct S-D channel.

Three relay location scenarios are considered in this chapter, as shown in Fig. 3.1. Generally, we can allocate the relay node closer to the source node (Location A) or closer to the destination (Location B), or the three components to keep the same distance from each other (Location C). In this dissertation, the subscripts $\bullet_1$, $\bullet_2$, and $\bullet_3$ are used to indicate the S-D, R-D and S-R channels, respectively. The geometric gain of the S-R channel with regard to the S-D channel can be defined as [28]

$$G_3 = \left(\frac{d_1}{d_3}\right)^{\alpha}, \tag{3.1}$$

where the path-loss exponent α is assumed to be 3.52 [29] in the simulations presented in Section 3.4. It is straightforward to derive the geometric gain of the R-D channel G_2 in the same way. Moreover, without

loss of generality, the geometric gain of the S-D channel, G_1, is fixed to one. Therefore, the received signals $\mathbf{y}_i$ (i=1, 2, 3) at the relay and the destination node can be expressed as:

$$\mathbf{y}_1 = \sqrt{G_1} \cdot h_1 \cdot \mathbf{s}_1 + \mathbf{n}_1, \tag{3.2}$$

$$\mathbf{y}_2 = \sqrt{G_2} \cdot h_2 \cdot \mathbf{s}_2 + \mathbf{n}_2, \tag{3.3}$$

$$\mathbf{y}_3 = \sqrt{G_3} \cdot h_3 \cdot \mathbf{s}_1 + \mathbf{n}_3, \tag{3.4}$$

where $\mathbf{s}_1$ and $\mathbf{s}_2$ represent the signal vectors transmitted from the source and the relay, respectively. $\mathbf{n}_i$ represents the zero-mean AWGN noise vector of the three channels with the variance σ_n^2 per dimension. The fading channel gain, h_i, is assumed to be one in the AWGN channel, and thereby the instantaneous received SNR is determined by the noise variation σ_n^2 and the geometric gains G_i. However, in fading channels, h_i becomes time-varying. The average received SNRs via different channels for each location scenario are evaluated as follows: given the path-loss parameter α equal to 3.52 [29], we have $\Gamma_3 = \Gamma_1 + 21.19$ and $\Gamma_2 = \Gamma_1 + 4.4$ in Location A; $\Gamma_3 = \Gamma_1 + 4.4$ and $\Gamma_2 = \Gamma_1 + 21.19$ in Location B; $\Gamma_1 = \Gamma_2 = \Gamma_3$ in Location C, where the unit is in dB.

3.2 Decoding Schemes

The block diagram of the proposed relay transmission system is shown in Fig. 3.2. In this system, since the relay does not aim to perfectly eliminate the intra-link errors, we do not need strong codes: only memory-1 half rate ($R_c = 1/2$) systematic non-recursive convolutional code (SNRCC) with generator polynomial $(3,2)_8$ is adopted for both encoders C_1 and C_2. At the source node, the original information sequence $\mathbf{b}_1$ is first encoded by C_1. Then, the encoded bit sequences are interleaved by a random interleaver Π_1 and doped-accumulated by a DACC (with a doping rate P_{d1}). Then, the outputs of DACC are mapped onto symbols $\mathbf{s}_1$ according to the specified BICM method, and broadcasted to both the relay and the destination nodes during the first time slot.

According to our proposed relay strategy, the broadcasted signal arrived at the relay node is first fed to the demapper, followed by the decoder DACC^{-1} of DACC. The *extrinsic* LLR output from DACC^{-1} is fed to the de-interleaver Π_1^{-1}. One of the choices is that, the relay aims to recover the original information bit sequence $\mathbf{b}_1$ by performing fully iterative decoding/detection between demapper-plus-DACC^{-1} and the decoder D_1 of C_1, and make hard decisions on the output of the decoder. However, instead

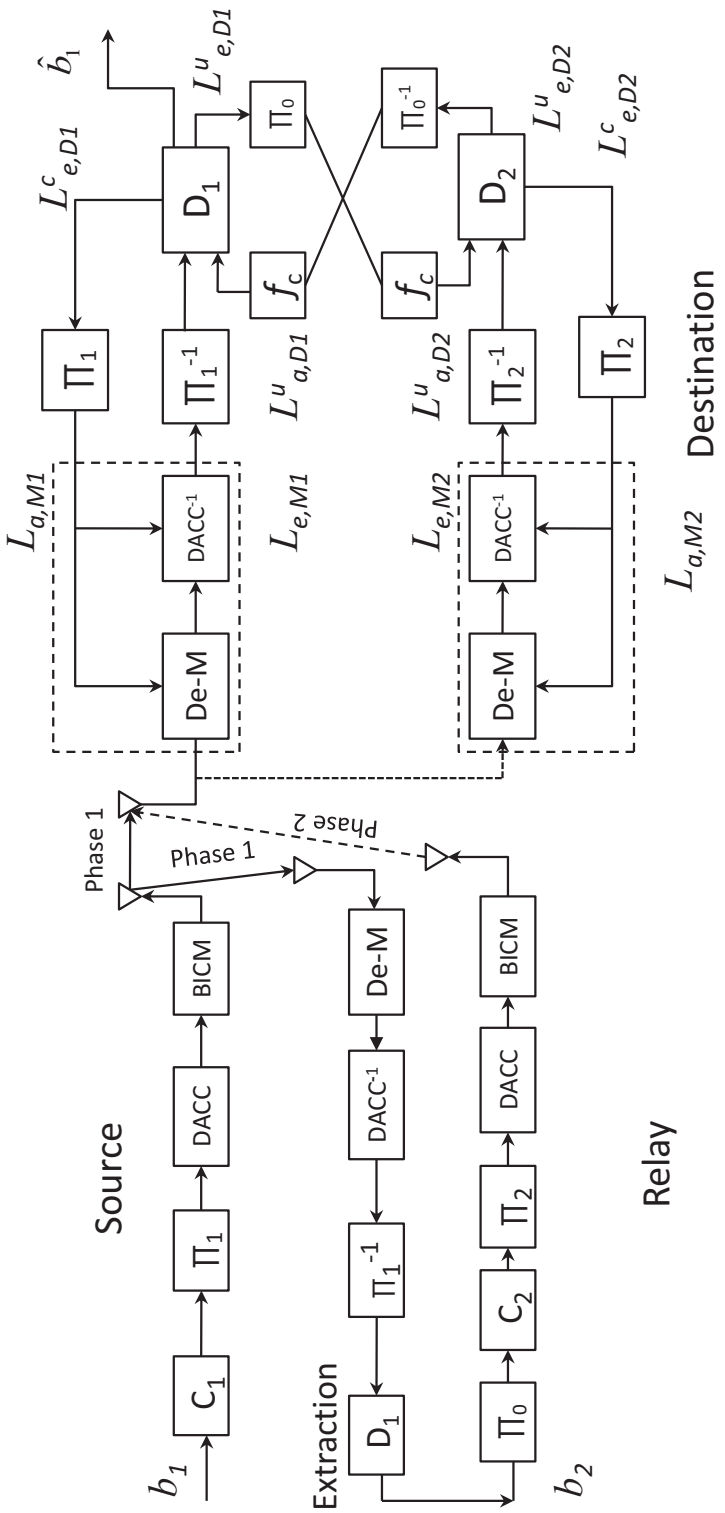

Figure 3.2: Structure of the proposed Slepian-Wolf relay system.

of performing the fully iterative decoding/detection between demapper-plus-DACC^{-1} and D_1, only one round of Viterbi decoding (referred to as one-round-Viterbi DF in the following sections) or even only extracting the systematic bits (referred to as EF) may result in similar performance at the destination. With this technique, we can significantly reduce the complexity due to performing iteratively the Bahl, Cocke, Jelinek and Raviv (BCJR) algorithm for *a posteriori* decoding of DACC and channel code C_1.

With our technique, the sequence $\mathbf{b}_2$ that may contain some errors is still allowed to be forwarded to the destination, which eliminates the error-free transmission requirement over the intra-link. In this case, the complexity of the relay can be further reduced. After that, the recovered bit sequence $\mathbf{b}_2$ is again random interleaved by Π_0, channel encoded by C_2, interleaved by a random interleaver Π_2 and fed to DACC (with doping ratio P_{d2}). The purpose of the use of Π_0 is such that the interleaved sequence $\Pi_0(\mathbf{b}_2)$ is made statistically independent of $\mathbf{b}_1$. Finally, the bit sequence is mapped into $\mathbf{s}_2$, and transmitted to the destination during the second time slot.

At the destination, detection processes for the signals $\mathbf{y}_1$ and $\mathbf{y}_2$ received during the first and second time slots, respectively, are first performed independently as shown in Fig. 3.2. At this stage, fully iterative docoding/detection is adopted between demapper-plus-DACC^{-1} and D_i, which is referred to as horizontal iterations (HIs) [6]. After each round of HI, the *extrinsic* systematic LLRs obtained from the two decoders D_1 and D_2 are further exchanged between them, of which process is referred to as vertical iterations (VIs), where the *extrinsic* systematic LLR is updated by the function f_c as detailed in sub-section 3.2.3. By utilizing the function f_c, the *extrinsic* systematic LLRs, forwarded by the relay, help the decoder eliminate the errors in the original bit sequence $\mathbf{b}_1$ by exploiting the correlation knowledge between the source and the relay. Finally, the detection of $\mathbf{b}_1$ can be completed by making hard decisions of the *a posteriori* LLRs of the uncoded (systematic) bits outputs from D_1.

3.2.1 Doped Accumulator

The doped accumulator has the same structure as the memory-1 half rate systematic recursive convolutional code (SRCC), as shown in Fig. 3.3.

The output of DACC is a mixture of systematic (input) bits and the coded bits, where only every P_d-th (P_d is referred to as the doping ratio)

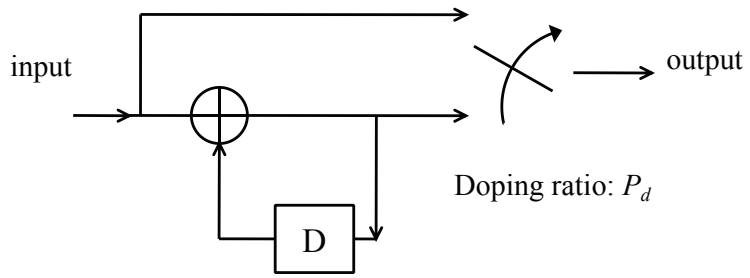

Figure 3.3: System model of Memory-1 doped accumulator.

.

of the systematic bits is replaced by the corresponding coded one, and the process is terminated within each frame. For instance, let a short sequence $s_1s_2s_3s_4s_5s_6$ be the input of DACC and $c_1c_2c_3c_4c_5c_6$ denote the coded sequence accordingly. If P_d is set at 2, the final output of DACC will be $s_1a_2s_3a_4s_5a_6$. It should be noted that DACC itself does not change the overall code rate because the rate of DACC is one. The purpose of using DACC is to reshape the EXIT curve of the demapper and keep the convergence tunnel open.

3.2.2 BICM-ID Demapper

As stated in Section 2.3, further improvement of decoding performance can be expected using the BICM-ID technique with the help of *a priori* LLR fed back from the decoder [30] over BICM. Also, as described in Section 2.3, non-Gray mapping, rather than Gray mapping, should achieve better performance of BICM-ID. The *extrinsic* LLRs of *v-th* bit of symbol **s** after the demapper can be expressed as [31]

$$\begin{aligned} L_e\left(s_v\right) &= \ln \frac{\mathrm{P_r}\left(s_v = 1 \mid y\right)}{\mathrm{P_r}\left(s_v = 0 \mid y\right)} \\ &= \ln \frac{\sum_{s \epsilon S_1} \left\{ \exp\left\{ -\frac{|y - h_i s|^2}{2\sigma_n^2} \right\} \prod_{w \neq v}^{M} \exp\left(s_w L_a\left(s_w\right)\right) \right\}}{\sum_{s \epsilon S_0} \left\{ \exp\left\{ -\frac{|y - h_i s|^2}{2\sigma_n^2} \right\} \prod_{w \neq v}^{M} \exp\left(s_w L_a\left(s_w\right)\right) \right\}}, \end{aligned} \tag{3.5}$$

where S_1 (S_0) denote the sets of mapping pattern having the *v-th* bit being one (zero), respectively. M represents the number of the bits per symbol and $L_a(s_w)$ represents the LLRs fed back from the decoder corresponding to the bit in the *w-th* position of the patterns. The output *extrinsic* LLRs of the demapper are then forwarded to the decoder DACC^{-1} of DACC.

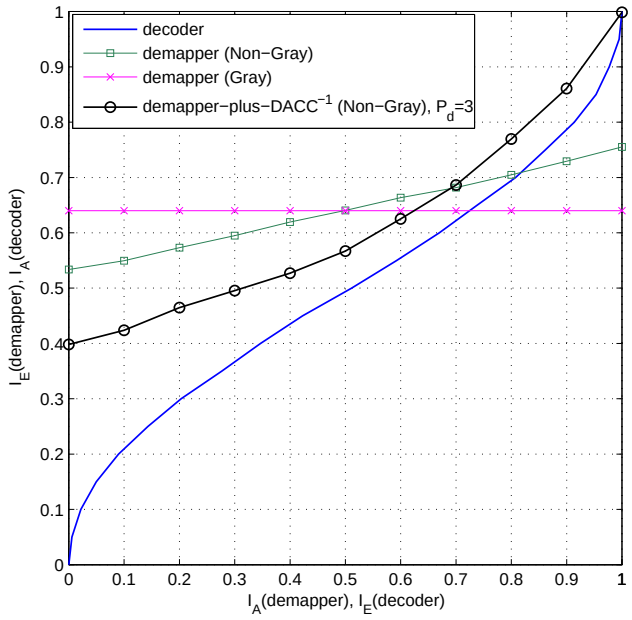

Figure 3.4: EXIT chart of the BICM-ID demapper, SNR = 2 dB.

Comparisons of the EXIT curves are shown in Fig. 3.4 between Gray mapping and non-Gray mapping using QPSK, assuming the SNR of the direct transmission being 2 dB. It is found that with Gray mapping, the EXIT curve is entirely flat regardless of the *a priori* information, which means that the feedback from the decoder does not help the demapper improve performance through the iterative process. By using non-Gray mapping, obviously, the righthand side of the EXIT curve rises up as the given *a priori* information increases, but still it can not achieve (1,1) mutual information point. However, the EXIT curve of demapper-plus-DACC^{-1} changes the shape of its EXIT curve and it finally reaches a point very close to the (1,1) mutual information point, which can be well matched with the EXIT curve of the decoder of convolutional codes. Therefore, the error floor is completely avoided (or at least reduced to a very small level) by this technique.

3.2.3 LLR Updating Function

As described above, our technique can improve the performance of the distributed relay system by utilizing the correlation knowledge between the source and the relay. The recovered information bits at the relay node may contain some errors, but they are still correlated with the original information. The correlation value is denoted by the error probability p_e of the intra-link, which can be estimated by using the *a posteriori* LLRs of the uncoded (systematic) bits, $L^u_{p,D1}$ and $L^u_{p,D2}$ [1] output from the two decoders D_1 and D_2, as [6]:

$$\tilde{p_e} = \frac{1}{N}\sum_{n=1}^{N} \frac{e^{L^u_{p,D_1}} + e^{L^u_{p,D_2}}}{\left(1+e^{L^u_{p,D_1}}\right)\left(1+e^{L^u_{p,D_2}}\right)}, \tag{3.6}$$

where N denotes the number of the *a posteriori* LLR pairs from the two decoders with sufficient reliability. Specifically, only the LLRs with their absolute values greater than a given threshold can be chosen. The threshold is set at 1 in our simulations, due to that the memory-1 code in our system is not strong [6].

With the error probability p_e, we can straightforwardly derive (3.7) [32] as follows:

$$\begin{aligned} \mathrm{P_r}(b_2 = 0) &= (1-p_e)\mathrm{P_r}(b_1 = 0) + p_e\mathrm{P_r}(b_1 = 1), \\ \mathrm{P_r}(b_2 = 1) &= (1-p_e)\mathrm{P_r}(b_1 = 1) + p_e\mathrm{P_r}(b_1 = 0). \end{aligned} \tag{3.7}$$

Based on the relationship in (3.7), the two decoders D_1 and D_2 exchange the LLRs updated by exploiting p_e, through the LLR updating function f_c [33], which can be defined as follows:

$$f_c(x) = \ln \frac{(1-p_e)\cdot \exp(x) + p_e}{(1-p_e) + p_e \cdot \exp(x)}, \tag{3.8}$$

where the input value x represents the interleaved and/or de-interleaved *extrinsic* LLRs of the uncoded bits, L^u_{e,D_1} and L^u_{e,D_2}, output from the two decoders D_1 and D_2, respectively. The outputs of f_c are the updated LLRs by exploiting p_e as the correlation knowledge of the intra-link. Specifically, the *extrinsic* information of one decoder is fed to the other one as the *a*

[1] In the dissertation, L^u_* and L^c_* denote LLRs of uncoded and coded bits, respectively, while L^*_{a,D_i}, L^*_{p,D_i} and L^*_{e,D_i} represent the *a priori*, *a posteriori* and extrinsic LLRs of channel decoder D_i, respectively.

priori information, and the VI operations at the destination node can be expressed as:

$$L^u_{a,D_1} = f_c\left\{\Pi_0^{-1}\left(L^u_{e,D_2}\right)\right\}, \tag{3.9}$$

$$L^u_{a,D_2} = f_c\left\{\Pi_0\left(L^u_{e,D_1}\right)\right\}. \tag{3.10}$$

3.3 EXIT Chart and Convergence Analysis

The three-dimensional (3D) EXIT analysis is provided in this section to evaluate the convergence behavior of the proposed relay system [33]. In this dissertation, we only focus on the decoder D_1 because the final target of the relay system is to successfully retrieve the original information bit sequence $\mathbf{b}_1$. As shown in Fig. 3.2, the *a priori* LLRs of the uncoded bits L^u_{a,D_1} (the updated version of L^u_{e,D_2}) and the coded bits L^c_{a,D_1} are exploited in D_1. Hence,

$$I^c_{e,D_1} = T^c_{D_1}(L^c_{a,D_1}, L^u_{e,D_2}, p_e), \tag{3.11}$$

where I^c_{e,D_1} denotes the *extrinsic* mutual information between the *extrinsic* LLR output L^c_{e,D_1} of D_1, and the channel-coded bits by C_1. L^u_{e,D_2} denotes *extrinsic* LLR of the uncoded bits, output from D_2, and it is fed to D_1 as its *a priori* information L^u_{a,D_1} with which the correlation knowledge can well be utilized at the destination.

The 3D EXIT chart can be used to examine the influence of the source-relay correlation. Fig. 3.5 shows that when the intra-link error probability p_e is small ($p_e = 0.02$), indicating that the source and relay are highly correlated, I^u_{e,D_2} has a significant influence on $T^c_{D_1}(\cdot)$. However, when p_e is large ($p_e = 0.25$), I^c_{e,D_1} does not increases much even when I^u_{e,D_2} becomes large, which can be clearly seen in Fig. 3.6. In other words, with small p_e values, the impact of D_2 has to be deeply examined since the decoder D_2 can provides significant help when the source and relay are highly correlated. When p_e approximates 0.5, the EXIT analysis for the decoder D_1 reduces to the two-dimensional case, since the effect of L^u_{e,D_2} tends to be negligible.

The convergency behaviors of the proposed relay system are presented in Figs. 3.7 to 3.10 for Locations B and C, with modulation schemes of QPSK and 8PSK. We plot *extrinsic* mutual information of the output of the decoder D_1, which is equivalent to the *a priori* mutual information of the input of demapper-plus-DACC^{-1} in 3D EXIT charts. The trajectories of the mutual information were obtained through simulations, by measuring the exchange of the LLRs between D_1 and the demapper-plus-DACC^{-1}, and the results are also plotted in Figs. 3.7 to 3.10. It is found

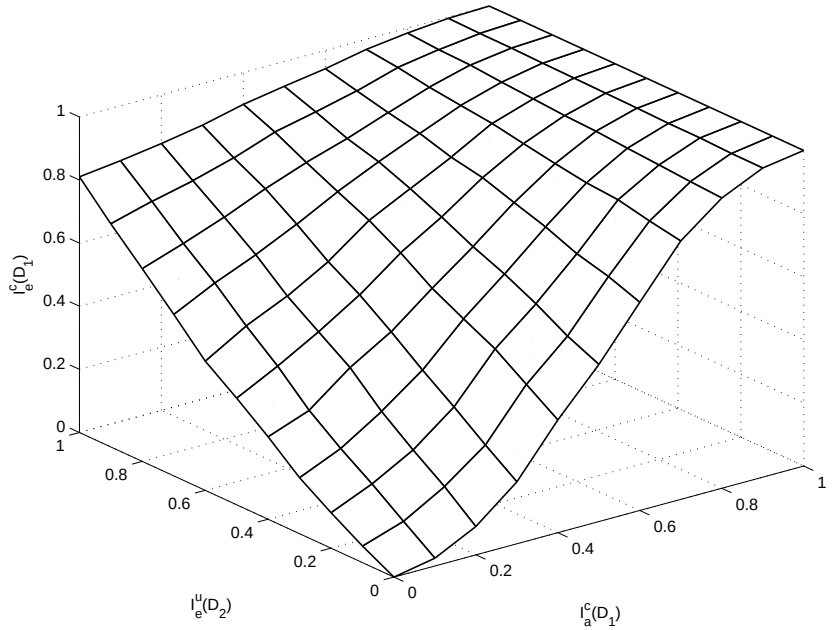

Figure 3.5: 3D EXIT chart, $p_e = 0.02$, Γ_1 = -4.5 dB, Location A, QPSK.

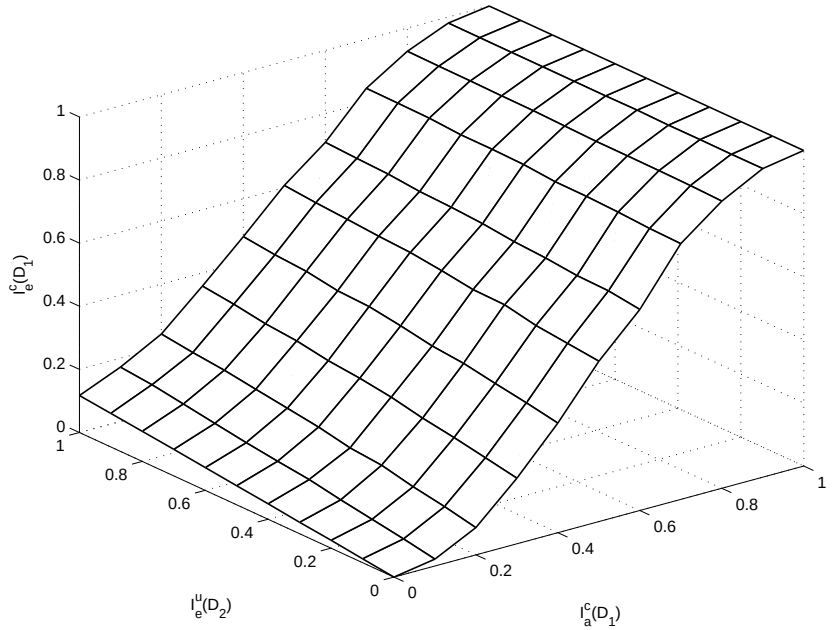

Figure 3.6: 3D EXIT chart, $p_e = 0.25$, Γ_1 = -4.5 dB, Location A, QPSK.

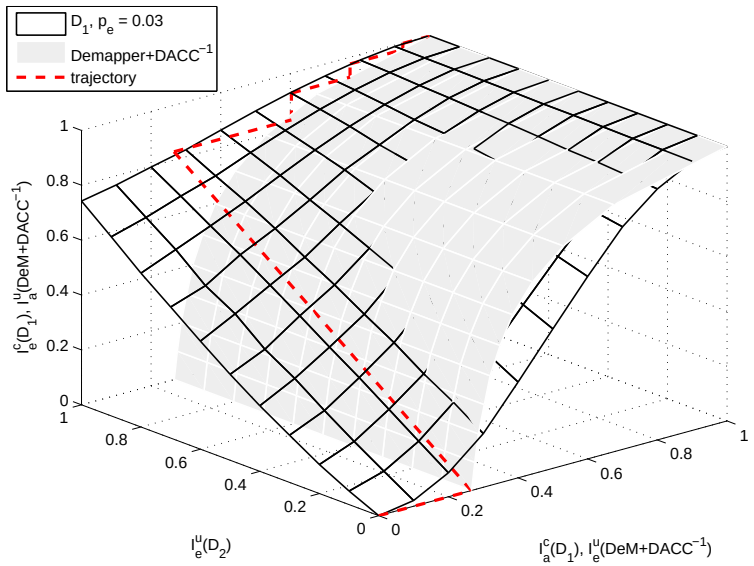

Figure 3.7: 3D EXIT chart and trajectory of the proposed system, Location B, QPSK, Γ_1 = -0.5 dB.

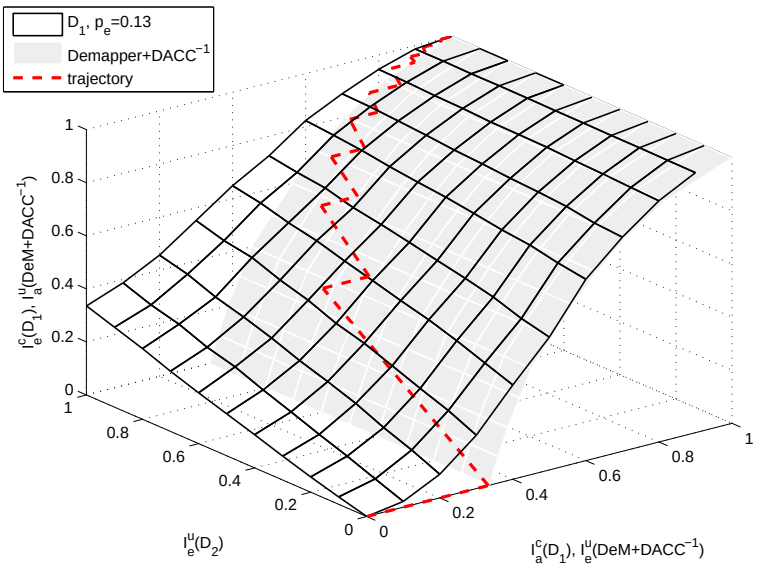

Figure 3.8: 3D EXIT chart and trajectory of the proposed system, Location C, QPSK, Γ_1 = 1.2 dB.

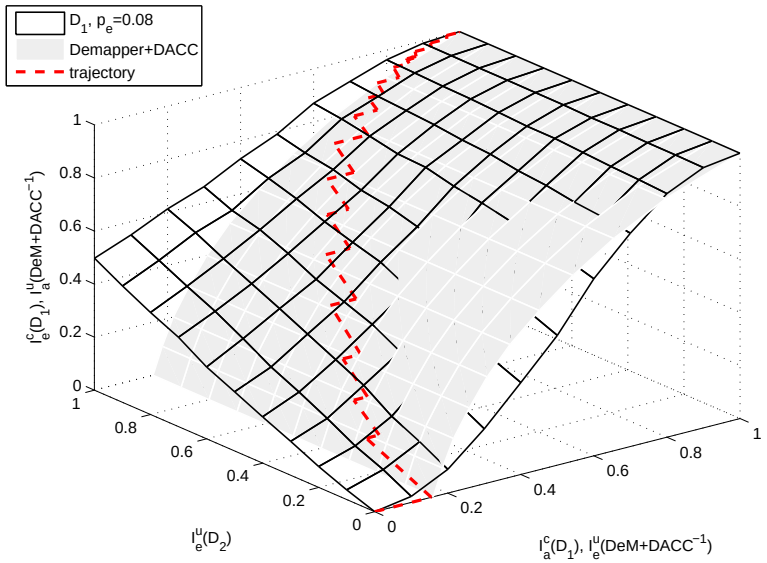

Figure 3.9: 3D EXIT chart and trajectory of the proposed system, Location B, 8PSK, $\Gamma_1 = 2.9$ dB.

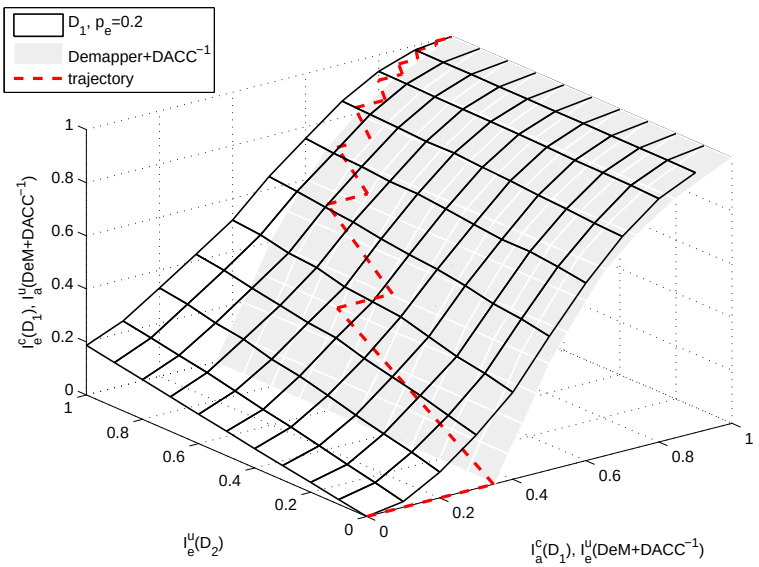

Figure 3.10: 3D EXIT chart and trajectory of the proposed system, Location C, 8PSK, $\Gamma_1 = 4.5$ dB.

that with our technique, if the SNR values are larger than the threshold at which the two EXIT surfaces open, the trajectory goes between the two surfaces and can finally reach a point very close to the (1,1,1) mutual information point. Based on the 3D EXIT chart analysis, the average SNR of S-D channel Γ_1 required for keeping convergence tunnel opening in the Locations A, B and C are around -4.6 dB, -0.5 dB and 1.2 dB for QPSK, and -2.4 dB, 2.9 dB and 4.5 dB for 8PSK. It should be noticed that the doping ratio of DACC also has the significant impact on the EXIT behaviour. In this dissertation, the optimal doping ratios were found by a brute-force search (the gap between the two EXIT surfaces with all the possible doping ratio values were tested, and the best pairs of P_{d1} and P_{d2} yielding the smallest threshold), which are found to be $P_{d1} = P_{d2} = 5$, 5, 3 for QPSK and = 4, 2, 8 for 8PSK, in scenarios A, B and C, respectively.

3.4 Simulation Results

Figs. 3.12 and 3.13 show results of the simulations conducted to evalute the BER performances of the proposed relay system with QPSK and 8PSK modulations in AWGN channels, respectively, where the frame length of the transmitted information was set at 10000 bits. Based on the EXIT analysis, 30 horizontal iterations were performed at the destination node and meanwhile 5 vertical iterations took place between the two decoders D_1 and D_2 during each horizontal iteration, totalling 150 iterations.

It is clearly seen that Turbo cliff can be achieved in our proposed relay system over AWGN channels. Fig. 3.12 shows that when performing the channel decoding at the relay node using QPSK modulation, the BER performance in Location A is much better than that of the other cases. However, the Location C scenario has the worst BER performance, due to the fact that no geometric gain is achieved when the three nodes are equally separated, compared to the other two scenarios. Actually, the BER performance of the whole system is affected by both the S-D and the R-D channels. There will be an optimal point between the source and the relay yielding the lowest error rate, which will be discussed in Chapter 5.

Fig. 3.12 also presents the BER curves by using EF relay strategy, where only the systematic part of the coded bits are extracted at the relay, without performing channel decoding. According to Fig. 3.11, the intra-link BER performances with the EF scheme are shown to be worse than that with the one-round-Viterbi DF scheme (only one round Viterbi decoding takes place for the both DACC^{-1} and D_1 at the relay; no fully iterative decoding between them is performed, as stated in Section 3.2)

for both QPSK and 8PSK modulations. However, it can be clearly seen in Fig. 3.12 that the EF scheme can achieve very close BER performance as that with the one-round-Viterbi DF strategy using our proposed relay system, especially in Location A. The reason is that, when the relay node is approaching the source, intra-link becomes very strong and therefore both one-round-Viterbi DF and EF schemes can almost fully recover the original bit sequence at the relay. However, when relay is close to the destination node as in Location B, a certain gap appears between BER curves of the system with the one-round-Viterbi DF and EF schemes. The reason is because, for example, when Γ_1 is around 0 dB (Γ_2 becomes 4.4 dB), the intra-link BER difference between the one-round-Viterbi DF and EF schemes becomes larger, and still roughly around 1 dB BER difference remains at the destination. In the case of Location C, the BER gap between one-round-Viterbi DF and EF is much less than that of Location B. This is because in Location C, when the Γ_1 is around 1.2 dB ($\Gamma_2 = \Gamma_3$), one-round-Viterbi DF and EF schemes still achieve very similar intra-link BERs as shown in Fig. 3.11, and hence the difference does not have significant impact on the system performance as a whole. In this sense, the EF scheme also achieves good performance, while the relay complexity can be further reduced. Similarly, the BER performances for the 8PSK modulation scheme are presented in Fig. 3.13 in AWGN channels.

Finally, the FER performance in block Rayleigh fading channels using QPSK and 8PSK modulation schemes are shown in Fig. 3.14 and Fig. 3.15. The interleaver lengths are set at 2400 bits for the both QPSK and 8PSK cases. The doping ratios of the DACCs are set at the same as in the AWGN channel's cases for Locations A, B and C. Comparisons are provided between our proposed Slepian-Wolf relay system and the conventional S-DF scheme. For the S-DF scheme, only the error-free re-constructed data sequences are forwarded from the relay to the destination. The FER performances can be seen in Fig. 3.14, where the point-to-point transmission with the same transmission parameters are also shown for comparison. Clearly, in Location B and Location C, there are around 1-2 dB gains with our proposed system over the S-DF system. However, this improvement becomes very small in Location A. The reason is that, when relay is very close to the source as in Location A, the intra-link error probability becomes almost 0 due to the large geometric gain, and therefore almost all the re-constructed sequences have no errors, and hence are forwarded to the destination with S-DF, which is almost equivalent to our proposed Slepian-Wolf relay system.

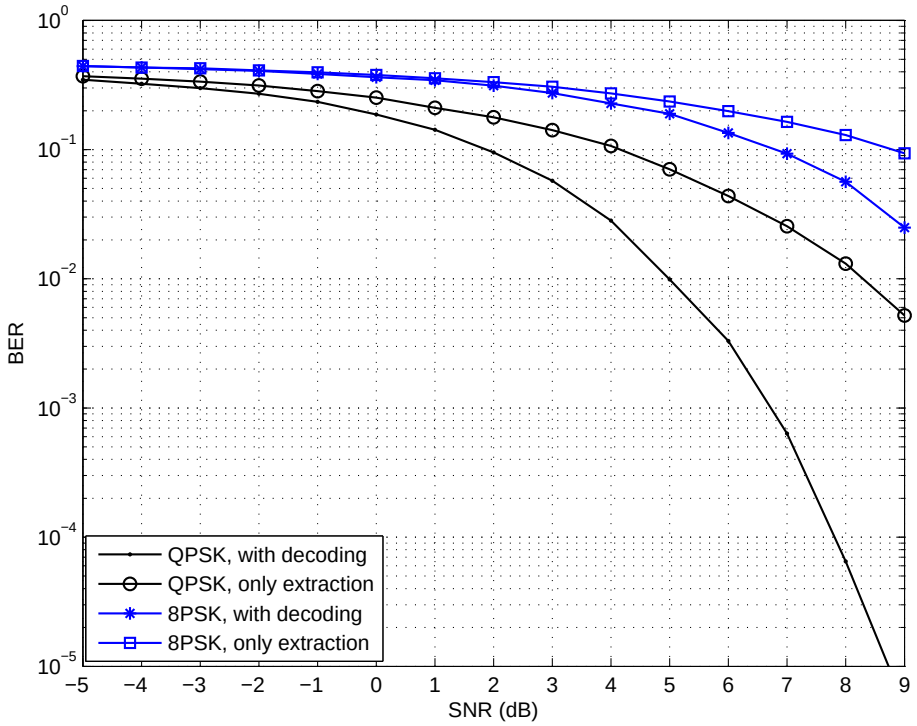

Figure 3.11: Comparison of intra-link BER performance between the case with channel decoding and that only extracts the systematic part.

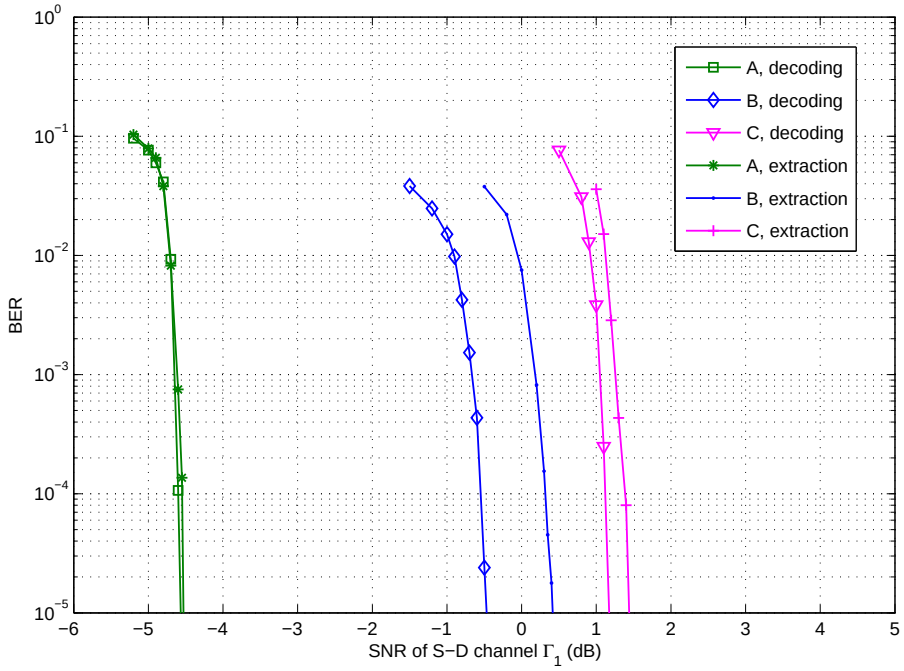

Figure 3.12: BER performances of the proposed system, QPSK.

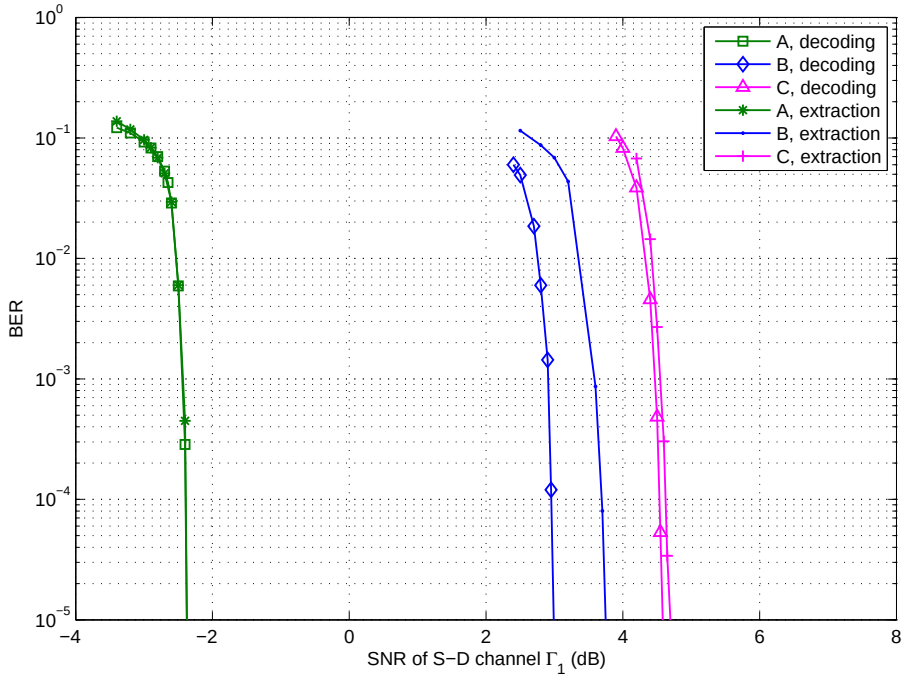

Figure 3.13: BER performances of the proposed system, 8PSK.

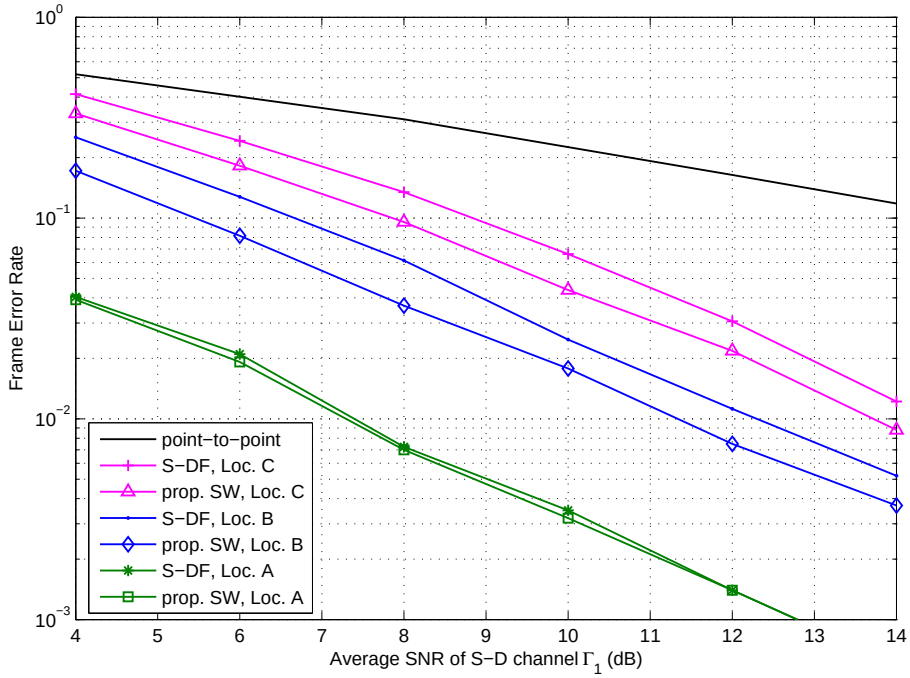

Figure 3.14: FER performances of the proposed system compared with S-DF scheme, QPSK.

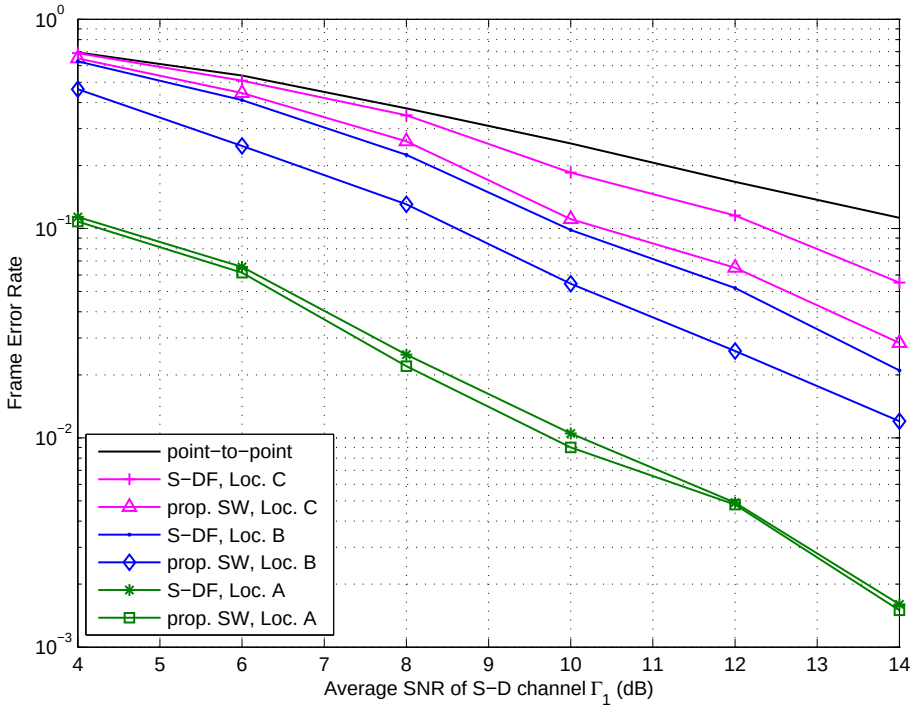

Figure 3.15: FER performances of the proposed system compared with S-DF scheme, 8PSK.

3.5 Relationship to ARQ Technique

If the intra-link of our propsed relay system is assumed to be error free, it is logically equivalent to a simple Automatic Repeat Request (ARQ) scheme, where the R-D channel corresponds to the re-transmission: no LLR updating by the f_c function is needed because $p_e = 0$ in this case. If the transmitter is acknowledged, indicating that the frame is correctly detected, it continues to transmit the next data frame. However, if errors are detected in the current frame, re-transmission is invoked. Unlike the conventional ARQ scheme, with our proposed scheme, the frame to be re-transmitted is first input to a random interleaver before being re-transmitted, which is equivalent to the case when relay perfectly recovers the source bits and interleaves them before re-encoding. The FER for the first and second transmission are denoted by P_1 and P_2, respectively. Finally, if both transmissions fail, the receiver works exactly the same as our proposed relay system, where the two received frames are connected by VI and HI. Let the error probability of this stage be denoted by P_3. Obviously, $P_3 << P_1$ and $P_3 << P_2$. Assuming selective repeat ARQ, the average throughput T_{ave} is given by

$$\begin{aligned} T_{ave} &= R_c \left[(1 - P_1) + 0.5P_1 (1 - P_2) + 0.5P_1P_2 (1 - P_1P_2P_3)\right] \\ &= R_c \left[1 - 0.5P_1 (1 + P_2P_3)\right], \end{aligned} \tag{3.12}$$

where R_c denotes the per-transmission normalized spectrum efficiency of the transmission chain, including the channel coding rate and modulation multiplicity. QPSK is used as the modulation scheme and half rare convolutional code, specified in Section 3.2, is used, hence $R_c = 1$. 10000 frames were transmitted and the frame length was set at 4000. It can be seen in Fig. 3.16 that the FER curves of P_1 and P_2 are almost the same, because the first and second transmissions use the same transmission parameters. By performing HI and VI decoding processes, errors are significantly reduced, and hence the P_3 value is dramatically reduced. The average throughput curve of the system is presented in Fig. 3.17. It is found that when SNR is around -2.5 dB, the average throughput suddenly increases and exhibits again a flat shape, when -2.5<SNR<2 (dB). At this stage, errors are significantly reduced by utilizing the correlated frames received from the first and second transmissions. $T_{ave} = 0.5$ indicates the per-transmission normalized spectrum efficiency assumed in the simulation (=1) divided by the total transmission times (=2). After the SNR reaches 2 dB, the curve again rises, and with SNR$\geq$ 3 dB, $T_{ave} = 1$,

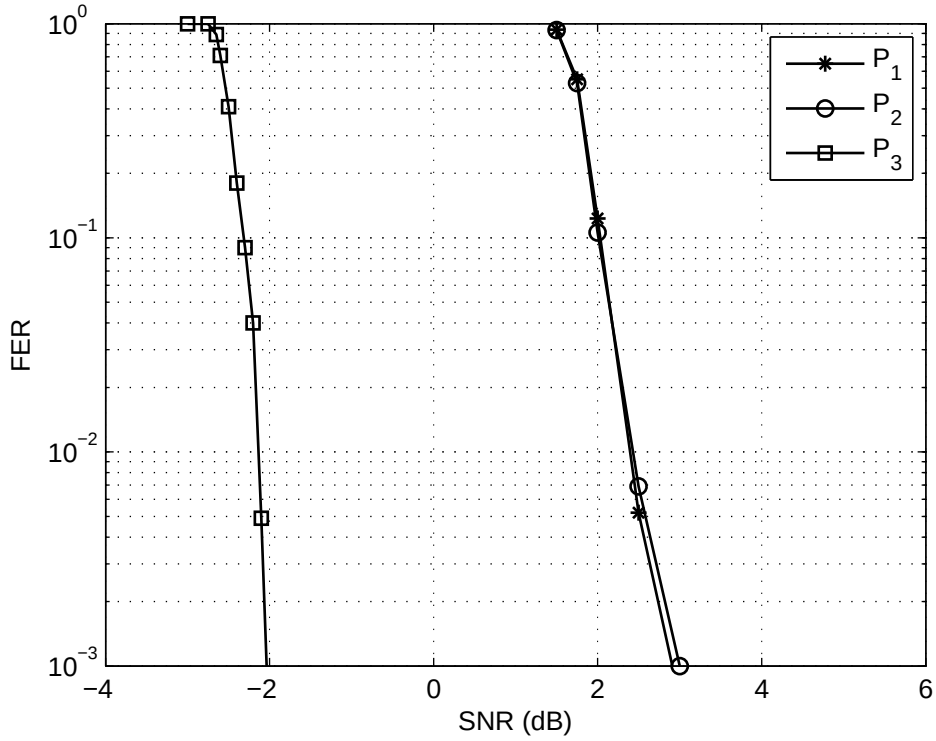

Figure 3.16: FER of the average throughput of the ARQ scheme using QPSK in AWGN channel.

which indicates that errors are all removed by decoding the received frame transmitted at the first transmission. Average throughput with the conventional ARQ that does not perform VI is also plotted in Fig. 3.17. It is found that with the conventional ARQ, the flat part of -2.5<SNR<2 (dB) diminishes.

3.6 Summary

The main objective of this chapter has been to propose a one-way relay system allowing intra-link errors with higher order modulations, in order to achieve higher spectrum efficiency.

First of all, a simple relay system model was proposed for the cooperative transmission over AWGN and block fading channels, which combines the BICM-ID technique with higher order modulation. The novelty of the proposed structure lies in the fact that the relay allows intra-link er-

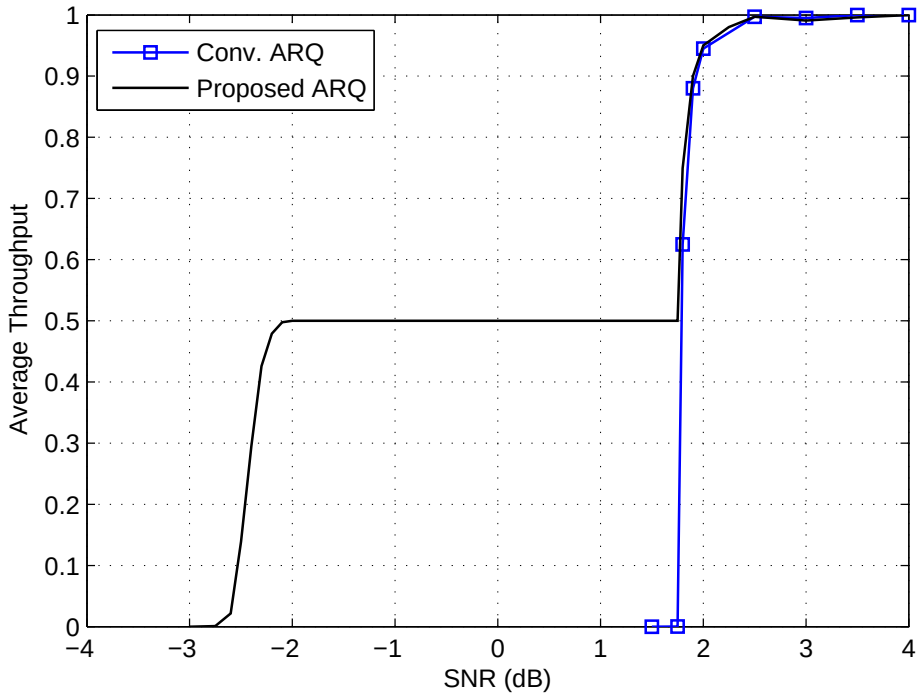

Figure 3.17: The average throughput of the ARQ scheme using QPSK in AWGN channel.

rors, remaining in the re-constructed information bit sequence. Instead of discarding the frame containing some errors after re-construction, which is the case of the conventional S-DF scheme, the frame containing errors are interleaved, re-encoded, and forwarded to the destination. The intra-link error probability is utilized as the correlation knowledge between the information sequence transmitted from the source and relay nodes. The correlation can be estimated and exploited at the destination via vertical iterations between the two decoders. It has been shown in the 3D EXIT charts that, the EXIT surface of demapper-plus-DACC^{-1} exhibits excellent matching with that of a memory-1 systematic convolutional code with the help of vertical iterations.

The proposed system does not require heavy decoding process at the relay, since only one-round-Viterbi-DF, is performed for DACC^{-1} and D_1. To further reduce the complexity of the relay, even simply extracting the systematic part of the coded bits recovered by the DACC^{-1} without performing channel decoding, EF, does not lead to significant performance loss at the destination. It is found from the BER simulation results that

very similar performances can be achieved with the two decoding techniques at the relay described above, especially in Location A and Location C. This observation implies the superiority of the correlation exploiting method used in the proposed system. Thereby, excellent BER performances can be achieved without requiring high computational complexity at the relay.

Finally, the relationship between the proposed relay system and an ARQ technique was set up based on the relay system described in this chapter. In contrast with conventional ARQ strategies, the re-transmitted information bit sequence has to be interleaved before being encoded. The advantages of the proposed ARQ structure over the conventional ARQ that does not perform VI have been shown in terms of the throughput efficiency.

Chapter 4

Theoretical Outage Probability Analysis of Slepian-Wolf Relay System

In the previous chapter, we analyzed the performance of a Slepian-Wolf relay system exploiting correlation knowledge between source and relay. However, no theoretical bound has been provided so far. The primary goal of this chapter is to derive the theoretical outage probability of the correlated source transmission system based on a distributed coding technique over block Rayleigh fading channels. As mentioned above, throughout this dissertation, a simple one-way relay system is considered in the framework of two correlated source transmission.

First of all, the Slepian-Wolf theorem is introduced in detail as our theoretical framework. Two cases of the relay system model are considered in this chapter: in Case 1, the intra-link error is modeled by a bit-flipping method and the error probability p_e is assumed to be constant; in Case 2 the intra-link is also assumed to suffer from block Rayleigh fading and p_e is assumed to be represented by the Hamming distortion, where the rate distortion function is used to describe the p_e value, given the instantaneous SNR of the intra-link. We define the theoretical outage probability of the proposed systems over block Rayleigh fading channels in both the two cases, based on the Slepian-Wolf theorem. Then, the mathematical expressions of the outage probabilities are derived as the main part of this chapter. Moreover, the asymptotic properties of the outage curves in Case 1 are mathematically proven, which are shown to be consistent with simulation results, for the practical system investigated in the previous chapter. The impact of the relay location on outage performance is

not theoretically investigated, because in practice, p_e depends on the relay location, however, in Case 1, it is used as a parameter indicating the intra-link error probability. The relay location is taken into account only in the simulations conducted to verify the consistency between the theoretical outage and FER performance results. In Case 2, the theoretical outage performances are presented considering the impact of different relay location scenarios. This is made possible because p_e is obtained theoretically as a function of the instantaneous SNR of the intra-link.

4.1 Slepian-Wolf Theorem

Slepian-Wolf theorem is well known when dealing with lossless compression of correlated sources with high efficiency. In the example of a distributed source coding model shown in Fig. 4.1, the physically isolated data sequences $\mathbf{b}_1$ and $\mathbf{b}_2$ are separately compressed by their own single encoders. At the receiver side, the two correlated data streams (with their rate after compression being R_1 and R_2, respectively) are jointly decoded by a single decoder. According to the contribution made by David Slepian and Jack K. Wolf in [27], it has been proven that by exploiting the correlation knowledge of data streams at the destination, the distributed source coding can achieve the same rate after compression as the optimum single encoder which compresses the sources jointly.

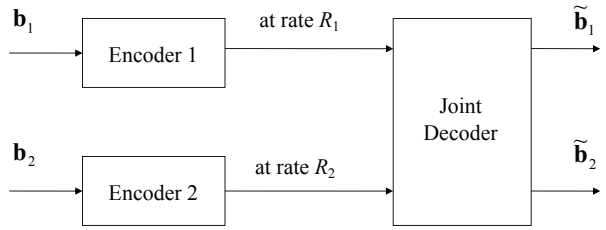

Figure 4.1: Block diagram of Slepian-Wolf coding.

According to the Slepian-Wolf theorem [27], if R_1 and R_2 satisfy the following three inequalities, the transmitted data can be recovered with arbitrary low error probability.

$$R_1 \geqslant H(\mathbf{b}_1 \mid \mathbf{b}_2), \tag{4.1}$$

$$R_2 \geqslant H(\mathbf{b}_2 \mid \mathbf{b}_1), \tag{4.2}$$

$$R_1 + R_2 \geqslant H(\mathbf{b}_1, \mathbf{b}_2), \tag{4.3}$$

where $H(\mathbf{b}_1 \mid \mathbf{b}_2)$ and $H(\mathbf{b}_2 \mid \mathbf{b}_1)$ denote the conditional entropy of $\mathbf{b}_1$ and $\mathbf{b}_2$, given the information of $\mathbf{b}_2$ and $\mathbf{b}_1$, respectively, and $H(\mathbf{b}_1, \mathbf{b}_2)$ denotes the joint entropy of the correlated information $\mathbf{b}_1$ and $\mathbf{b}_2$. The admissible rate region identified by this theorem is shown in Fig. 4.2. When the rate R_1 for transmitting the information stream $\mathbf{b}_1$ is equal to its entropy $H(\mathbf{b}_1)$, the rate R_2 for transmitting the information stream $\mathbf{b}_2$ can be less than its entropy $H(\mathbf{b}_2)$, but it has to be larger than the conditional entropy $H(\mathbf{b}_2 \mid \mathbf{b}_1)$, as indicated by the point X_1 in Fig. 4.2. Similarly, when $\mathbf{b}_2$ is transmitted at the rate $H(\mathbf{b}_2)$, then $\mathbf{b}_1$ can be transmitted at the rate which is less than $H(\mathbf{b}_1)$, but should be larger than $H(\mathbf{b}_1 \mid \mathbf{b}_2)$. Since the binary symmetric source model (Pr(1)=Pr(0)=0.5) is assumed in this dissertation, $H(\mathbf{b}_1) = H(\mathbf{b}_2) = 1$, $H(\mathbf{b}_1 \mid \mathbf{b}_2) = H(\mathbf{b}_2 \mid \mathbf{b}_1) = H(p_e)$, $H(\mathbf{b}_1, \mathbf{b}_2) = 1 + H(p_e)$ with $H(p_e) = -p_e \log_2(p_e) - (1 - p_e) \log_2(1 - p_e)$.

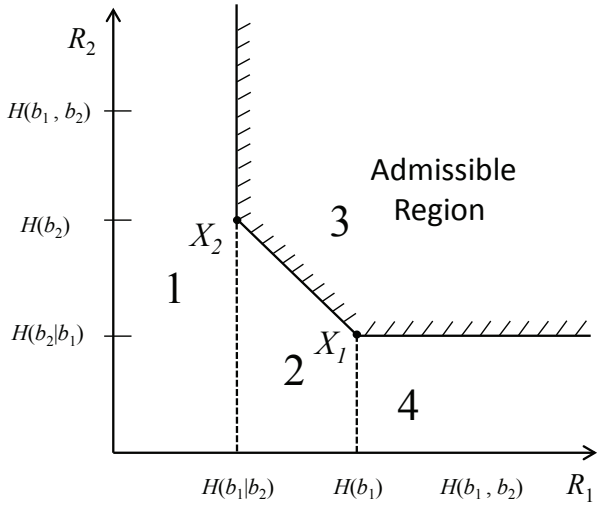

Figure 4.2: Admissible Slepian-Wolf rate region.

4.2 Case 1: Slepian-Wolf Relay with Parameterized Intra-link

4.2.1 System Model

The proposed one-way relay transmission model of Case 1, as shown in Fig. 4.3, is the same as the system described in Chapter 3, only with a difference that neither practical transmission chain nor its related parameters is considered. In practice, the value of p_e depends on many

parameters, related to the intra-link transmission such as modulation-and-detection schemes and/or encoding-and-decoding methods. p_e does not have to represent the bit error probability of the *real* raw intra-link signal transmission. It represents the error probability of the *virtual* link between source and relay node.

The intra-link of this relay system is assumed to be represented by a simple bit-flipping model [34], where some of the information bits reconstructed at the relay node are the flipped versions of their corresponding original information bits at the source. Specifically, $\mathbf{b}_1$ denotes the original information bit sequence broadcasted from the source node, while $\mathbf{b}_2$ is the recovered bit sequences at the relay node, regardless of whether the strategy is one-round-Viterbi DF or EF. Therefore, the model is more abstract than that described in Chapter 3, because the goal of this chapter is to derive the outage probability theoretically. $\mathbf{b}_2 = \mathbf{b}_1 \oplus \mathbf{e}$ with probability $\Pr(e = 1) = p_e$. The p_e value can be estimated by the destination, block-by-block, as presented by [6], and hence, making an assumption that p_e is known to the destination is reasonable in the theoretical analysis.

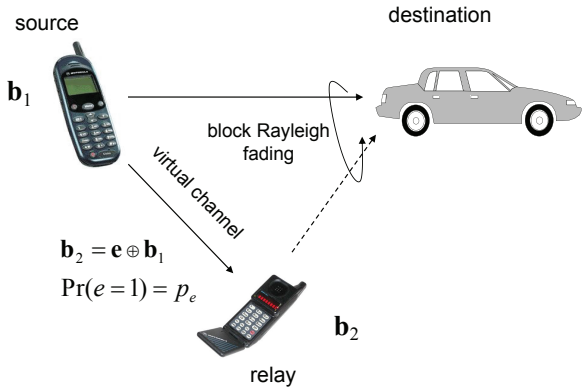

Figure 4.3: System model of the proposed relay system of Case 1.

In this model, both S-D and R-D channels are assumed to suffer from block Rayleigh fading. Two scenarios, the two channels are temporally uncorrelated and correlated, are analyzed in the following sub-sections.

4.2.2 Outage Probability Definition

In this sub-section, outage probability of the relay model described above is defined over block Rayleigh fading channels. The outage probability definition has been already provided in Sub-section 2.1.4.

As shown in Fig. 4.2, the entire rate region for the rate pair R_1 and R_2 can be divided into 4 parts, with P_j ($j = \{1, 2, 3, 4\}$), representing the probability that the rate pair (R_1, R_2) falls into Part j. The common admissible rate region for the case of two correlated sources can be expressed by an unbounded polygon, which corresponds to Part 3 of the rate region shown in Fig. 4.2. The two correlated bit streams can not be successfully recovered if the rate pair (R_1, R_2) does not falls into the admissible region Part 3. Hence, the outage event happens when R_1 and R_2 fall outside the Slepian-Wolf admissible region, with the probability of

$$\begin{aligned} P_{out,sw} =& 1 - P_3 \\ =& P_1 + P_2 + P_4. \end{aligned} \tag{4.4}$$

However, considering the relay system described before, Part 4 should also be included in the admissible rate region [35], because in the one-way Slepian-Wolf relay system investigated in this dissertation, we only focus on the transmission of the source information $\mathbf{b}_1$. The data to be transmitted from the relay node is actually the erroneous copy of the original information bit stream, interleaved by Π_0 as shown in Fig. 4.3. In other words, an arbitrary value of R_2 is satisfactory as long as R_1 is larger than $H(\mathbf{b}_1)$. In this case, the outage event happens when the pair (R_1, R_2) falls in Part 1 or Part 2, and the outage probability of the Slepian-Wolf relay model considered in this dissertation is defined as

$$\begin{aligned} P_{out} =& 1 - P_3 - P_4, \\ =& P_1 + P_2. \end{aligned} \tag{4.5}$$

According to Shannon's source-channel separation theorem, the relationship between the threshold instantaneous SNR and its corresponding rate R_i allocated to the source i is given by

$$R_i = \frac{1}{R_{ci}} \log(1 + \gamma_i), \quad i = 1, 2 \tag{4.6}$$

where R_{c1} and R_{c2} represent the spectrum efficiency of the transmission chain, including the channel coding rate and the modulation multiplicity of the S-D channel and R-D channel, respectively [34]. According to [36], the conditions on R_1 and R_2 to achieve arbitrary low bit error rate are given by[1]

$$\begin{aligned} P_1 =& \Pr\left[0 < R_1 < H(\mathbf{b}_1 \mid \mathbf{b}_2), R_2 > 0\right] \\ =& \Pr\left[0 < \gamma_1 < 2^{R_{c1} H(\mathbf{b}_1 | \mathbf{b}_2)} - 1, \gamma_2 > 0\right]. \end{aligned} \tag{4.7}$$

[1] A Gaussian codebook is assumed for channel coding.

$$
\begin{aligned}
P_2 &= \Pr\left[H(\mathbf{b}_1 \mid \mathbf{b}_2) < R_1 < H(\mathbf{b}_1), R_1 + R_2 < H(\mathbf{b}_1, \mathbf{b}_2)\right] \\
&= \Pr\Big[2^{R_{c1}H(\mathbf{b}_1|\mathbf{b}_2)} - 1 < \gamma_1 < 2^{R_{c1}H(\mathbf{b}_1)} - 1, \\
&\qquad 0 < \gamma_2 < 2^{\left[R_{c2}H(\mathbf{b}_1,\mathbf{b}_2) - \frac{R_{c2}}{R_{c1}}\log(1+\gamma_1)\right]} - 1\Big].
\end{aligned} \tag{4.8}
$$

4.2.3 Outage Calculation

In this sub-section, the outage probability of the Slepian-Wolf relay system over block Rayleigh fading channels is derived.

Temporally Uncorrelated Channels

With an assumption that both S-D channel and R-D channel suffer from statistically uncorrelated (here, independent, because the complex envelop h_i of the Rayleigh fading can be represented by two dimensional Gaussian random process) block Rayleigh fading, the joint PDF of the instantaneous SNR can be expressed as $p(\gamma_1, \gamma_2) = p(\gamma_1)p(\gamma_2)$ [37], with

$$
p\left(\gamma_i\right) = \frac{1}{\Gamma_i}\exp(-\frac{\gamma_i}{\Gamma_i}), \quad i = 1, 2 \tag{4.9}
$$

where $\Gamma_i = G_i E_{s,i} \left\langle \mid h_i \mid^2 \right\rangle / \left(2\sigma^2\right)$ $(i = 1, 2)$, denoting the normalized average SNR of S-D channel and R-D channel, respectively, with $E_{s,i}$ being the per-symbol energy of the signal. Based on (4.7) and (4.8), the probabilities P_1 and P_2 can be mathematically derived as follows

$$
\begin{aligned}
P_1 &= \int_{\gamma_1=0}^{2^{R_{c1}H(\mathbf{b}_1|b_2)}-1} \int_{\gamma_2=0}^{\infty} p\left(\gamma_1\right) p\left(\gamma_2\right) d\gamma_1 d\gamma_2, \\
&= \int_{\gamma_1=0}^{2^{R_{c1}H(\mathbf{b}_1|\mathbf{b}_2)}-1} \frac{1}{\Gamma_1}\exp(-\frac{\gamma_1}{\Gamma_1}) d\gamma_1 \\
&= 1 - \exp\left[-\frac{2^{R_{c1}H(\mathbf{b}_1|\mathbf{b}_2)} - 1}{\Gamma_1}\right].
\end{aligned} \tag{4.10}
$$

and

$$
\begin{aligned}
P_2 &= \int_{\gamma_1=2^{R_{c1}H(\mathbf{b}_1)}-1}^{2^{R_{c1}H(\mathbf{b}_1)}-1} \int_{\gamma_2=0}^{2^{\left[R_{c2}H(\mathbf{b}_1,\mathbf{b}_2)-\frac{R_{c2}}{R_{c1}}\log_2(1+\gamma_1)\right]}-1} p\left(\gamma_1\right) p\left(\gamma_2\right) d\gamma_1 d\gamma_2 \\
&= \int_{\gamma_1=2^{R_{c1}H(\mathbf{b}_1|\mathbf{b}_2)}-1}^{2^{R_{c1}H(\mathbf{b}_1)}-1} p\left(\gamma_1\right) \left[-\exp\left(-\frac{\gamma_2}{\Gamma_2}\right)\right]_{\gamma_2=0}^{2^{\left[R_{c2}H(\mathbf{b}_1,\mathbf{b}_2)-\frac{R_{c2}}{R_{c1}}\log_2(1+\gamma_1)\right]}-1} d\gamma_1 \\
&= \frac{1}{\Gamma_1} \int_{\gamma_1=2^{R_{c1}H(\mathbf{b}_1|\mathbf{b}_2)}-1}^{2^{R_{c1}H(\mathbf{b}_1)}-1} \exp\left(-\frac{\gamma_1}{\Gamma_1}\right) \left[1-\exp\left(\frac{1}{\Gamma_2}-\frac{2^{R_{c2}H(\mathbf{b}_1,\mathbf{b}_2)}}{\Gamma_2(1+\gamma_1)^{\frac{R_{c2}}{R_{c1}}}}\right)\right] d\gamma_1.
\end{aligned}
\tag{4.11}
$$

Unfortunately, the derivation of an explicit expression of (4.11) may not be possible. Hence, instead, the trapezoidal numerical integration [38] method is used to calculate P_2 in Section 4 of this chapter.

Correlated Channels

This sub-section derives P_1 and P_2 taking into account the correlation $\rho = \langle h_1 h_2^* \rangle$ of the fading variations. According to [37], when S-D channel and R-D channel are correlated, the signal amplitudes A_1 and A_2 ($A_i = \sqrt{G_i \left\langle |h_i| \right\rangle^2 E_{s,i}}$) follow the joint PDF $p(A_1, A_2)$, as shown in (4.12):

$$
p(A_1, A_2) = \frac{4A_1A_2}{P_{r1}P_{r2}(1-|\rho|^2)} I_0\left[\frac{2|\rho| A_1A_2}{\sqrt{P_{r1}P_{r2}}(1-|\rho|^2)}\right] \exp\left[-\frac{\frac{A_1^2}{P_{r1}}+\frac{A_2^2}{P_{r2}}}{1-|\rho|^2}\right], \tag{4.12}
$$

where $I_0(\cdot)$ is the zero-th order modified Bessel's function of the first kind. We define the average SNR $\Gamma_i = P_{ri}/\left(2\sigma^2\right)$ $(i = 1, 2)$, where $P_{ri} = \left\langle G_i E_{s,i} |h_i|^2 \right\rangle$ denotes the average received signal power. Since $I_0(x)$ can be expanded into a series $I_0(x) = \sum_{n=0}^{\infty} \frac{(x/2)^{2n}}{(n!)^2}$, (4.12) can be re-written as [39]

$$
\begin{aligned}
p(A_1, A_2) =& \frac{4A_1A_2}{P_{r1}P_{r2}(1-|\rho|^2)} \exp\left(-\frac{A_1^2/P_{r1}}{1-|\rho|^2}-\frac{A_2^2/P_{r2}}{1-|\rho|^2}\right) \\
& \sum_{n=0}^{\infty} \frac{1}{(n!)^2} \left(\frac{|\rho| A_1A_2}{\sqrt{P_{r1}P_{r2}}(1-|\rho|^2)}\right)^{2n} \\
=& \sum_{n=0}^{\infty} q_1^{(n)} q_2^{(n)},
\end{aligned}
\tag{4.13}
$$

where $q_1^{(n)}$ and $q_2^{(n)}$ can be expressed as

$$q_1^{(n)} = \frac{2A_1^{2n+1}\,|\rho|^n}{P_{r1}^{n+1}(1-|\rho|^2)^{n+1/2}} \exp\left(-\frac{A_1^2/P_{r1}}{1-|\rho|^2}\right)\left(\frac{1}{n!}\right), \tag{4.14}$$

$$q_2^{(n)} = \frac{2A_2^{2n+1}\,|\rho|^n}{P_{r2}^{n+1}(1-|\rho|^2)^{n+1/2}} \exp\left(-\frac{A_2^2/P_{r2}}{1-|\rho|^2}\right)\left(\frac{1}{n!}\right). \tag{4.15}$$

Since $p(A_1, A_2)$ can be factored into a product of two independent terms, each for its corresponding random variable, it is easy to calculate P_1 and P_2 by substituting (4.13)–(4.15) and $\gamma_i = A_i^2/(2\sigma^2)$ into (4.10) and (4.11), with the aid of the trapezoidal methods.

Outage of MRC

For a comparison with our proposed Slepian-Wolf relay system, the outage probability of the maximum ratio combining (MRC) scheme is derived, with the assumptions that $\rho = 0$, $\Gamma_1 = \Gamma_2$ and $p_e = 0$. The reason why $p_e \neq 0$ is not considered is because, even without the interleaver Π_0 at the relay node, a serious error propagation is expected in the case of MRC, due to the use of DACC. Hence, performing MRC at the destination by ignoring the intra-link errors even degrades the performance. However, without DACC, HI can not reach a point in EXIT chart close enough to the (1,1) mutual information point.

It is well known that the output of the MRC combiner is a weighted sum of signals received via all the transmission channels. The PDF $p_{\gamma_\Sigma}(\gamma)$ of the instantaneous SNR γ in the block Rayleigh channel after the MRC combining is given by [40]

$$p_{\gamma_\Sigma}(\gamma) = \frac{\gamma^{N-1}\exp\left(-\frac{\gamma}{\Gamma}\right)}{\Gamma^N\,(N-1)!}, \tag{4.16}$$

where N denotes the diversity order, and we have assumed each channel has the same average SNR Γ. The outage probability of MRC is defined as the probability that the instantaneous SNR after combining is less than a given threshold. For a fair comparison, the threshold of the transmission rate is chosen to be $R_{c1}H(b_1)$. Then, the outage probability of the 2nd

order MRC diversity can be calculated as follows

$$\begin{aligned} P_{out,mrc} &= \int_{\gamma=0}^{2^{R_{c1}H(b_1)}-1} p_{\gamma_\Sigma}(\gamma)d\gamma_1 \\ &= \int_{\gamma=0}^{2^{R_{c1}H(b_1)}-1} \frac{\gamma \exp\left(-\frac{\gamma}{\Gamma}\right)}{\Gamma^2} d\gamma \\ &= 1 - \exp(\frac{1-2^{R_{c1}H(b_1)}}{\Gamma}) \sum_{k=1}^{2} \frac{\left[(2^{R_{c1}H(b_1)}-1)/\Gamma\right]^{k-1}}{(k-1)!}. \end{aligned} \tag{4.17}$$

4.2.4 Asymptotic Tendency Analyses

Tendency 1: In the case $p_e = 0$

This sub-section provides the proof of the fact that, when $\mathbf{b}_1$ and $\mathbf{b}_2$ are fully correlated ($p_e = 0$), the 2nd order diversity of the outage curves can be achieved. In this case, we have $H(\mathbf{b}_1 \mid \mathbf{b}_2) = 0$, $H(\mathbf{b}_1, \mathbf{b}_2) = 1$ and the value of P_1 is always equal to 0 as found from (4.10). Hence, the outage probability is determined by P_2 only. By assuming that the fading variations of the two channels are statistically independent ($\rho = 0$) and $R_{c1} = R_{c2} = 1$, the derivation of P_2 can be reduced to

$$\begin{aligned} P_2 &= \int_{\gamma_1=0}^{1} \int_{\gamma_2=0}^{2^{[1-\log_2(1+\gamma_1)]}-1} p(\gamma_1)p(\gamma_2)d\gamma_1 d\gamma_2, \\ &= \int_0^1 p(\gamma_1)d\gamma_1 \left[-\exp\left(-\frac{\gamma_2}{\Gamma_2}\right)\right]_0^{2^{[1-\log_2(1+\gamma_1)]}-1} \\ &= \frac{1}{\Gamma_1}\int_0^1 \left[\exp(-\frac{\gamma_1}{\Gamma_1}) - \exp\left(-\frac{\gamma_1}{\Gamma_1} + \frac{1}{\Gamma_2} - \frac{2}{\Gamma_2(1+\gamma_1)}\right)\right] d\gamma_1. \end{aligned} \tag{4.18}$$

By using (4.19) for very small x:

$$\mathrm{e}^{-x} = \sum_{n=0}^{\infty} \frac{(-x)^n}{n!} \approx 1 - x, \tag{4.19}$$

(4.18) can be approximated as

$$\begin{aligned} P_2 \approx & \frac{1}{\Gamma_1}\int_0^1 \left[\left(1-\frac{\gamma_1}{\Gamma_1}\right)-\left(1-\frac{\gamma_1}{\Gamma_1}+\frac{1}{\Gamma_2}-\frac{2}{\Gamma_2\left(1+\gamma_1\right)}\right)\right] d\gamma_1 \\ = & \frac{1}{\Gamma_1}\int_0^1 \left[-\frac{1}{\Gamma_2}+\frac{2}{\Gamma_2\left(1+\gamma_1\right)}\right] d\gamma_1 \\ = & \frac{1}{\Gamma_1}\left[\frac{2\ln\left(1+\gamma_1\right)-\gamma_1}{\Gamma_2}\right]_0^1 \\ = & \frac{2\ln 2-1}{\Gamma_1\Gamma_2}. \end{aligned} \tag{4.20}$$

Obviously, the final result shows that with $p_e = 0$, the outage probability curve is inversely proportional to the product of Γ_1 and Γ_2, which achieves the 2nd order diversity.

Tendency 2: Slepian-Wolf Relay Versus MRC

In this sub-section, the proof of the advantage of the Slepian-Wolf relay system over MRC is presented, assuming that $\Gamma_1 = \Gamma_2$, $p_e = 0$, $\rho = 0$ and $R_{c1} = R_{c2} = 1$ for both the schemes. Then, (4.11) and (4.17) can be further reduced to

$$P_2 = \frac{1}{\Gamma_1}\int_{\gamma_1=0}^1 \left\{\exp\left(-\frac{\gamma_1}{\Gamma_1}\right)-\exp\left[\frac{1}{\Gamma_1}\left(1-\gamma_1-\frac{2}{1+\gamma_1}\right)\right]\right\} d\gamma_1, \tag{4.21}$$

and

$$P_{out,mrc} = \frac{1}{\Gamma_1}\int_{\gamma_1=0}^1 \frac{\gamma_1}{\Gamma_1}\exp\left(-\frac{\gamma_1}{\Gamma_1}\right) d\gamma_1. \tag{4.22}$$

To prove that $P_{out,mrc} - P_2 > 0$, we define $P_{gap} = P_{out,mrc} - P_2$

$$\begin{aligned} P_{gap} = & \frac{1}{\Gamma_1}\int_{\gamma_1=0}^1 \left\{\exp\left[\frac{1}{\Gamma_1}\left(1-\gamma_1-\frac{2}{1+\gamma_1}\right)\right]+\left(\frac{\gamma_1}{\Gamma_1}-1\right)\exp\left(-\frac{\gamma_1}{\Gamma_1}\right)\right\} d\gamma_1 \\ = & \frac{1}{\Gamma_1}\left\{\int_{\gamma_1=0}^1 \exp\left[\frac{1}{\Gamma_1}\left(1-\gamma_1-\frac{2}{1+\gamma_1}\right)\right] d\gamma_1 - \exp\left(-\frac{1}{\Gamma_1}\right)\right\}. \end{aligned} \tag{4.23}$$

Let $y_1(x) = \exp\left(1-x-\frac{2}{1+x}\right)$. It is found that $y_1(x) \geqslant -1$ within the range of [0, 1] if $y_1(x)$ is concave, since $y_1(x) \geqslant min\left\{y_1(0), y_1(1)\right\} = -1$,

according to the property of the concave function. $y_1(x)$ can be proven to be concave by showing that

$$y_1(x)'' = \exp(1 - x - \frac{2}{1+x}) \left[\frac{2}{(1+x)^2} - 1\right]^2 - \frac{4\exp(1 - x - \frac{2}{1+x})}{(1+x)^3} < 0. \tag{4.24}$$

By ignoring the common exponential terms in (4.24), because they are positive, it is found that giving a proof to (4.24) is equivalent to proving that $y_2(x) = \left[2 - (1+x)^2\right]^2 - 4(1+x) < 0$. Let $t = 1 + x$ ($t \in [1, 2]$). Then, $y_2(t) = (2 - t^2)^2 - 4t = t^4 - 4t^2 - 4t + 4$. The second order derivative of $y_2(t)$ can be expressed as

$$y_2(t)'' = 12t^2 - 8. \tag{4.25}$$

Obviously, $y_2(t)'' > 0$ within the range of $[1, 2]$. Therefore $y_2(t)$ is convex, and $y_2(t) < max\{y_2(1), y_2(2)\} = -3$. Hence, $y_2(t) < 0$, which is equivalent to $y_1(x)'' < 0$. Now $y_1(x)$ is proven to be concave, and consequently P_{gap} is proven to be positive. As a result, Slepian-Wolf relaying yields a lower outage probability than MRC, if $p_e = 0$.

Tendency 3: In the case $p_e \neq 0$

When b_1 and b_2 are not fully correlated ($p_e \neq 0$), the asymptotic tendency of the outage curve is proven to converge into that of the 1st order diversity. With $\rho = 0$, when $\Gamma_1 \to \infty$ and $\Gamma_2 \to \infty$, $P_2 \to 0$ according to (4.8). Therefore only P_1 dominates the outage probability. Assuming $R_{c1} = 1$, (4.7) can be approximated by using (4.19), as

$$\begin{aligned} P_1 =& 1 - \exp\left[-\frac{2^{H(b_1|b_2)} - 1}{\Gamma_1}\right] \\ \approx& \frac{2^{H(b_1|b_2)} - 1}{\Gamma_1}. \end{aligned} \tag{4.26}$$

Obviously, when the average SNRs Γ_1 and Γ_2 become large, the value of P_1 is inversely proportional to Γ_1 and hence the outage curve converges to the 1st order diversity.

Tendency 4: Correlated channel variation

When the fading variation correlation $\rho \neq 0$, regardless of the value of the bit flipping probability p_e, increasing the average SNRs Γ_1 and Γ_2, or equivalently increasing P_{r1} and P_{r2} yields [39]:

$$\frac{2\left|\rho\right|A_1A_2}{\sqrt{P_{r1}P_{r2}}(1-\left|\rho\right|^2)} \approx 0 \quad (P_{r1}\to\infty,\ P_{r2}\to\infty) \tag{4.27}$$

Hence, with $I_0(0)\to 1$, (4.12) can be approximated as

$$\begin{aligned} p(A_1,A_2) \approx & \frac{4A_1A_2}{P_{r1}P_{r2}(1-\left|\rho\right|^2)}\exp\left(-\frac{A_1^2/P_{r1}}{1-\left|\rho\right|^2}-\frac{A_2^2/P_{r2}}{1-\left|\rho\right|^2}\right) \\ = & \frac{2A_1}{P_{r1}\sqrt{1-\left|\rho\right|^2}}\exp\left(-\frac{A_1^2}{P_{r1}(1-\left|\rho\right|^2)}\right) \\ & \frac{2A_2}{P_{r2}\sqrt{1-\left|\rho\right|^2}}\exp\left(-\frac{A_2^2}{P_{r2}(1-\left|\rho\right|^2)}\right) \\ = & p(A_1')p(A_2'), \end{aligned} \tag{4.28}$$

where $A_1' = A_1\sqrt{1-\left|\rho\right|^2}$ and $A_2' = A_2\sqrt{1-\left|\rho\right|^2}$, with $P_{r1}' = P_{r1}(1-\left|\rho\right|^2)$ and $P_{r2}' = P_{r2}(1-\left|\rho\right|^2)$. Obviously, $p(A_i') = \frac{2A_i'}{P_{ri}'}\exp\left(-\frac{{A_i'}^2}{P_{ri}'}\right)$, which corresponds to the well-known PDF of the Rayleigh-distributed signal amplitude [40]. Hence, with $P_{r1}\to\infty$ and $P_{r2}\to\infty$ (equivalently, $P_{r1}'\to\infty$ and $P_{r2}'\to\infty$), the asymptotic property of the outage probability exhibits the same tendency as in the case of independent channels, which indicates that the tendency of the diversity order only depends on the source correlation.

4.2.5 Numerical Results

In this section, the numerical results of the theoretical outage probability calculation and the FER performance of the BICM-ID based Slepian-Wolf relay system obtained through simulations are presented. In the simulations for the BICM-ID based Slepian-Wolf relay system, we use the same transmission chain parameters, as those used in the previous chapter, i.e., the half rate non-recursive systematic convolutional code with generator polynomials $(3,2)_8$ for both C_1 and C_2, and with DACC, non-Gray QPSK used for both S-D channel and R-D channel. Hence, the coefficients R_{ci} $(i=1,2)$ representing channel coding rate and modulation multiplicity is equal to one $(=\frac{1}{2}\times 2)$ in theoretical calculations of the outage probability. The random interleaver length was 4000 and the doping ratio P_{d1} and P_{d2} are set at 4. The LLR threshold for (3.6) was set to one, as in [6], to select the reliable LLRs output from D_1 and D_2.

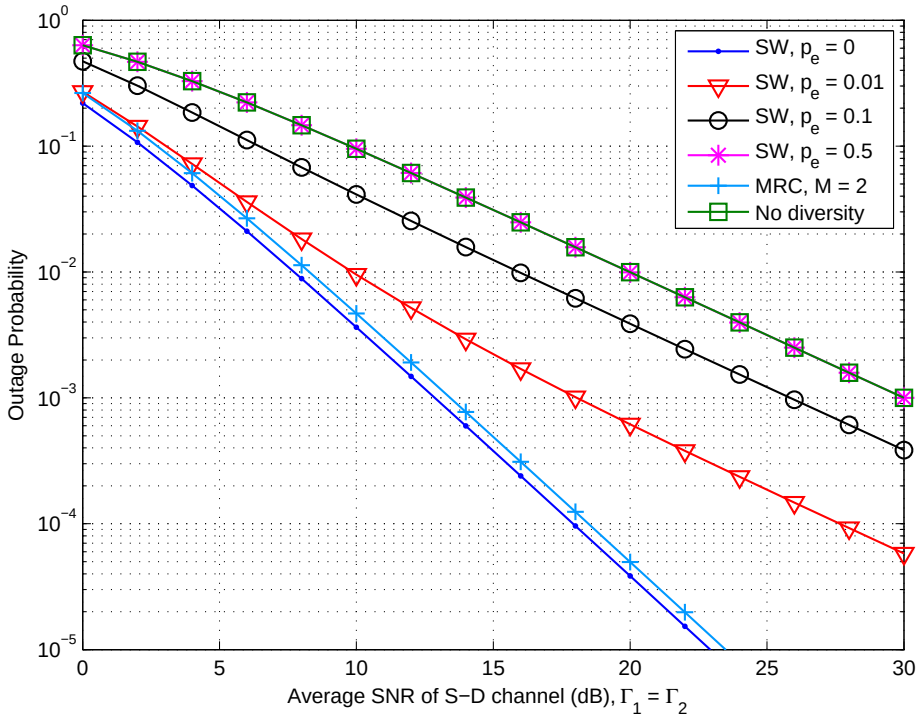

Figure 4.4: The theoretical outage probability of the Slepian-Wolf relay system.

Fig. 4.4 shows the theoretical outage probabilities of the proposed Slepian-Wolf relay system, in the case $\rho = 0$ and average SNRs $\Gamma_1 = \Gamma_2$. It is found that, only when $\mathbf{b}_1$ and $\mathbf{b}_2$ are fully correlated ($p_e = 0$), the 2nd order diversity can be achieved, which is consistent to the asymptotic analysis of Tendency 1 presented in sub-section 4.2.4. Moreover, it should be noticed that with $p_e = 0$ the Slepian-Wolf relay system can achieve slightly better outage performance than that with MRC, which is also consistent to the mathematical proof of Tendency 2 provided in Sub-section 4.2.4. The superiority of signal combining by the Slepian-Wolf system over MRC is also used in the framework of Hybrid-ARQ system in [41]; the reason for the superiority is assessed by making comparison between combining before decoding (CBD) and combining after decoding (CAD) [41]. In the case $p_e \neq 0$, the diversity order of the outage curves always plateaus at one as the average SNR increases. This asymptotic tendency agrees with the mathematical proof of Tendency 3. When $\mathbf{b}_1$ and $\mathbf{b}_2$ are completely independent ($p_e = 0.5$), obviously, the outage curves of the Slepian-Wolf relay is the same as that without diversity.

Fig. 4.5 demonstrates the FER performance of the BICM-ID based Slepian-Wolf relay system for $\rho = 0$, where the theoretical outage curve is also plotted for comparison. It is found that the FER and the theoretical outage curves exhibit the same decay, however, there is a 2–3 dB gap in average SNR between them. This is because the BICM-ID technique used in this example does not achieve close-capacity performance. This indicates that there is a possibility that the gap can further be reduced by using very strong, close-capacity achieving techniques [16] [42].

Fig. 4.6 shows the impact of the relay location on the outage probability, by assuming that the relay location is in a line between source and destination nodes, where $d_r = d_3/d_1$ is the relay distance ratio. According to (3.1), $\Gamma_2 = \Gamma_1 + 10\log_{10}\left[(d_1/d_2)^{3.52}\right]$ (dB). Because of the very stable intra-link assumption that we made in the theoretical analysis, in the simulation for the impact evaluation of the relay location, we assume an AWGN source-relay channel. The received average SNR Γ_R at the relay is given by $\Gamma_R = \Gamma_1 + 10\log_{10}\left[(d_1/(d_1 - d_2))^{3.52}\right]$ (dB). We assume the Slepian-Wolf relaying technique presented in the previous chapter, where the coding and modulation parameters are exactly the same as that described in the previous section.[2] The only difference from the technique presented in the previous section is that in the simulation, the intra-link signal detection process is also included, where only systematic part is

[2]In practice, the p_e value depends on the transmission techniques and their related parameters.

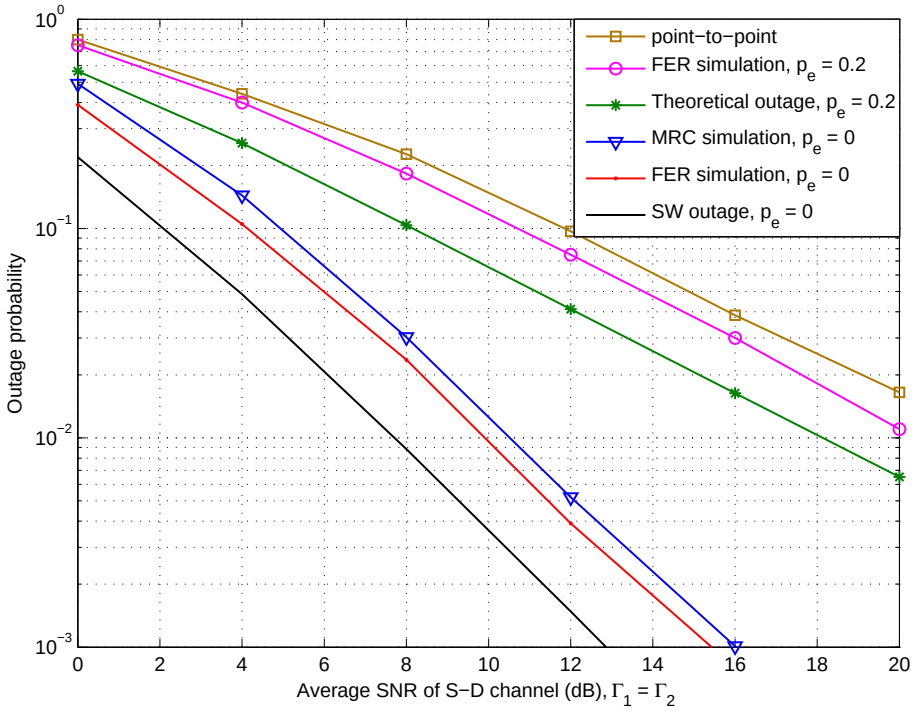

Figure 4.5: Comparison of the theoretical outage probability and the FER of the BICM-ID based Slepian-Wolf relay system.

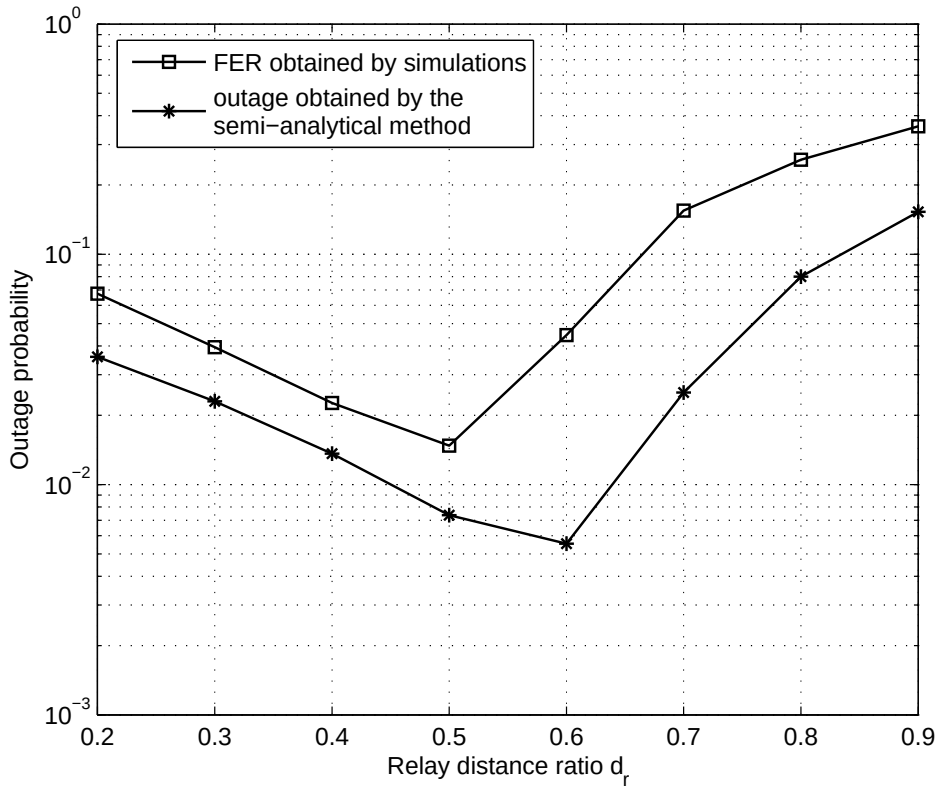

Figure 4.6: Outage probability comparison between theoretical and simulated results versus the distance ratio, where intra-link is modelled as a AWGN channel.

extracted (no decoding for C_1 is performed after the Viterbi decoding of DACC), and the extracted sequence was compared to the actually transmitted sequence to identify the p_e value. The obtained p_e value is then substituted into the equations presented in the previous chapters.

The SNR values were calculated at different locations using the equation shown above, and then we obtain p_e values corresponding to the SNR at each relay location. With the fixed p_e value obtained via the methodology described above, we evaluate the FER performance via simulations, where S-D channel and R-D channel are assumed to suffer from statistically independent block Rayleigh fading. The FER curves are shown in Fig. 4.6 for $\Gamma_1 = 3$ dB. The semi-theoretical outage curve is also shown where only p_e with the intra-link was obtained by the simulation, and the result is substituted to the theoretical expressions.

Interestingly, it is found in Fig. 4.6 that there is an optimal relay location between the source and the destination. If the relay node is either too close to the source or to the destination, the FER performances become worse than that at the optimal location. In fact, there are two factors that improve the FER/outage performance: one is the correlation exploitation, and the other is the energy of each channel. At the optimal point, the effect of combining the information through VI are maximized. It is also found that there is a gap between the FER simulation result and theoretical outage curve, because the BICM-ID relay system assumed in the simulation does not achieve close-capacity performance as stated before.

Fig. 4.7 shows the theoretical outage curves in the presence of fading correlation ρ between S-D channel and R-D channel while the source bits $\mathbf{b}_1$ and $\mathbf{b}_2$ are fully correlated ($p_e = 0$). Obviously, the larger the fading correlation, the larger the outage probability. The 2nd order diversity can asymptotically be achieved with arbitrary value of $|\rho| \neq 1$ by increasing the average SNRs, which is consistent to the asymptotic tendency analysis provided in Sub-section 4.2.4.

Duality consideration

In this part, the duality of source and channel correlations is investigated [39]. As an example, the intra-link error probability p_e is set at 0.01 which indicates that $\mathbf{b}_1$ and $\mathbf{b}_2$ are not fully correlated. It can be clearly seen in Fig. 4.8 that three outage cavers differ within a certain SNR range for different channel correlation factors ρ (=0, 0.8, 0.99). It should be noted that, they can not achieve the 2nd order diversity as the average SNRs further increase, the proof of which can be seen in Tendency 4.

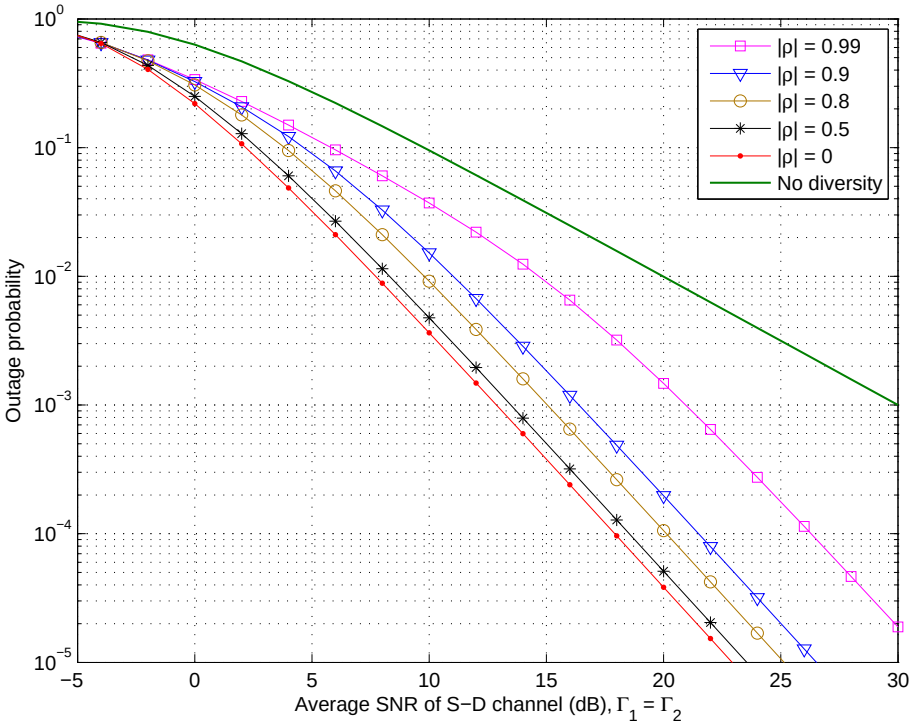

Figure 4.7: The theoretical outage probability when fading of the two channels is correlated and $p_e = 0$.

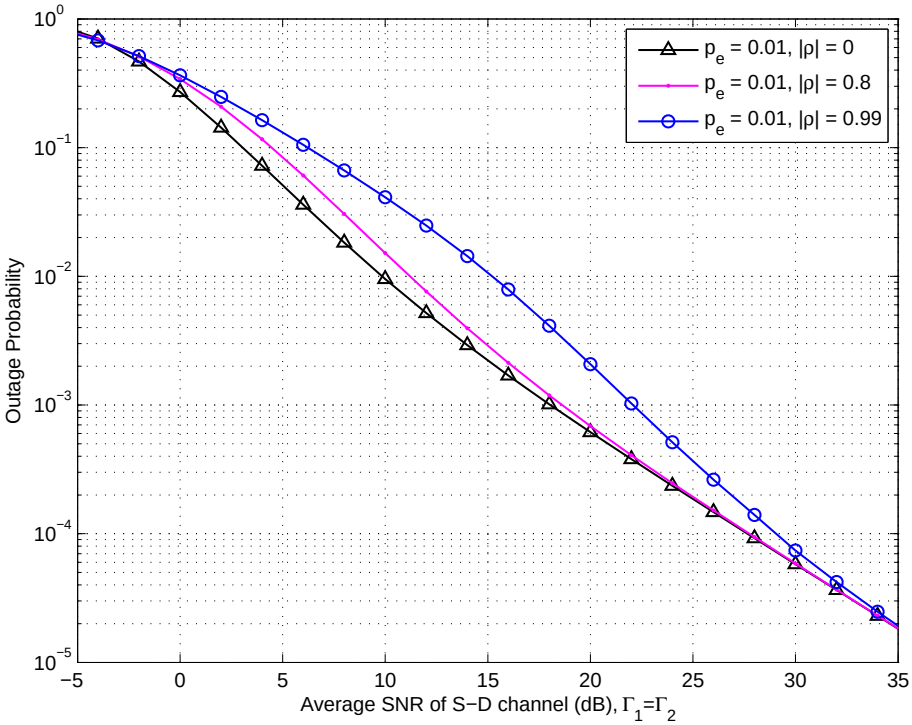

Figure 4.8: Outage probabilities in the duality of source-channel correlation.

As observed before, when $\Gamma_1 \to \infty$, $\Gamma_2 \to \infty$ and $|\rho| = 0$, the outage probability yields the equivalent diversity order 1 asymptotically, as far as $p_e \neq 0$. On the other hand, when $p_e = 0$, the equivalent diversity order converges into two, so far as $|\rho| \neq 1$. This duality can easily be understood by considering that when $\Gamma_1 \to \infty$, $\Gamma_2 \to \infty$, only either the source bits transmitted from the two transmitters being different, or the complex fading envelops of the two channels having different values determine the diversity order.

4.3 Case 2: Slepian-Wolf Relay with Rate Distortion Function

4.3.1 System Model

In this section, the same relay structure is examined, as described above. However, instead of parameterizing the intra-link errors by a bit flipping model, the assumption made in this section is more practical, in the sense that the intra-link is also suffering from block Rayleigh fading as in the other two channels.

4.3.2 Outage Probability Definition

In Case 1, the intra-link bit error probability p_e is used as a constant parameter for outage probability calculation. However, in the block Rayleigh fading assumption used in Case 2, p_e also varies according to the intra-link fading variation. Specifically, the intra-link behavior can be classified into two scenarios. In the case when intra-link SNR can support the rate $R_3 > H(\mathbf{b}_1) = 1$, the transmission is assumed to be lossless and therefore $p_e = 0$. However, if $p_e \neq 0$, the intra-link transmission is lossy and R_3 is expressed by a rate distortion function $R_D(\mathcal{D})$ $(0 \leq R_D(\mathcal{D}) < 1)$. With Shannon's source-channel separation theorem,

$$R_{c3} R_D(\mathcal{D}) \leqslant C_3(\gamma_3), \tag{4.29}$$

where R_{c3} (the same with R_{c1}) denotes the spectrum efficiency of the intra-link, including channel coding and modulation multiplicity, and $C_3(\gamma_3)$ is the channel capacity of the intra-link. $R_D(\mathcal{D})$ is the rate-distortion function of the source (with Hamming distortion measure, the distortion level $\mathcal{D}$ is equal to the intra-link probability p_e). According to [13],

$R_D(\mathcal{D}) = R_D(p_e) = H(\mathbf{b}_1) - H(p_e)$ defines the minimum rate after compression that allows the received sequences to be re-constructed with a distortion no larger than $\mathcal{D}$. Therefore, it is straightforward to obtain the relationship between the intra-link SNRs and p_e value which is shown in Fig. 4.9.[3]

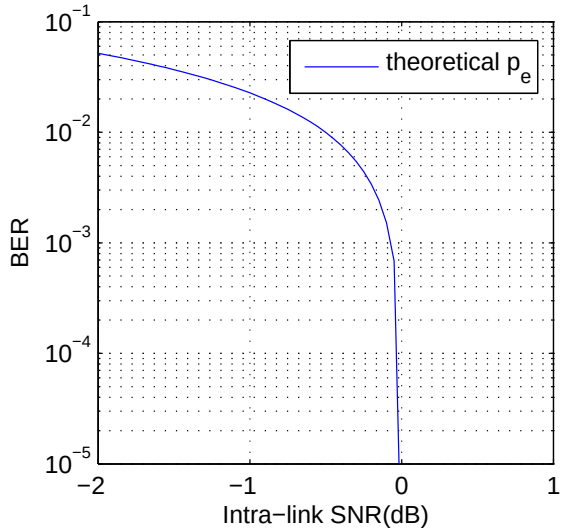

Figure 4.9: Theoretical BER of intra-link with rate distortion function.

The rate distortion function is introduced in this model for calculating the outage probability of the proposed relay system. Consequently, the rate constrains are given by [43]:

$$\begin{aligned} R_1 &\geqslant H(\mathbf{b}_1 \mid \mathbf{b}_2), \\ R_2 &\geqslant H(\mathbf{b}_2 \mid \mathbf{b}_1), \\ R_1 + R_2 &\geqslant H(\mathbf{b}_1, \mathbf{b}_2) \\ &= 1 + H(p_e) \\ &= 1 + H\left[R_D^{-1}\left(\frac{C_3(\gamma_3)}{R_{c3}}\right)\right]. \end{aligned} \tag{4.30}$$

(4.30) can be understood from the viewpoint of the Slepian-Wolf rate region presented in Fig. 4.10, the principle of which was explained in

[3]The outage happens mostly when SNR is low, and hence the Gaussian capacity and the constellation constrained capacity are almost the same in the small SNR range.

the previous section. According to the value of R_3, we divide the rate constrains into two ranges: 1) $R_3 \geq 1$ ($p_e = 0$), implying that perfect decoding is achieved at the relay. The outage event happens when R_1 and R_2 are within Part 1 shown in Fig. 4.10(a) with a probability P_1; 2) $0 \leqslant R_3 < 1$ ($0 < p_e \leqslant 0.5$), which is expressed by the rate distortion function $R_D(\mathcal{D})$ indicating that decoding at the relay is imperfect. The outage event occurs when R_1 and R_2 are within Part 2 and Part 3 shown in Fig. 4.10(b) with probabilities P_2 and P_3, respectively. Hence, the total outage probability of the relay system can be defined as

$$P_{out} = P_1 + P_2 + P_3. \tag{4.31}$$

The constrains on the rate R_3 can be converted into the instantaneous SNR constrains as follows:

$$\begin{aligned} P_1 =& \Pr\left[0 < R_1 < H(\mathbf{b}_1), 0 < R_2 < H(\mathbf{b}_1, \mathbf{b}_2), R_3 \geq 1\right] \\ =& \Pr\Big[0 < \gamma_1 < 2^{R_{c1} H(\mathbf{b}_1)} - 1, 0 < \gamma_2 < 2^{R_{c2} H(\mathbf{b}_1, \mathbf{b}_2) - \frac{R_{c2}}{R_{c1}} \log(1+\gamma_1)} - 1, \\ & \gamma_3 > 2^{R_1 R_3} - 1\Big], \end{aligned} \tag{4.32}$$

$$\begin{aligned} P_2 =& \Pr\left[0 < R_1 < H(\mathbf{b}_1 \mid \mathbf{b}_2), R_2 > 0, 0 \leq R_3 < 1\right] \\ =& \Pr\left[0 < \gamma_1 < 2^{R_{c1} H(\mathbf{b}_1 | \mathbf{b}_2)} - 1, \gamma_2 > 0, 0 < \gamma_{sr} < 2^{R_1 R_D(p_e)} - 1\right], \end{aligned} \tag{4.33}$$

$$\begin{aligned} P_3 =& \Pr\left[H(\mathbf{b}_1 \mid \mathbf{b}_2) < R_1 < H(\mathbf{b}_1), 0 < R_2 < H(\mathbf{b}_1, \mathbf{b}_2) - R_1, 0 \leq R_3 < 1\right] \\ =& \Pr\Big[2^{R_{c1} H(\mathbf{b}_1 | \mathbf{b}_2)} - 1 < \gamma_1 < 2^{R_{c1} H(b_1)} - 1, \\ & 0 < \gamma_2 < 2^{R_{c2} H(\mathbf{b}_1, \mathbf{b}_2) - \frac{R_{c2}}{R_{c1}} \log(1+\gamma_1)} - 1, 0 < \gamma_3 < 2^{R_1 R_D(p_e)} - 1\Big], \end{aligned} \tag{4.34}$$

where γ_3 represents the instantaneous SNR of the intra-link.

4.3.3 Outage Probability Calculation

By assuming independent block Rayleigh fading scenario, the PDF of the instantaneous SNR with the intra-link is given by $p(\gamma_3) = \frac{1}{\Gamma_3} \exp(-\frac{\gamma_3}{\Gamma_3})$,

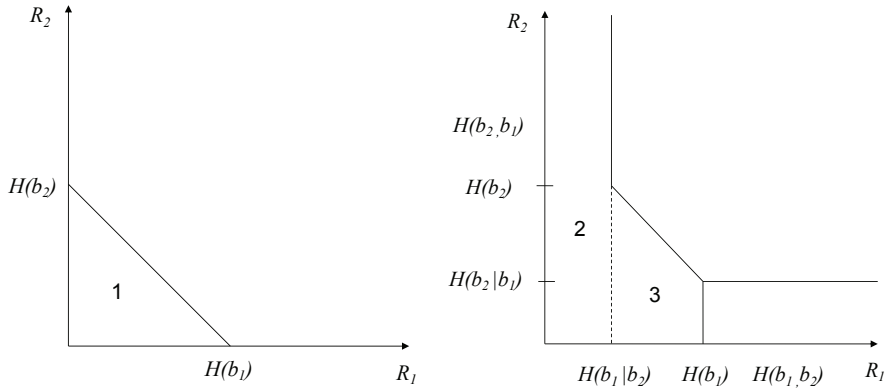

(a) In the case of lossless transmission of the Intra-link.

(b) In the case of lossy transmission of the Intra-link.

Figure 4.10: Slepian-Wolf region of the proposed relay system in Case 2.

where Γ_3 is the average SNR of the intra-link. The PDFs for the other channels are given by (4.9). P_1, P_2 and P_3 are then calculated as

$$\begin{aligned}
P_1 &= \int_{\gamma_1=0}^{1} \int_{\gamma_2=0}^{2^{1-\log_2(1+\gamma_1)}-1} \int_{\gamma_3=1}^{\infty} p(\gamma_1)p(\gamma_2)p(\gamma_3)d\gamma_1 d\gamma_2 d\gamma_3 \\
&= \int_{\gamma_3=1}^{\infty} p(\gamma_3)d\gamma_3 \int_{\gamma_1=0}^{1} p(\gamma_1)d\gamma_1 \left[-\exp\left(-\frac{\gamma_2}{\Gamma_2}\right)\right]_{\gamma_2=0}^{2^{1-\log_2(1+\gamma_1)}-1} \\
&= \int_{\gamma_3=1}^{\infty} p(\gamma_3)d\gamma_3 \int_{\gamma_1=0}^{1} p(\gamma_1) \left[1-\exp\left(-\frac{2^{1-\log_2(1+\gamma_1)}-1}{\Gamma_2}\right)\right] d\gamma_1 \\
&= \frac{1}{\Gamma_1}\exp\left(-\frac{1}{\Gamma_3}\right) \int_{\gamma_1=0}^{1} \exp\left(-\frac{\gamma_1}{\Gamma_1}\right) \left[1-\exp\left(-\frac{2^{1-\log_2(1+\gamma_1)}-1}{\Gamma_2}\right)\right] d\gamma_1,
\end{aligned} \tag{4.35}$$

$$
\begin{aligned}
P_2 &= \int_{\gamma_1=0}^{2^{H(p_e)}-1} \int_{\gamma_2=0}^{\infty} \int_{\gamma_3=0}^{1} p(\gamma_1)p(\gamma_2)p(\gamma_3)d\gamma_1 d\gamma_2 d\gamma_3 \\
&= \int_{\gamma_3=0}^{1} p(\gamma_3)d\gamma_3 \int_{\gamma_1=0}^{2^{H(p_e)}-1} \frac{1}{\Gamma_1} \exp\left(-\frac{\gamma_1}{\Gamma_1}\right) d\gamma_1 \\
&= \int_{\gamma_3=0}^{1} \frac{1}{\Gamma_3} \exp\left(-\frac{\gamma_3}{\Gamma_3}\right) \left[1 - \exp\left(-\frac{2^{H(p_e)}-1}{\Gamma_1}\right)\right] d\gamma_3 \\
&= \frac{1}{\Gamma_3} \int_{\gamma_3=0}^{1} \exp\left(-\frac{\gamma_3}{\Gamma_3}\right) \left[1 - \exp\left(-\frac{2^{1-\log_2(1+\gamma_3)}-1}{\Gamma_1}\right)\right] d\gamma_3, \quad (4.36)
\end{aligned}
$$

$$
\begin{aligned}
P_3 &= \int_{\gamma_1=2^{H(p_e)}-1}^{1} \int_{\gamma_2=0}^{2^{1+H(p_e)-\log_2(1+\gamma_1)}-1} \int_{\gamma_3=0}^{1} p(\gamma_1)p(\gamma_2)p(\gamma_3)d\gamma_1 d\gamma_2 d\gamma_3 \\
&= \int_{\gamma_1=2^{H(p_e)}-1}^{1} \int_{\gamma_2=0}^{2^{2-\log_2(1+\gamma_3)-\log_2(1+\gamma_1)}-1} \int_{\gamma_3=0}^{1} p(\gamma_1)p(\gamma_2)p(\gamma_3)d\gamma_1 d\gamma_2 d\gamma_3 \\
&= \int_{\gamma_1=2^{H(p_e)}-1}^{1} \int_{\gamma_3=0}^{1} p(\gamma_1)p(\gamma_3)d\gamma_1 d\gamma_3 \left[-\exp\left(-\frac{\gamma_2}{\Gamma_2}\right)\right]_0^{2^{2-\log_2(1+\gamma_3)-\log_2(1+\gamma_1)}-1} \\
&= \frac{1}{\Gamma_1}\frac{1}{\Gamma_3} \int_{\gamma_1=2^{1-\log(1+\gamma_3)}-1}^{1} \int_{\gamma_3=0}^{1} \exp\left(-\frac{\gamma_1}{\Gamma_1}\right) \exp\left(-\frac{\gamma_3}{\Gamma_3}\right) \\
&\quad \left[1 - \exp\left(-\frac{2^{2-\log_2(1+\gamma_3)-\log_2(1+\gamma_1)}-1}{\Gamma_2}\right)\right] d\gamma_1 d\gamma_3. \quad (4.37)
\end{aligned}
$$

It may be difficult to derive explicit expressions of (4.35), (4.36) and (4.37), therefore, the outage probability is calculated using a numerical technique.

4.3.4 Numerical Results

In this sub-section, theoretical outage probabilities of the Slepian-Wolf relay system in Case 2 are provided. Specifically, different relay location scenarios are considered for comparison, and the relay is assumed to move only in the line between the source and the destination nodes.

By fixing the average SNR of S-D channel Γ_1 to 3 dB as an example, the outage probabilities over different d_r values are presented in Fig. 4.11, where $d_r = d_{sr}/d_{sd} (0 < d_r < 1)$, denoting the distance ratio of the S-R and the S-D channel. The geometric gains are calculated according to (3.1) with the path-loss factor set at 3.52. It is clear that the outage probabilities change with different relay location scenarios, given a fixed

average SNR of the S-D channel. Theoretically, the optimal distance ratio yielding the lowest outage probability is found to be 0.5, which indicates that the relay is placed exactly at the midpoint between the source and the relay nodes. Moreover, the outage probability increases symmetrically when relay node moves towards to either the source and the destination side.

Since the frame found to contain some errors at the relay are still forwarded, the optimal distance ratio is identified as a point where the both S-R and R-D channels equally make influence to the outage probability. More specifically, the conditions of the S-R channel determines the p_e value at the relay, while the condition of the R-D channel determines the accuracy of detecting $\mathbf{b}_2$ at the destination.

The FER obtained as the simulation results of the proposed practical system using BICM-ID as described in Chapter 3, are also provided, where the intra-link also suffers from block Rayleigh fading, and the p_e value corresponding to instantaneous SNR was obtained by simulating the decoding/detection process at the relay. It can be observed that the optimal distance ratio is not exactly 0.5 in the practical system, and is slightly smaller than 0.5 (around 0.4). The theoretical analysis assumes capacity-achieving code, however, in practice, the S-R transmission is obviously not capacity-achieving, and therefore the error probability p_e is worse than the theoretical one. As a consequence, the accuracy of the recovered $\mathbf{b}_2$ also decreases even though with the fixed R-D channel gain. In order to compensate the this problem, the relay node has to be moved slightly closer to the source to acquire higher geometric gain, yielding the lowest outage, where the influence of the S-R and R-D channels qualities are properly balanced. This indicates that the influence of the correlation p_e is more significant than that of the R-D channel quality. It is the reason why the optimal relay distance ratio is found to be slightly smaller than 0.5 in the FER simulation for the practical system. In addition, the gap between theoretical outage and the FER obtained by the simulation is found to be larger when the relay is moving towards the destination side.

Finally, both the theoretical outage probability and the FER simulation results versus the average SNRs Γ_1 of S-D channel are presented in Fig. 4.12, considering the relay distance ratio d_r being 0.2, 0.4 and 0.6 for comparisons. Clearly, the theoretical outage probability curves with $d_r = 0.4$ and $d_r = 0.6$ overlap with each other and hence symmetric, which follows the observation of Fig. 4.11. For the FER obtained by the simulation, it is found that among those scenarios considered, the scenario with $d_r = 0.4$ achieves the best performance among the three examples,

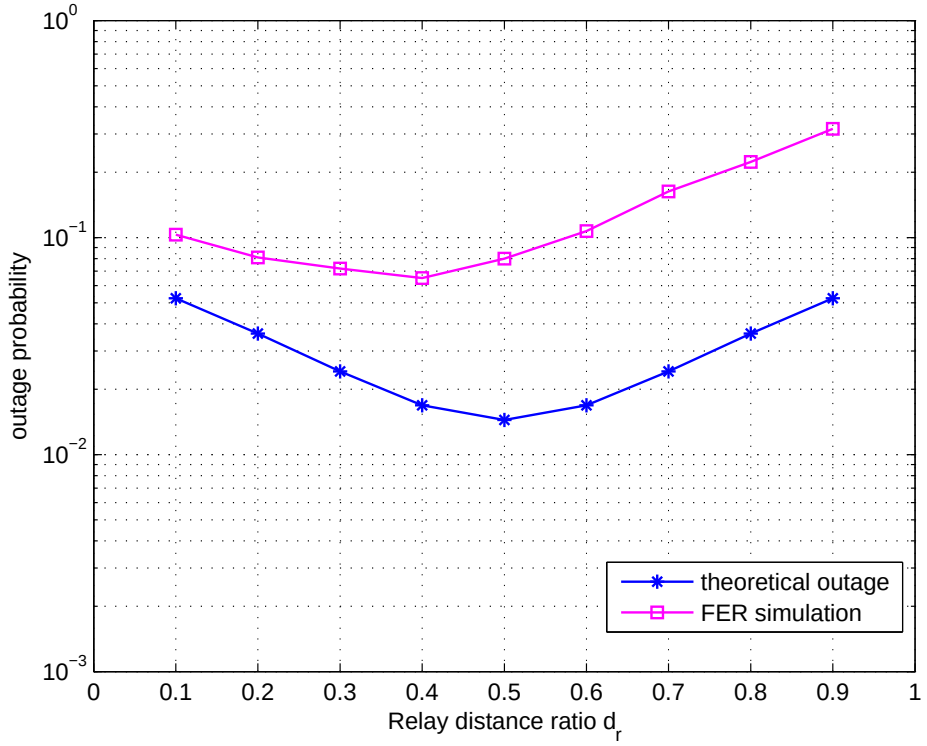

Figure 4.11: Comparisons of theoretical outage probabilities and simulated FER results over different relay distance ratios in Case 2, $\Gamma_1 = 3$ dB.

while $d_r = 0.6$ indicates the worst. This observation is consistent to the investigation described above.

4.4 Summary

In this chapter, we have theoretically analyzed the outage probability and its asymptotic properties of a simple one-way Slepian-Wolf relay system in two cases, where the source-relay correlation is exploited in the joint decoding process at the destination node. In both cases, the outage probabilities have been calculated by a set of integrals corresponding to the admissible rate region with respect to the PDF of the instantaneous SNRs of the transmission channels, identified by the Slepian-Wolf theorem.

In Case 1, the intra-link error is modeled by a bit-flipping probability p_e, which is regarded as a constant parameter, virtually representing the intra-link quality. This assumption is reasonable because the intra-link

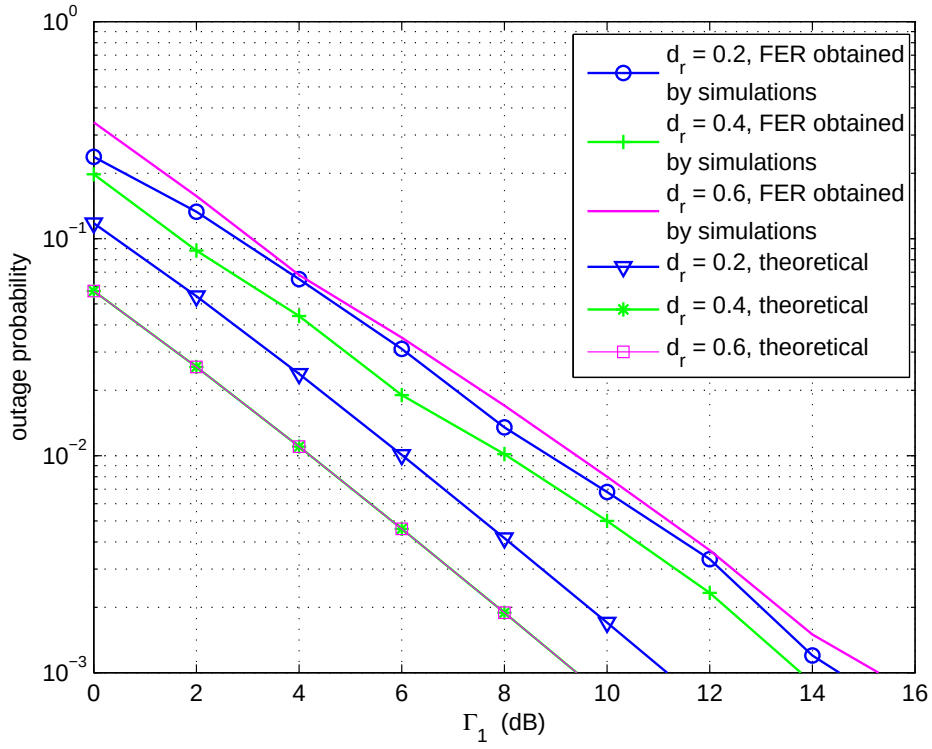

Figure 4.12: Comparisons of theoretical outage probabilities and simulated FER results in Case 2.

quality depends on many factors related to practical transmission designs. It has been found through the asymptotic tendency analysis that the 2nd order diversity can be achieved only when the information bit sequences transmitted from the source and the relay are fully correlated. Otherwise, the diversity order asymptotically converges into one as the average SNRs of S-D and/or R-D channels increase. Moreover, when $p_e = 0$, the outage probability of the Slepian-Wolf relay system is found to be lower than the case where the signals received via the two channels are maximum-ratio-combined before decoding. A mathematical proof of this discovery has been provided. It has to be noted that this proof is only for the case where the two channels suffer from independent block Rayleigh fading with the same average SNR. However, this discovery is commonly expected to hold with the arbitrary distance ratio d_2/d_1, and/or for correlated fading variation, considering the physical meaning, as stated in [41], which is still an open hypothesis.

Furthermore, the correlation ρ of the fading variations [39] of S-D and R-D channels were also taken into account, together with the correlation between the original bit sequence $\mathbf{b}_1$ at the source and re-constructed sequence $\mathbf{b}_2$ at the relay. It has been found that the diversity order of outage probability curves is only determined by the correlation between $\mathbf{b}_1$ and $\mathbf{b}_2$, and is independent of the channel variation correlation, so far as $|\rho| < 1$.

We evaluated the FER performance of the BICM-ID based Slepian-Wolf relay system, where the intra-link error p_e was obtained by the simulation. The FER performance results were then compared to the theoretical outage probability for $\rho = 0$. It has been found that the decay of FER and outage curves are consistent with each other, however, with a 2-3 dB loss in average SNR from the theoretical result. This is because the BICM-ID technique used in this example does not achieve close-capacity performance. There is a possibility that the gap can be reduced by utilizing very strong, close-capacity achieving code.[4] Interestingly, we also found that with $p_e \neq 0$, the decay of the outage curves with different ρ values all asymptotically converges to that with 1st order diversity. Conversely, with $p_e = 0$, the decay of the outage curve converges to the 2nd order diversity, so far as the fading correlation $|\rho| < 1$. It can be concluded that the source and the channel correlations are dual with each other.

In Case 2, instead of fixing the intra-link error probability p_e value as

[4]It should be noted that with the BICM-ID structure, very strong, capacity-achieving code should not necessarily require high computational burden, as shown in [44].

a parameter, it is represented by the Hamming distortion supported by the capacity of the channel, given the instantaneous SNR. With this assumption, it is made possible to evaluate the impact of the block Rayleigh fading experienced by the intra-link, as well as the S-D and R-D channels. Therefore, one more integral has to be added in the outage calculations, as presented in this chapter. By comparing the theoretical results in different relay location scenarios, it is found that the outage performances are symmetric with respect to the midpoint of the S-D channel, and this midpoint also indicates the optimal relay position that achieves the lowest outage probability. However, the FER simulation results conducted assuming Slepian-Wolf relay system using BICM-ID, presented in Chapter 3, exhibit that the optimal relay location is slightly closer to the source from the midpoint. This is because the codes used in our simulation are not capacity achieving, while the theoretical derivation is based on the use of capacity achieving codes.

Chapter 5

Optimal Power allocation

In future wireless communication systems, tremendously massive mobile devices will be involved, which results in an increasing consumption of transmit power. However, the battery life of mobile devices is still a crucial bottleneck of wireless networks. Therefore, it is quite reasonable that optimal power allocation is sought for, in order to improve the transmission efficiency of the network, as a whole. In this chapter, we present optimal power allocation schemes for the relay models in the two cases as described in Chapter 4.

In Case 1, the intra-link quality is parameterized by the fixed channel BER for simplicity while the other channels are assumed to suffer from block Rayleigh fading. A closed-form expression of the outage probability derived in the previous chapter is approximated by setting the average SNRs of S-D and R-D channels being sufficiently large while keeping the allocated power ratio to each transmit node (the source and the relay) constant. Then, it is shown that our optimal power allocation scheme can be formulated as a convex optimization problem. This chapter presents solutions to the optimization problem, and the numerical results as well.

In addition, optimal power allocation is determined in Case 2, where it is assumed that the intra-link also suffers from block Rayleigh fading, and the error probability p_e describes the Hamming distortion given by the inverse rate-distortion function. Comparisons are made between with equal power allocation and with the optimized power for different relay location scenarios.

5.1 Problem Setup

In this section, we aim to set up an optimal power allocation problem for the Slepian-Wolf relay system described in Chapter 4. Specifically, assuming that the total transmit power E_{T} for each transmit node is fixed, the allocated power for the source and the relay are represented by E_1 and E_2, respectively. Let k $(0 < k < 1)$ denote the transmit power ratio. Then, E_1 and E_2 are given by

$$\begin{aligned} E_1 &= E_{\mathrm{T}} k, \\ E_2 &= E_{\mathrm{T}}(1-k). \end{aligned} \tag{5.1}$$

Obviously, according to (5.1), $100k$ percent of the total power is given to the source node, while the rest is to the relay. Our targets are 1) Minimizing the entire outage performance while keeping the total power E_{T} fixed; 2) Minimizing the total transmit power E_t while fixing the outage probability.

5.2 Case 1: Slepian-Wolf Relay with Bit-flipping Intra-link Error Model

The system assumption here is the same as the one described in Chapter 4.2, where the intra-link error is represented by a bit-flipping model. Even though the intra-link error probability p_e may, in practice, vary as the power allocation changes, we assume that p_e is kept constant. The physical meaning of this assumption can be understood by either (1) the obtained power allocation is optimized, and as the result of the optimization, the specific p_e value is yielded, or (2) the relay location is changeable such that the p_e value does not vary with different power allocations to the source and relay.

5.2.1 Closed-form Expression of Outage Probability

In this section, we assume the spectrum efficiency R_{c1} and R_{c2} are fixed to 1 (corresponding to the case where, for example, rate 1/2 channel codes are used with QPSK modulation). According to Chapter 4.2, P_{out} can be mathematically expressed by

$$P_{out} = 1 - \exp\left(-\frac{1}{\Gamma_1}\right) - \frac{\exp\left(\frac{1}{\Gamma_2}\right)}{\Gamma_1} \int_{2^{H(p_e)}-1}^{1} \exp\left(-\frac{\gamma_1}{\Gamma_1} - \frac{2^{1+H(p_e)}}{\Gamma_2(1+\gamma_1)}\right) d\gamma_1. \tag{5.2}$$

Based on (5.2), by bringing the average SNRs Γ_1 and Γ_2 to infinity while keeping their ratio k fixed, the closed-form expression of the outage can then be obtained, by invoking the Taylor expansion approximation $\mathrm{e}^{-x} \approx 1 - x$ for a very small x, as:

$$P_{out} \approx \frac{1 - M_1}{\Gamma_1} + \frac{M_2}{{\Gamma_1}^2} + \frac{M_3 - M_1}{\Gamma_1\Gamma_2} + \frac{M_2}{{\Gamma_1}^2\Gamma_2} + \frac{M_3}{\Gamma_1{\Gamma_2}^2}, \tag{5.3}$$

where the three constants are defined as

$$\begin{aligned} M_1 &= 2 - 2^{H(p_e)}, \\ M_2 &= 2^{H(p_e)} - 2^{2H(p_e)-1}, \\ M_3 &= 2^{1+H(p_e)} \left[\ln 2 - \ln 2(2^{H(p_e)})\right]. \end{aligned} \tag{5.4}$$

5.2.2 Optimal Power Allocation

First of all, the geometrical gains of both S-D and R-D channels are assumed to be 1 without loss of generality with the system model described in Section 4.2. By normalizing the noise variance σ_n^2 of both S-D and R-D channels to unity, E_1 and E_2 are equivalent to their corresponding average SNRs Γ_1 and Γ_2, respectively, and $\Gamma_\mathrm{T} = E_T/\sigma_n^2$ is the transmit average SNR. Notice that the last two terms in (5.3) are negligible with high SNRs, then, the closed-form expression of $P_{out}(k, E_\mathrm{T})$ can be re-written as

$$P_{out}(k, E_\mathrm{T}) \approx \frac{1 - M_1}{E_\mathrm{T} k} + \frac{M_2}{E_\mathrm{T}^2 k^2} + \frac{M_3 - M_1}{{E_\mathrm{T}}^2 k(1-k)}. \tag{5.5}$$

In Fig. 5.1, the outage probability are shown over the entire range of k given different p_e values, by using the numerical calculation according to (5.2) and the approximated method as in (5.5), respectively. It is found that, the outage curves obtained using the both two methods match with each other very well, especially in the range when $k > 0.5$, which indicates that the approximation is accurate. Moreover, (5.5) can be proven to be a convex function [45], of which proof is detailed in Appendix A.

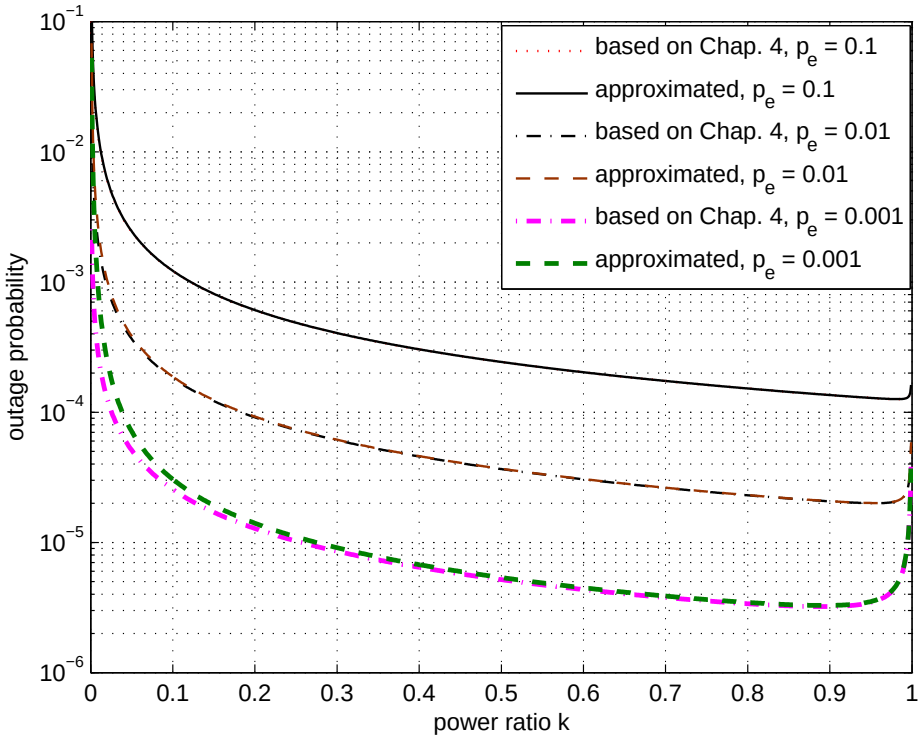

Figure 5.1: Comparison of outage curves obtained by using the numerical calculation (5.2) and approximation method (5.5), when $E_{\mathrm{T}}/\sigma_n^2 = 35$ dB.

Total power fixed

The goal of this part is to minimize the outage probability while keeping the total power E_{T} fixed. The convex problem can be formulated as

$$\begin{array}{ll} \text{minimize} & P_{out}(k, E_{\mathrm{T}}) \\ \text{subject to} & k - 1 < 0 \\ & -k < 0. \end{array} \tag{5.6}$$

By using a convex optimization toolbox in Matlab, the optimal values of k can be found, and the results are shown in Table 5.1, which compares the cases $p_e = 0.1$ and 0.01. It is found that the larger the p_e value, the more transmit power should be allocated to the source node in order to improve the quality of the S-D channel. On the other hand, the optimal k value changes according to the total transmit power E_{T}. According to Table 5.1, the optimal power ratio k becomes larger as the total power E_{T} is increasing.

Table 5.1: Optimal power ratio k, E_{T} fixed, Case 1.

E_{T}(dB)	optimal k ($p_e = 0.1$)	optimal k ($p_e = 0.01$)
20	0.893	0.778
22	0.915	0.817
24	0.933	0.851
26	0.947	0.879
28	0.958	0.902
30	0.967	0.921

The comparisons of outage probability curves between equal and optimal power allocation schemes are shown in Fig. 5.2, both using theoretical calculations. It is clearly found that in both scenarios when $p_e = 0.1$ and $p_e = 0.01$, by properly selecting the k value listed in Table 5.1, roughly 2 dB gain can be achieved in terms of the transmit SNR, compared to the case without optimization (only equal power power allocation is adopted).

Fig. 5.3 presents the simulation results for the FER evaluation with and without optimal power allocation, where we employed the same transmission chain and its related parameters as those used in the Slepian-Wolf relay system with BICM-ID presented in Section 4.2. It is found that, by selecting the optimal k values, the Slepian-Wolf relay system can achieve roughly 2 dB gain compared with the cases with equal power allocation. This tendency is consistent with the theoretical analysis demonstrated in Fig. 5.2.

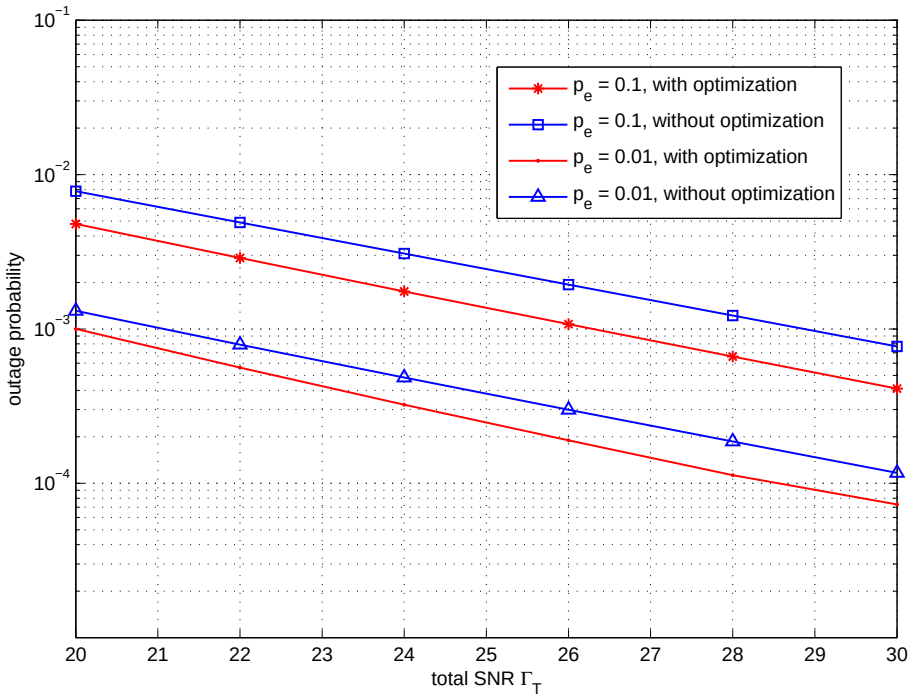

Figure 5.2: Comparison of theoretical outage probabilities with and without power allocation scheme.

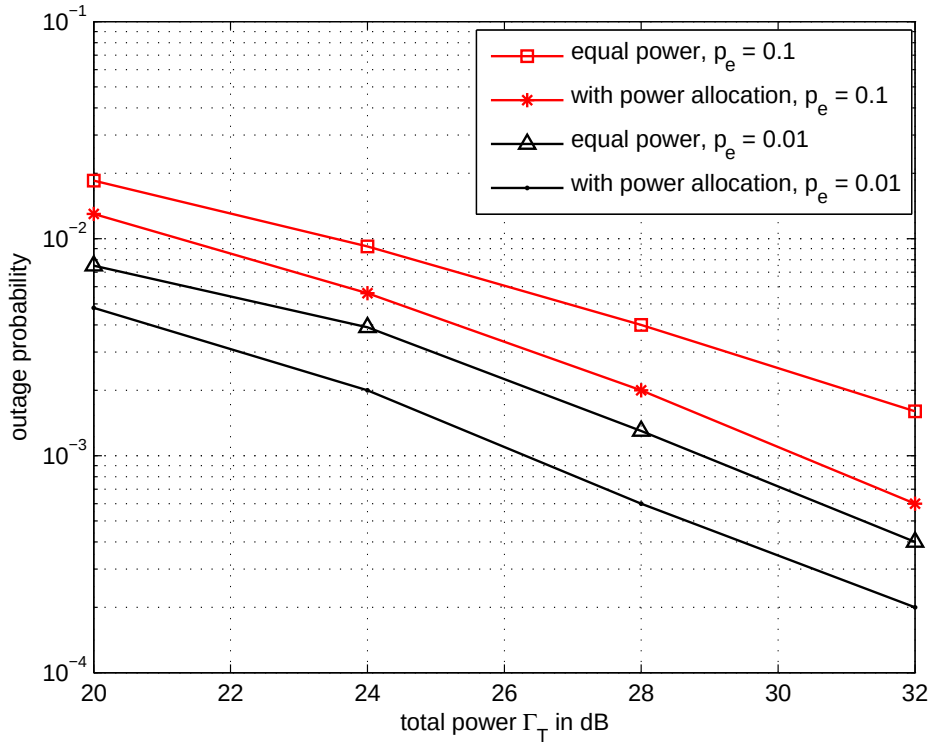

Figure 5.3: Comparison of simulated FER with and without power allocation scheme.

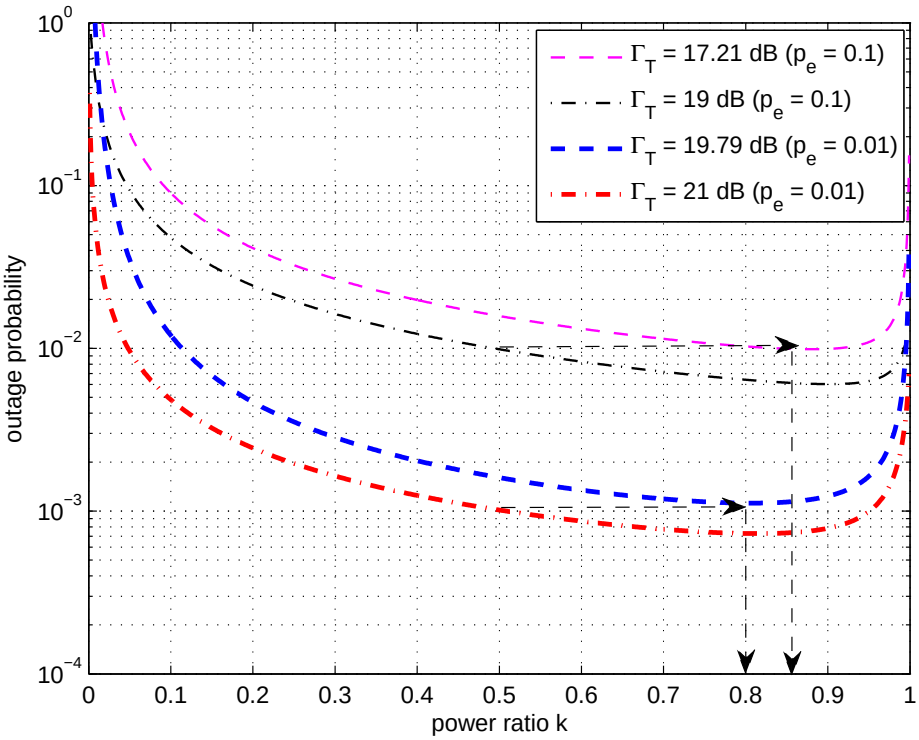

Figure 5.4: Theoretical outage probabilities with different total power.

Outage Probability Requirement Fixed

The goal of this sub-section is to minimize the total transmit power E_{T} while keeping the outage probability fixed. We formulate the problem in the following way to find the minimum power as well as its corresponding k, given the outage probability requirement C_{out}:

$$\begin{array}{ll} \text{minimize} & E_{\mathrm{T}} + 0k \\ \text{subject to} & P_{out}(k, E_{\mathrm{T}}) - C_{out} \leqslant 0 \\ & k - 1 < 0 \\ & -k < 0 \\ & -\Gamma_{\mathrm{T}} < 0 \end{array} \tag{5.7}$$

This problem is proved to be convex, which is detailed in Appendix A. The Karush-Kuhn-Tucker (KKT) conditions [45] corresponding to this problem is shown in Appendix B.

Table 5.2: Optimized total power and k, P_{out} fixed, Case 1.

P_{out} requirement	required Γ_{T} (equal power)	required Γ_{T} (optimized)	Gain
0.01 (p_e=0.1)	19 dB	17.21 dB (k=0.85)	1.79 dB
0.001 (p_e=0.01)	21 dB	19.79 dB (k=0.8)	1.21 dB

As shown in Table 5.2, for the Slepian-Wolf relay system with equal power allocation scheme, we need 19 dB total power, when $p_e = 0.1$, in order to achieve the outage probability $P_{out} = 0.01$. However, by using the optimal $k = 0.85$ obtained as the solution to the optimization problem, it can be reduced to 17.21 dB. Fig. 5.4 shows the theoretical outage curves obtained by using a numerical technique [38], without using the high average SNR assumption. For equal power allocation, the only selectable k value is 0.5, while for optimal power allocation, the optimal k yielding the smallest outage probability varies. It can be clearly seen that the optimal k values corresponding to p_e and outage requirements of 0.01 and 0.001 are exactly consistent to the values obtained as the solution to the optimization problem.

5.3 Case 2: Slepian-Wolf Relay with Rayleigh-Fading Intra-link

In this section, the optimal power allocation is performed in a more practical case, where the intra-link, as well as the S-D and R-D channels, are all suffering from block Rayleigh fading. In this case, the intra-link error probability p_e will no longer be fixed, but changes according to the fading variation, as described in Section 4.3 [43]. In other words, depending on the power allocated to the source, the p_e value also changes given a certain relay location scenario.

5.3.1 Total Transmit Power Fixed

In this sub-section, the relay location scenarios with $d_r = 0.25$, 0.5 and 0.75 are considered, which means that the relay moves in the line between the source and destination nodes. The geometric gains of S-R, S-D and R-D channels are all calculated according to (3.1). Furthermore, by normalizing the AWGN noise variance σ_n^2 of each channel to 1, the average SNRs of each channel (Γ_1 Γ_2 and Γ_3) are equal to the multiplication of transmit power and the geometric gain, where k is still used to represent the transmit power ratio, according to (5.1).

Based on the numerical calculations for (4.32), (4.33) and (4.34), the outage probabilities over the entire range of k with different relay distance ratios are shown in Fig. 5.5, with $E_{\mathrm{T}}/\sigma_n^2 = 16$ dB. An interesting observation is that, when relay is close to the source node (d_r=0.25), the optimal transmit power ratio yielding the lowest outage probability is around 0.5. In other words, the total transmit power is mostly equally allocated to both source and relay nodes (As emphasized in the previous chapter, the influence should be equally shared by the two channels at the optimal point. Hence, the optimal allocation differ as the relay location changes.). If the relay node is moved towards the destination (d_r =0.75), more transmit power has to be allocated to the source node to achieve the lowest outage probability.

Table 5.3: Optimal transmit power ratio k, different relay distance ratios, Case 2.

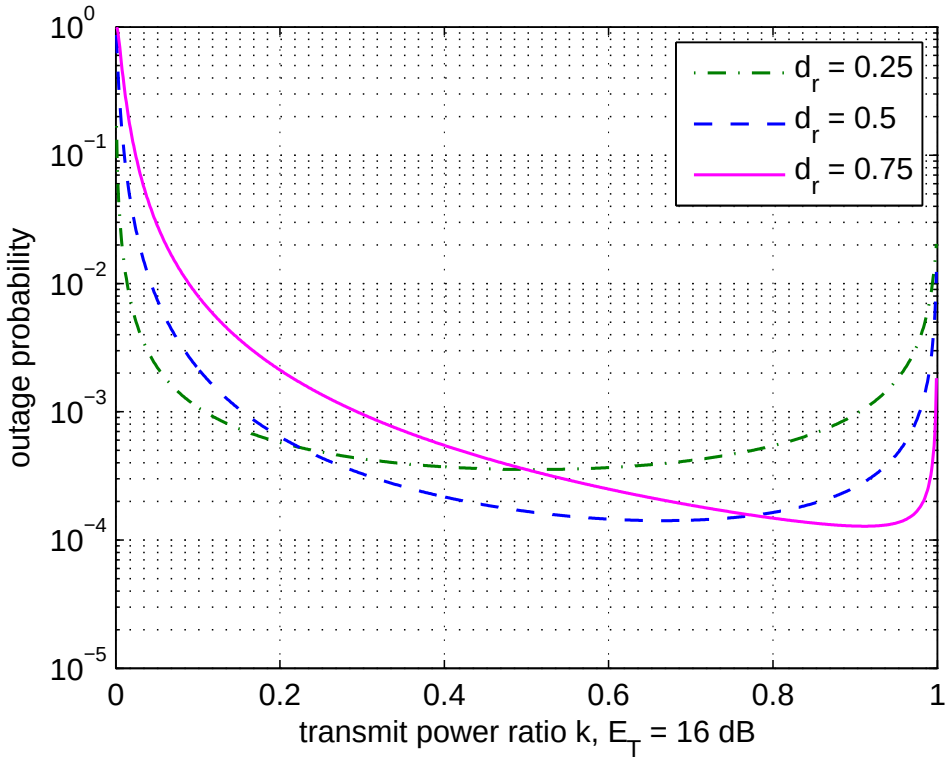

Figure 5.5: Theoretical outage probabilities versus the power ratio k in different relay locations in Case 2. $E_{\mathrm{T}}/\sigma_n^2$ =16 dB.

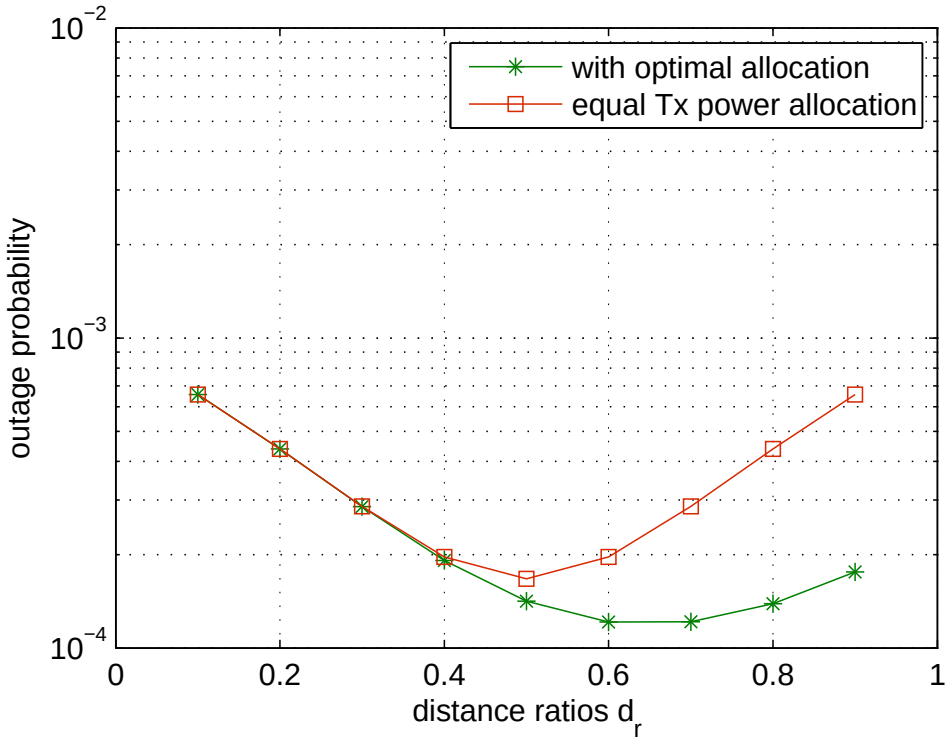

Figure 5.6: Comparisons of theoretical outage probabilities between equal and optimal power allocation in different relay locations. $E_{\mathrm{T}}/\sigma_n^2$ =16 dB.

d_r	optimal k
0.1	0.500
0.2	0.502
0.3	0.520
0.4	0.574
0.5	0.666
0.6	0.774
0.7	0.871
0.8	0.943
0.9	0.985

In Table 5.3, the optimal transmit power ratio k obtained by the numerical outage calculation is listed in different relay distance scenarios, for the $E_{\mathrm{T}}/\sigma_n^2 = 16$ dB. By substituting the obtained k value into the theoretical outage expressions, it can be clearly seen in Fig. 5.6 that, lower outage probabilities can be achieved when the relay is approaching the destination (as indicated by the green line), compared with the scenario with equal power allocation (by the red line). However, the decrease in the outage becomes smaller and even invisible as the relay is moving towards the source node. This observation can be understood as follows: when the relay node is located near the source, sufficiently small intra-link error can be easily achieved, and therefore it is reasonable to reach the lowest outage probability with equal power allocation, for the relay location. However, in the case when relay is located near the destination node, the intra-link error becomes large which leads to more significant impact on the convergence of the decoding/detection process at the destination, and hence, more power is needed for the transmitter at the source to enhance the intra-link transmission.

5.3.2 Outage Requirement Fixed

This sub-section examines how much total transmit power can be saved given a fixed outage probability requirement, by using our power allocation scheme. Table 5.4(a) shows for the relay distance ratio of 0.6, the required total transmit power with equal and optimal power allocations for outage requirements, P_{out} =0.00001, 0.0001 and 0.001. Table 5.4(b) shows for $d_r = 0.7$.

Table 5.4: Optimal k values, P_{out} fixed, Case 2

(a) Optimal k values, d_r =0.6

P_{out} requirement	required E_{T} (equal power)	required E_{T} (optimized)	Gain
0.001	12.45 dB	11.35 dB (k=0.774)	1.1 dB
0.0001	17.45 dB	16.40 dB (k=0.774)	1.05 dB
0.00001	22.50 dB	21.42 dB (k=0.774)	1.08 dB

(b) Optimal k values, d_r =0.7

P_{out} requirement	required E_{T} (equal power)	required E_{T} (optimized)	Gain
0.001	13.25 dB	11.47 dB (k=0.871)	1.88 dB
0.0001	18.30 dB	16.42 dB (k=0.872)	1.88 dB
0.00001	23.31 dB	21.44 dB (k=0.872)	1.87 dB

According to Tables 5.4(a) and 5.4(b), it is clearly seen that given the relay location, the transmit power gains with the optimal power allocation over the equal power allocation are almost the same, independently of the outage requirements. Moreover, as shown in Fig. 5.7 and Fig. 5.8, it is found that the optimal k stays almost unchanged, regardless of relay location scenarios.

5.4 Summary

In this chapter, we proposed optimal power allocation schemes for the Slepian-Wolf relay system in two cases. In Case 1, by deriving the closed-form of the outage expression assuming high average SNR, the power allocation is found to be formulated by a convex optimization problem. Roughly 2 dB SNR gain can be achieved by selecting the optimal power allocation ratios compared to the case of equal power allocation. The results obtained by solving the convex optimization is almost the same as the power allocation ratios obtained by evaluating the outage probabilities shown in the previous chapter, by using a numerical technique.

Furthermore, the optimal power allocation is also analysed in Case 2 for different relay location scenarios. It is found that when the relay node

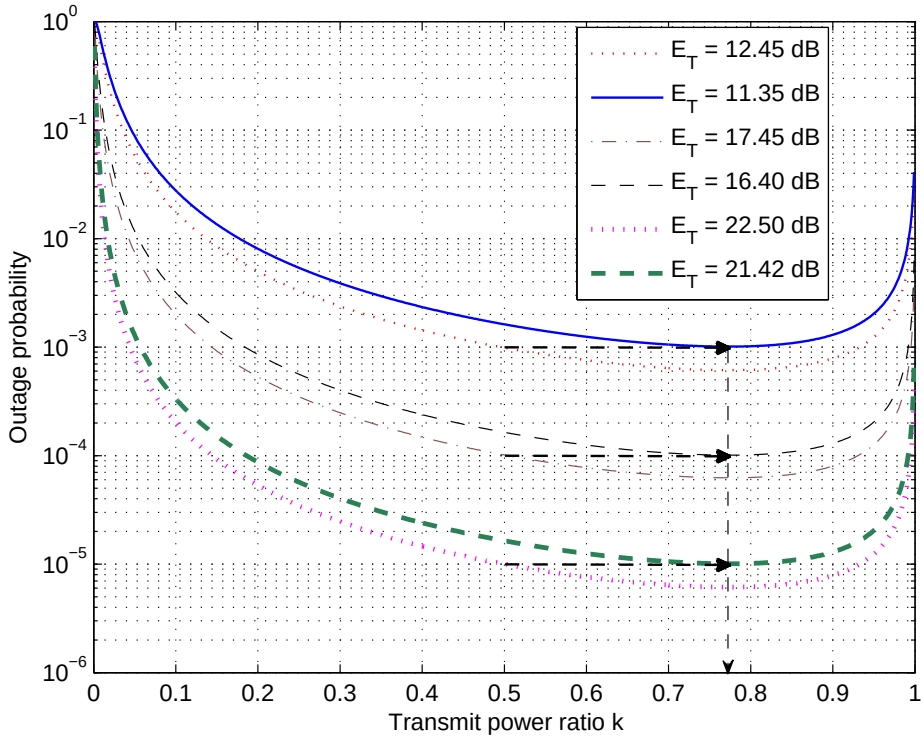

Figure 5.7: Theoretical outage probabilities versus the power ratio k with different total transmit powers, $d_r = 0.6$.

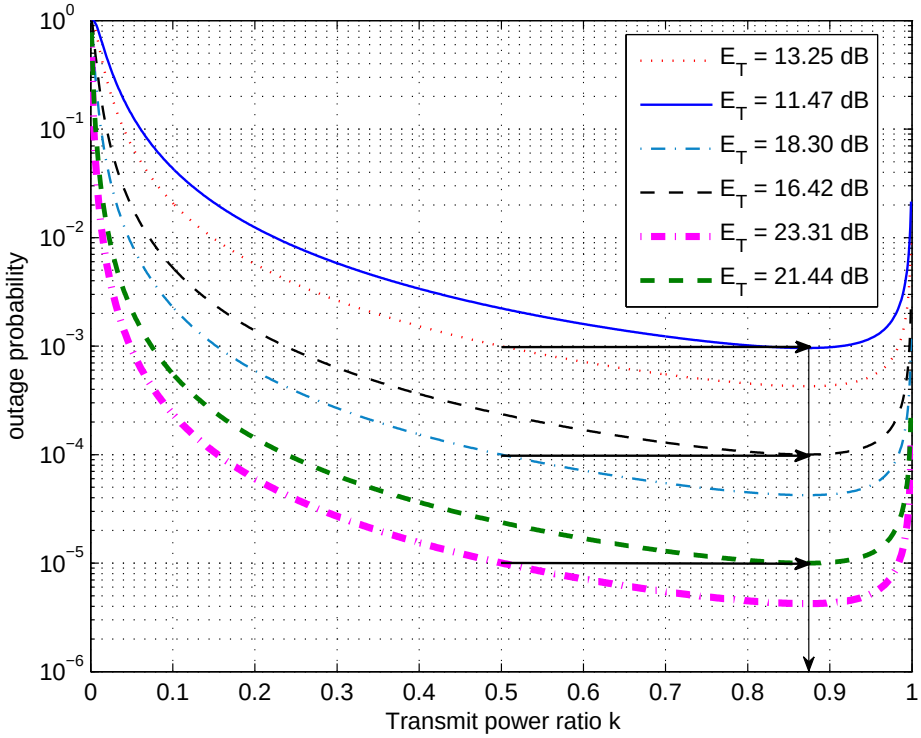

Figure 5.8: Theoretical outage probabilities versus the power ratio k with different total transmit powers, $d_r = 0.7$.

is very close to the source, lowest outage probability can be achieved by equally allocating the transmit power. When the relay is moving towards the destination node, more power should be allocated to the source in order to achieve the lowest outage probability.

Chapter 6

Conclusions and Future Work

6.1 Conclusions

In this dissertation, we have intensively investigated the cooperative communication system which exploits the source correlation from the viewpoint of the Slepian-Wolf theorem. The main contributions of this research are that both the practical coding/decoding strategies and the theoretical bases, including outage bound derivations and power optimization techniques have been identified. In particular, a simple one-way relay model using DF relaying scheme allowing intra-link errors has been investigated. It has been shown that the classic three-node relay model can be regarded as a simple distributed coding structure, where the original information sequence at the source node and the decoded sequence at the relay node are highly correlated. Our technique aims to best exploit the correlation of the two bit sequences which are independently encoded and transmitted to the destination, in order to improve the system performance.

First of all in Chapter 3, a DACC-assisted Slepian-Wolf relay system is proposed with BICM-ID technique for QPSK and 8PSK modulations. In our proposed DF strategy, the re-constructed bit sequence obtained, as the decoding result at the relay, is always interleaved, re-encoded, and forwarded to the destination, regardless of whether or not the re-constructed sequence contains some errors. The interleaver converts the relay model into a form of distributed Turbo code structure. At the destination side, the intra-link error probability, representing as the source-relay correlation, is utilized at the destination via an LLR updating function. Therefore, heavy decoding load at the relay is not needed, even we can just extract the information part of the coded bit sequence, instead of performing fully iterative decoding of the channel codes. It has also been shown that

the EXIT curve of the BICM-ID demapper-plus-DACC^{-1} matches very well with that of the decoder of convolutional codes. Parameters used in the transmission chain including inner/outer codes and doping ratios of DACC are chosen based on EXIT chart analysis. Furthermore, the relationship of system model described above to an ARQ system was investigated. A series of simulations were conducted to evaluate the system performance of the proposed system in both AWGN and block Rayleigh fading channels, where account is taken of the different relay location scenarios.

According to the Slepian-Wolf theorem, for distributed source coding, the rate after the source coding of each single transmission chain can be further reduced by exploiting the correlation knowledge in joint decoding process. As a core contribution of this dissertation, the one-way relay system allowing intra-link errors is formulated where the framework is the Slepian-Wolf theorem. Specifically, the outage probability of such a system model has been formulated by a set of integrals over the admissible Slepian-Wolf rate region with respect to the PDF of the instantaneous SNR of the each transmission channel. Two cases were considered to evaluate the outage probability. In Case 1, the intra-link error is parameterized by a bit-flipping model, with a flipping probability p_e indicating the correlation between the original information sequence and the reconstructed bit sequence at the relay. It has been found that the 2nd order diversity of the outage curves can be achieved only when the two bit sequences are fully correlated ($p_e = 0$). Otherwise it will asymptotically converge to the 1st diversity, regardless of the correlation of the fading variations. In Case 2, by introducing the rate distortion function with the Hamming distortion measure, the intra-link transmission error probability is derived where p_e is no longer a constant. With this technique, the optimal relay location, indicating the lowest outage performance, is found to be at the midpoint between the source and destination.

Based on the theoretical framework of the outage probability derivation, we provided optimal power allocation schemes aiming at (1) minimizing the outage probability while keeping the total transmit power fixed, and (2) minimizing the total transmit power while keeping the outage requirement fixed. In Case 1, an asymptotic closed-form expression of the outage probability is derived. The optimal power allocation scheme is formulated by a convex optimization problem. The simulation results have shown that with the optimal transmit power allocation, the system can reduce 2 dB of the total transmit power compared with equal power allocation. In Case 2, when the relay is very close to source node, the op-

timal transmit power ratio, which achieves the lowest outage probability, is found to be around 0.5. However, when the relay is moving towards the destination side, more transmit power has to be allocated to the source in order to achieve the lowest outage performance.

Although the system structure considered in this dissertation is simple, the techniques and theoretical formulations can be straightforwardly extended to more complex topologies for future wireless cooperative networks having many network nodes.

6.2 Future Work

Based on the achievements of this dissertation, we can provide several directions as the future work.

- The outage probabilities of the system with more than two correlated sources have to be considered. In that case, the admissible Slepian-Wolf rate region is more complex, and hence outage derivation is expected to be more complicated.
- It is also interesting to investigate the asymptotic tendency of outage curves with a increased number of correlated sources.
- The transmission strategy proposed in this dissertation can be changed to a multiple access channel model (MAC), so that the MAC region should also be considered in the outage calculation.
- Power allocation considering the transmission over temporally correlated channels has to be identified.
- We can also apply our methodology to a more complicated wireless mesh network (WMN), from the viewpoint of lossy correlated source coding exemplified by the Chief Executive Officer (CEO) problem.

Appendix A

Convexity Proof

The convexity of the approximated outage probability expression (5.5) is proven in Appendix A. It is clear to see that (5.5) is composed of three terms. If each of the three terms can be proven to be convex, (5.5) is also convex because it is a sum of the convex terms. The Hessian matrix of the first term $\frac{1-M_1}{kE_\mathrm{T}}$ can be calculated as

$$\mathbb{H}\left[\frac{1-M_1}{kE_\mathrm{T}}\right] = \frac{1-M_1}{k^3E_\mathrm{T}^3}\begin{bmatrix}2E_\mathrm{T}^2 & kE_\mathrm{T}\\ kE_\mathrm{T} & 2k^2\end{bmatrix}. \tag{A.1}$$

Since $1-M_1 = 2^{H(p_e)}-1 \geq 0$, the eigenvalues of the Hessian matrix in (A.1) are calculated as $\lambda_{1,2} = 0.5\frac{1-M_1}{k^3E_\mathrm{T}^3}\left(\sqrt{k^2+E_\mathrm{T}^2} - \sqrt{k^2+E_\mathrm{T}^2-3k^2E_\mathrm{T}^2}\right)$, which are clearly non-negative. Therefore, the Hessian matrix of $\left[\frac{1-M_1}{kE_\mathrm{T}}\right]$ is positive semi-definite and hence its convexity has been proven.

The Hessian matrix of the second term $\frac{M_2}{k^2E_\mathrm{T}^2}$ can be calculated as

$$\mathbb{H}\left[\frac{M_2}{k^2E_\mathrm{T}}\right] = \frac{2M_2}{k^4E_\mathrm{T}^4}\begin{bmatrix}3E_\mathrm{T}^2 & 2kE_\mathrm{T}\\ 2kE_\mathrm{T} & 3k^2\end{bmatrix}. \tag{A.2}$$

Since $M_2 = 2^{H(p)} - 2^{2H(p)=1} \geq 0$, the eigenvalues of the Hessian matrix in (A.3) are obtained as $\lambda_{1,2} = \frac{M_2}{k^4E_\mathrm{T}^4}\left(\sqrt{6k^2+3E_\mathrm{T}^2} - \sqrt{6k^2+3E_\mathrm{T}^2-56k^2E_\mathrm{T}^2}\right)$, which are clearly non-negative. Therefore, the Hessian matrix of $\frac{M_2}{k^2E_\mathrm{T}^2}$ is positive semi-definite and hence its convexity has been proven.

The Hessian matrix of the third $\frac{M_3-M_1}{E_{\mathrm{T}}^2 k(k-1)}$ can be calculated as

$$\mathbb{H}\left[\frac{M_3-M_1}{{E_{\mathrm{T}}}^2 k(1-k)}\right] = \frac{2(M_3-M_1)}{k^3(1-k)^3 {E_{\mathrm{T}}}^4}\begin{bmatrix} k^2{E_{\mathrm{T}}}^2 - k{E_{\mathrm{T}}}^2 + {E_{\mathrm{T}}}^2 & kE_{\mathrm{T}} - kE_{\mathrm{T}} \\ kE_{\mathrm{T}} - kE_{\mathrm{T}} & 3k^4 - 6k^3 + 3k^2 \end{bmatrix}, \tag{A.3}$$

Letting $m(k) = 3k^2(k-1)^2 + {E_{\mathrm{T}}}^2(k^2+1-k)$ and $n(k) = 3k^4 - 9k^3 + 11k^2 - 7k + 2$, the eigenvalues are $\lambda_{1,2} = \frac{M_3-M_1}{k^3(1-k)^3 E_{\mathrm{T}}^4}\left(m - \sqrt{m^2 - 4k^2 E_{\mathrm{T}}^2 n}\right)$. For $0 < k < 1$, obviously, $m(k) > 0$. Since $n(k)^{''} = 36k^2 - 54k + 22 > 0$, $n(k)^{'}$ is proven to be monotonically increasing until the boundary $n(k)^{'} < n(k=1) = 0$, and furthermore $n(k)^{'} < 0$ indicates $n(k)$ is monotonically decreasing until the boundary $n(k) > n(k=1) = 0$. This proves the non-negativity of n(k).

Now, let $y = M_3 - M_1 = 2^x\left[2\ln 2 - 2\ln(2^x) + 1\right] - 2$, where $x = H(p_e)$ with $0 \le x \le 1$. Due to the fact that

$$\begin{aligned} y^{''} &= 2^x \ln 2\left[\ln 2\left(2\ln 2 - 2\ln 2^x + 1\right) - 4\right] \\ &< 2^x \ln 2\left[\ln 2\left(2\ln 2 - 2\ln 2^0 + 1\right) - 4\right] \\ &< 0, \end{aligned} \tag{A.4}$$

y is concave and $M_3 - M_1 > min(y(0), y(1)) = 0$. Therefore, the Hessian matrix of $\frac{M_3-M_1}{E_{\mathrm{T}}^2 k(k-1)}$ is proven to be positive semi-definite and hence its convexity has been proven.

Appendix B

KKT Condition

The KKT condition for the optimization problem presented in Section 5.2 is summarized below:

$$\begin{aligned}
&P_{out}(k, E_{\mathtt{T}}) - M_{out} \leqslant 0 \\
&k - 1 < 0 \\
&-k < 0 \\
&-E_{\mathtt{T}} < 0 \\
&\lambda_1 \geq 0 \\
&1 + \lambda_1 \tfrac{\partial P_{out}(k, E_{\mathtt{T}})}{\partial E_{\mathtt{T}}} = 0 \\
&\lambda_1 \tfrac{\partial P_{out}(k, E_{\mathtt{T}})}{\partial k} = 0
\end{aligned} \tag{B.1}$$

The formulation and notations are all consistent to [45], where $f_0 = E_{\mathtt{T}} + 0k$, $f_1 = P_{out}(k, E_{\mathtt{T}}) - M_{out}$, $f_2 = k - 1$, $f_3 = -k$, $f_4 = -E_{\mathtt{T}}$ and they are all differentiable.

Bibliography

[1] M. Torlak and T. Duman, "Mimo communication theory, algorithms, and prototyping," in *Signal Processing and Communications Applications Conference (SIU), 2012 20th*, pp. 1–2, 2012.

[2] A. Goldsmith, S. Jafar, N. Jindal, and S. Vishwanath, "Capacity limits of mimo channels," *Selected Areas in Communications, IEEE Journal on*, vol. 21, no. 5, pp. 684–702, 2003.

[3] E. C. van der Meulen, "Three-terminal Communication Channels," *Adv. Appl. Prob.*, vol. 3, pp. 120–154, June 1971.

[4] G. Kramer, M. Gastpar, and P. Gupta, "Cooperative strategies and capacity theorems for relay networks," *Information Theory, IEEE Transactions on*, vol. 51, no. 9, pp. 3037–3063, 2005.

[5] S.-Q. Huang, H.-H. Chen, and M.-Y. Lee, "On performance bounds of mixed amplify-and-forward and decode-and-forward cooperative relay systems," in *Communications and Networking in China (CHINACOM), 2011 6th International ICST Conference on*, pp. 521–527, 2011.

[6] K. Anwar and T. Matsumoto, "Accumulator-assisted distributed turbo codes for relay system exploiting source-relay correlation," *IEEE Communications Letter*, vol. 16, pp. 1114 –1117, Jul. 2012.

[7] E. Zehavi, "8-psk trellis codes for a rayleigh channel," *IEEE Transactions on Communications*, vol. 40, no. 5, pp. 873–884, 1992.

[8] A. Chindapol and J. Ritcey, "Design, analysis, and performance evaluation for bicm-id with square qam constellations in rayleigh fading channels," *Selected Areas in Communications, IEEE Journal on*, vol. 19, no. 5, pp. 944–957, 2001.

[9] S. ten Brink, "Convergence behavior of iteratively decoded parallel concatenated codes," *IEEE Transactions on Communications*, vol. 49, no. 10, pp. 1727–1737, 2001.

[10] R. Y. S. Tee, S. X. Ng, and L. Hanzo, "Three-dimensional exit chart analys'is of iteraltive detecltion aided coded modulaltion schemes," in *Vehicular Technology Conference, 2006. VTC 2006-Spring. IEEE 63rd*, vol. 5, pp. 2494–2498, 2006.

[11] B. Sklar, *Digital Communications: Fundamentals and Applications*. Prentice Hall; 2 edition, 2001.

[12] T. S. Rappaport, *Wireless Communications: Principles and practice, Second Edition*. Prentice Hall, 2002.

[13] T. M. Cover and J. A. Thomas, *Element of Information Theory, 2nd Edition*. John Wiley & Sons, Inc., 2006.

[14] M. Dohler and Y. Li, *Cooperative Communications hardware, Channel & PHY*. John Wiley & Sons, Ltd., 2010.

[15] C. Berrou, A. Glavieux, and P. Thitimajshima, "Near shannon limit error-correcting coding and decoding: Turbo-codes. 1," in *Communications, 1993. ICC '93 Geneva. Technical Program, Conference Record, IEEE International Conference on*, vol. 2, pp. 1064–1070 vol.2, 1993.

[16] L. Hanzo and T. H. Liew and B. L. Yeap and R. Y. S. Tee and S. X. Ng, *Turbo Coding, Turbo Equalisation and Space-Time Coding*. John Wiley and Sons, LTD, Second Edition, 2002.

[17] X. Li and J. Ritcey, "Bit-interleaved coded modulation with iterative decoding," *Communications Letters, IEEE*, vol. 1, no. 6, pp. 169–171, 1997.

[18] S. Alamouti, "A simple transmit diversity technique for wireless communications," *Selected Areas in Communications, IEEE Journal on*, vol. 16, no. 8, pp. 1451–1458, 1998.

[19] L. Qijia, Z. Wei, X. Ma, and G. Zhou, "Designing peak power constrained amplify-and-forward relay networks with cooperative diversity," *Wireless Communications, IEEE Transactions on*, vol. 11, no. 5, pp. 1733–1743, 2012.

[20] S. Simoens, J. Vidal, and O. Munoz, "Compress-and-forward cooperative relaying in mimo-ofdm systems," in *Signal Processing Advances in Wireless Communications, 2006. SPAWC '06. IEEE 7th Workshop on*, pp. 1–5, 2006.

[21] A. Wyner and J. Ziv, "The rate-distortion function for source coding with side information at the decoder," *Information Theory, IEEE Transactions on*, vol. 22, no. 1, pp. 1–10, 1976.

[22] Z. Zhang and T. Duman, "Capacity-approaching turbo coding for half-duplex relaying," *Communications, IEEE Transactions on*, vol. 55, no. 10, pp. 1895–1906, 2007.

[23] C. Li, G. Yue, M. Khojastepour, X. Wang, and M. Madihian, "Ldpc-coded cooperative relay systems: performance analysis and code design," *IEEE Transactions on Communications*, vol. 56, no. 3, pp. 485–496, 2008.

[24] H. Jun and T. Duman, "Cooperation over frequency-selective fading relay channels," *Wireless Communications, IEEE Transactions on*, vol. 7, no. 12, pp. 5072–5081, 2008.

[25] B. Zhao and M. Valenti, "Distributed turbo coded diversity for relay channel," *Electronics Letters*, vol. 39, no. 10, pp. 786–787, 2003.

[26] A. Chakrabarti, A. de Baynast, A. Sabharwal, and B. Aazhang, "Low density parity check codes for the relay channel," *IEEE Journal on Selected Areas in Communications*, vol. 25, no. 2, pp. 280–291, 2007.

[27] D. Slepian and J. K. Wolf, "Noiseless coding of correlated information sources," *IEEE Transactions on Information Theory*, vol. 19, pp. 471 – 480, Jul. 1973.

[28] D. Liang, S. X. Ng, and L. Hanzo, "Relay-induced error propagation reduction for decode-and-forward cooperative communications," in *Global Telecommunications Conference (GLOBECOM 2010), 2010 IEEE*, pp. 1–5, 2010.

[29] R. Youssef and A. Graell i Amat, "Distributed Serially Concatenated Codes for Multi-source Cooperative Relay Networks," *IEEE Transections on Wireless Communications*, vol. 10, pp. 253–263, Jan. 2011.

[30] D. Zhao, A. Dauch, and T. Matsumoto, "BICM-ID Using Extended Mapping and Repetition Code with Irregular Node Degree Allocation," in *IEEE Vehicular Tech. Conf.-Spring*, (Barcelona), Sept. 2009.

[31] K. Anwar and T. Matsumoto, "Very simple BICM-ID using repetition code and extended mapping with doped accumulator," *Wireless Personal Communications, Springer US*, vol. 67, pp. 573–584, Dec. 2012.

[32] K. Anwar and T. Matsumoto, "Spatially Concatenated Coded with Turbo Equalization for Correlated Sources," *IEEE Trans. on Signal Processing*, vol. 60, pp. 5572–5577, Oct. 2012.

[33] P.-S. Lu, V. Tervo, K. Anwar, and T. Matsumoto, "Low-Complexity Strategies for Multiple Access Relaying," in *Vehicular Technology Conference (VTC Spring)*, (Hungary), pp. 1–6, May 2011.

[34] J. Garcia-Frias and Y. Zhao, "Near-shannon/slepian-wolf performance for unknown correlated sources over awgn channels," *IEEE Transactions on Communications*, vol. 53, pp. 555 – 559, Apr. 2005.

[35] M. Cheng, K. Anwar, and T. Matsumoto, "Outage analysis of correlated source transmission in block rayleigh fading channels," in *Vehicular Technology Conference (VTC Fall), 2012 IEEE*, pp. 1 – 5, sept. 2012.

[36] M. Cheng, K. Anwar, and T. Matsumoto, "Outage probability of a relay strategy allowing intra-link errors utilizing slepian-wolf theorem," *EURASIP Journal on Advances in Signal Processing*, vol. 2013, no. 1, p. 34, 2013.

[37] M. Schwartz, W. R. Bennett, and S. Stein, *Communication Systems and Techniques*. John Wiley & Sons, 1995.

[38] V. E. Dale, P. J. Edwin, and R. Steven, *Calculus*. Prentice Hall, 2007.

[39] M. Cheng, K. Anwar, and T. Matsumoto, "On the duality of source and channel correlations: Slepian-wolf relaying viewpoint," in *International Conference on Communication Systems (ICCS) 2012*, pp. 388 – 392, Nov. 2012.

[40] A. Goldsmith, *Wireless Communications*. Stanford University, United States: Cambridge University Press, 2005.

[41] A. Irawan, K. Anwar, and T. Matsumoto, "Combining-after-decoding turbo hybrid arq by utilizing doped-accumulator," *IEEE Communications Letters*, vol. 17, no. 6, pp. 1212–1215, 2013.

[42] L. Hanzo, R. Maunder, J. Wang, and L. L. Yang., *Near-Capacity Variable-Length Coding.* John Wiley & Sons, 2010.

[43] X. Zhou, M. Cheng, X. He, and T. Matsumoto, "Exact and approximated outage probability analyses for decode-and-forward relaying system allowing intra-link errors," *IEEE Transactions Wireless Communications*, 2013. submitted.

[44] K. Fukawa, S. Ormsub, A. Tlli, K. Anwar, and T. Matsumoto, "Exit-constrained bicm-id design using extended mapping," *Wireless Communications, IEEE Transactions on*, vol. 2012, no. 1, p. 40, 2012.

[45] S. Boyd and L. Vandenberghe, *Convex Optimization.* Cambridge University Press, 2004.

Publications

Journal Articles

[1] **M. Cheng**, X Zhou, K. Anwar, T. Matsumoto, "Simple Relay Systems with BICM-ID Allowing Intra-link Errors". *IEICE Transactions on Communications*, vol. E95-B, No.12, pp. 36713678, December 2012.

[2] **M. Cheng**, K. Anwar, T. Matsumoto, "Outage Probability of a Relay Strategy Allowing Intra-link Errors Utilizing Slepian-Wolf Theorem", *EURASIP Journal on Advances in Signal Processing*, 2013, doi:10.1186/1687-6180-2013-34.

[3] X Zhou, **M. Cheng**, K. Anwar and T. Matsumoto, "Distributed Joint Source-Channel Coding for Relay Systems Exploiting Source-Relay Correlation and Source Memory", *EURASIP Journal on Wireless Communications and Networking*, 2012:260doi:10.1186/1687-1499-2012-260.

[4] X. Zhou, **M. Cheng**, X. He and T. Matsumoto, "Exact and Approximated Outage Probability Analyses for Decode-and-Forward Relaying System Allowing Intra-link Errors", *IEEE Trans. on Wireless Communications*. (under review)

Conference Proceedings

[5] **M. Cheng**, A. Irawan, K. Anwar, T. Matsumoto, "BICM-ID for Relay System Allowing Intra-link Errors and a Similarity Constellation to ARQ Schemes", *Progress In Electromagnetics Research Symposium* (*PIERS*), pp. 281286, Kuala Lumper, Malaysia, March 2012.

[6] **M. Cheng**, K. Anwar, T. Matsumoto, "Outage Analysis of Correlated Source Transmission in Block Rayleigh Fading Channels", *IEEE 76th Vehicular Technology Conference* (*VTC2012-Fall*) , pp. 15, Quebec, Canada, September 2012.

[7] **M. Cheng**, K. Anwar, T. Matsumoto, "On the duality of source and channel correlations: Slepian-Wolf relaying viewpoint", *IEEE International Conference on Communication Systems* (*ICCS 2012*) , pp. 388392, Singapore, November 2012.

[8] **M. Cheng**, K. Anwar and T. Matsumoto, "Outage Based Power Allocation: Slepian-Wolf Relaying Viewpoint", *IEEE Globecom 2013*, *First International Workshop on Cloud-Processing in Heterogeneous Mobile Communication Networks*, Atlanta, USA, December 2013. (Accepted)

[9] X. Zhou, **M. Cheng**, K. Anwar and T Matsumoto, "Distributed Joint Source-Channel Coding for Relay Systems Exploiting Spatial and Temporal Correlations", *IEEE Wireless Advanced 2012*, pp. 79-84, London, UK, June 2012.

[10] S. Qian, **M. Cheng**, K. Anwar, and T. Matsumoto, "Outage probability analysis for correlated sources transmission over rician fading channels, *2013 IEEE 24rd International Symposium on Personal Indoor and Mobile Radio Communications* (*PIMRC*), pp. 1087 - 1091, London, UK, September 2013.

[11] X. Zhou, **M. Cheng**, X. He, K. Anwar and T Matsumoto, "Outage Analysis of Decode-and-Forward Relaying System Allowing Intra-link Errors", submitted to *European Wireless* (*EW 2014*). (under review)